New Temporal Scour Depth Formula for Spur Dike using Statistical Analysis of Literature Data and Formulas

A thesis submitted towards partial fulfilment of the requirements for the degree of

Master of Engineering

in

Water Resources and Hydraulic Engineering

Submitted by

Sudarshan Mondal

Examination Roll No. M6WRP24016

Registration No. 121439 of 2012-2013

Under the guidance of

Dr. Subhasish Das

Associate Professor

School of Water Resources Engineering

Jadavpur University

School of Water Resources Engineering

M.E. (Water Resources & Hydraulic Engineering)

Course affiliated to ***Faculty Council of Engineering & Technology***

Jadavpur University

Kolkata-700032, West Bengal, India

2024

Declaration of Originality and Compliance of Academic Ethics

I hereby declare that this thesis contains a literature survey and original research work by the undersigned candidate, as part of my **Master of Engineering (Six Semester)** in **Water Resources and Hydraulic Engineering** in the Faculty Council of Interdisciplinary Studies, Law & Management, Jadavpur University during the academic session 2023-24.

All information in this document have been obtained and presented in accordance with academic rules and ethical conduct.

I also declare that, as required by these rules and conduct, I have fully cited and referenced all material and results that are not original to this work.

Name	**:**	**Sudarshan Mondal**
Exam. Roll Number	**:**	**M6WRP24016**
Thesis Title	**:**	New Temporal Scour Depth Formula for Spur Dike using Statistical Analysis of Literature Data and Formulas.
Signature with Date	**:**	

M.E. (Water Resources & Hydraulic Engg.) course affiliated to
Faculty Council of Engineering & Technology
Jadavpur University
Kolkata, India

Certificate of Recommendation

This is to certify that the thesis entitled **"*New Temporal Scour Depth Formula for Spur Dike using Statistical Analysis of Literature Data and Formulas*"** is a Bonafide work carried out by **Mr. Sudarshan Mondal** under my supervision and guidance for partial fulfilment of the requirement for the Post Graduate Degree of Master of Engineering in Water Resources and Hydraulic Engineering during the academic session 2023-24.

THESIS ADVISOR
Dr. Subhasish Das
Associate Professor
School of Water Resources Engineering
Jadavpur University

DIRECTOR
Prof. (Dr.) Asis Mazumdar
School of Water Resources Engineering
Jadavpur University

DEAN
Prof. (Dr.) Ratan Mondal
Faculty Council of Interdisciplinary Studies, Law & Management
Jadavpur University

M.E. (Water Resources & Hydraulic Engg.) course affiliated to
Faculty Council of Engineering & Technology
Jadavpur University
Kolkata, India

CERTIFICATE OF APPROVAL **

This foregoing thesis is hereby approved as a credible study of an engineering subject carried out and presented in a manner satisfactorily to warranty its acceptance as a prerequisite to the degree for which it has been submitted. It is understood that by this approval the undersigned do not endorse or approve any statement made or opinion expressed or conclusion drawn therein but approve the thesis only for the purpose for which it has been submitted.

Committee of

Final Examination

for the evaluation

of the thesis

** Only in case the thesis is approved.

ACKNOWLEDGEMENTS

I express my sincere gratitude to my supervisor, ***Dr. Subhasish Das,*** *Associate Professor, School of Water Resources Engineering, Jadavpur University, under whose supervision and guidance this work has been carried out. It would have been impossible to carry out this thesis work with confidence without his wholehearted involvement, advice, support and constant encouragement throughout. He has not only helped me in carrying out my thesis but also has given me valuable advice to proceed further in my life.*

I also express my sincere gratitude to, ***Prof. (Dr.) Asis Mazumdar****, Director,* ***Prof. (Dr.) Arunabha Majumder****, Emeritus Professor;* ***Prof. (Dr.) Pankaj Kr. Roy, Dr. Rajib Das, Dr. Gourab Banerjee,*** *Faculty members of School of Water Resources Engineering, Jadavpur University for their valuable suggestions.*

I would also express my sincere thanks to ***Mr., Buddhadev Nandi,*** *Research Scholar; of School of Water Resources Engineering, Jadavpur University for his unconditional support and affection during my work. Also, thanks to my classmates* ***Mr. Asraf Hossain*** *and* ***Ms. Moumita Nandi*** *for their help.*

Thanks, are also due to all staff of the School of Water Resources Engineering and the Regional-cum-Facilitation Centre (RCFC), NMPB, Jadavpur University for their help and support.

Date :

Place : Jadavpur University

Mr. Sudarshan Mondal
(Exam. Roll No: M6WRP24016)

ABSTRACT

Temporal scour depth (d_{st}) estimation at spur dikes is a significant issue for application engineers and researchers because accurate prediction is required for real-time monitoring. Although several formulas were employed, a definitive study is still needed to determine which formula predicts most accurately. Therefore, this study aims to address this need by conducting a comparative analysis of d_{st} prediction formulas at spur dikes under clear water conditions using laboratory datasets spanning the last 20 years. The analysis encompasses 14 parameters, each playing a significant role in scour depth prediction. These parameters include sediment coarseness, flow shallowness, porosity, densimetric Froude number, Reynolds number, spur dike length, height, thickness, orientation, width of flume, relative density, sediment uniformity, flow intensity and time. By considering these parameters, the study aims to identify the best option that will provide a more promising temporal scour depth formula based on a statistical analysis of data and formulas in literatures. Therefore, useful statistical influence factors are used to evaluate eight existing literature formulas alongside a newly derived formula concerning their effectiveness in predicting temporal scour depth. The model has been evaluated using different statistical performance indicators including Coefficient of Determination (R^2), Root Mean Squared Error (RMSE), Nash Sutcliffe Efficiency (NSE), and Mean Bias Error (MBE). The weightage of each influencing factor on the accuracy of predictions is calculated using CRITIC, Entropy, and AHP methods. Ranking of each formula based on their performance is determined using PROMETHEE and TOPSIS. The findings of the study reveal that the newly proposed formula most accurately predicts the d_{st} in terms of P_{in} as well as comparing statistical influence indicators such as $R^2 = 0.84$, RMSE = 0.13, NSE = 0.86, and MBE=0.003. The ranking of the formulas indicates that the newly developed formula consistently achieves the top position for each combination of weightage, for both the corresponding rankings. The formula of Coleman et al. (2003) is found useful for predicting d_{st}, particularly when equilibrium scour depth (d_{se}) and equilibrium time (t_e) are known. Additionally, the formulas proposed by Nasrollahi et al. (2008) and Karimi et al. (2012*a*, *b*) are found with similar accuracy compared to Coleman et al. (2003). Overall, this study not only identifies the most reliable formula for predicting d_{st} but also emphasizes the importance of considering practical constraints and real-world applicability in engineering solutions. By prioritizing practicality over idealistic approaches, engineers can make informed decisions that strike a balance between accuracy and feasibility.

CONTENT

Serial Number	Chapter No	Topic	Page No
		Declaration	iii
		Certificate of Recommendation	v
		Certificate of Approval	vii
		Acknowledgement	ix
		Abstract	xi
1	Chapter 1	**Introduction**	
		1.1 Brief Description	1
		1.2 Spur Dike	1
		1.3 Scouring Around Spur Dike	2
		1.4 Classification of Scour	3
		1.4.1 Contraction Scour	3
		1.4.2 Local Scour	4
		1.4.3 Live Bed Scour	5
		1.4.4 Clear Water Scour	6
2	Chapter 2	**Review of Literatures**	
		2.1 Literature Review	8
		2.2 Research Gap	15
		2.3 Need of The Study	16
3	Chapter 3	**Local Scour Characteristics Around Spur Dike**	
		3.1 Local Scour Mechanism	17
		3.1.1 Flow Diversion	17
		3.1.2 Horseshoe Vortex Formation	17
		3.1.3 Down Flow Formation	18
		3.1.4 Wake Vortex Formation	18
		3.1.5 Scour Hole Formation	18
		3.2 Classification of Spur Dikes	18
		3.2.1 Classification Based on Permeability	18
		3.2.2 Classification Based on Submergence	19
		3.2.3 Classification Based on Angle of Inclination	20
		3.2.4 Classification Based on Geometry	21
		3.3 Classification of Scour Parameters	22
		3.3.1. Spur Dike Properties	22
		3.3.2. Flume Properties	23
		3.3.3. Bed Properties	23

		3.3.4. Fluid Properties	24
		3.3.5. Flow Properties	24
		3.3.6. Time Properties	25
		3.3.7. Scour Depth Properties	25
		3.3.8. Structural Properties	26
		3.3.9. Environmental Properties	26
4	Chapter 4	**Classification of Data, Methods and Equations from Literatures**	
		4.1 Experimental Procedures followed by Research Groups	27
		4.2 Literature Equations to predict Temporal Scour	31
		4.3 New Functional Relationship developed based on Literatures	32
		4.4 Temporal Scour Depth Formulas developed by Researchers	33
		4.5 Datasets selected for Present Study	34
5	Chapter 5	**Objectives And Methodology**	
		5.1 Research Objectives	37
		5.2 Research Methodology	37
		5.3 Statistical Influencing Parameters	39
6	Chapter 6	**Dimensional Analysis**	
		6.1 Dimensional Framework	41
		6.1.1 Analyses of Scouring Parameters	41
		6.1.2 Ratio-Based Analysis	42
		6.2 Classification of Dimensional Parameters	46
		6.3 Dimensionless Parameters taken by Research Groups	48
7	Chapter 7	**Analysis of Parameters Using Feature Selection**	
		7.1 Feature Selection	50
		7.1.1 Goodman and Kruskal's Gamma Statistics Test	50
		7.1.2 Pearson Correlation Coefficient	52
		7.1.3 Spearman's Rho Correlation Coefficient	53
		7.1.4 Kendall's Tau B Correlation Coefficient	54
		7.1.5 Principal Component Analysis	55
		7.1.6 Discriminant Analysis	56
		7.1.7 Line of Least Squares Regression Analysis	57
		7.1.8 Enter Regression Analysis	58
		7.1.9 Forward Regression Analysis	59
		7.1.10 Backward Regression Analysis	60
		7.1.11 Removed Regression Analysis	60

7.1.12 Stepwise Regression Analysis 61
7.1.13 Subset Regression Analysis 62
7.1.14 Mandatory and Additional Components Contributing to Dimensionless Parameters 63
7.1.15 Identify Optimal Technique Using Weighted Mean Percentage Method 66
8 Chapter 8 Results And Discussion
8.1 Literature Data Compared to Empirical Formulas 67
8.2 Findings and Interpretations 79
8.2.1 New Formula Developed for Temporal Scour 79
8.2.2 Comparison of New and Literature Formulas Using Statistical Measures 81
8.2.3 Weightage and Ranking of Formulas 87
8.2.3.1 Weight Criteria Technique 87
8.2.3.2 Ranking Criteria Technique 91
8.2.4 Overall Discussion 98
8.2.5 Limitations of The Present Study 100
9 Chapter 9 Conclusive Remarks
9.1 Conclusions 102
9.2 Future Scopes 103
9.3 Notations 104
9.4 References 105

Chapter 1
Introduction

1.1 Brief Description

Scour occurs due to the erosive action of flowing water (Barbhuiya and Dey, 2004; Kothyari and Ranga Raju, 2001; Pandey et al., 2018b). Scour is responsible for the failure of many hydraulic structures (Chavan and Kumar, 2017; Kothyari et al., 2007; Lodhi et al., 2016; Pandey et al., 2018a; Singh et al., 2020). Hence, it is crucial to accurately predict the scour depth around the hydraulic structures such as bridge piers, abutments, and spur dikes experimentally, numerically as well as using machine learning techniques. There are numerous studies available for isolated bridge piers and a combination of bridge piers. The study on isolated pier scour depth computation formula conducted by Melville and Chiew, 1999; Oliveto and Hager, 2002; Azamathulla et al., 2010; Nandi and Das, 2023a; Nandi et al., 2024a; and Nandi et al., 2024b. The study of eccentric multiple piers conducted by several researchers (Das et al., 2014a; Das et al., 2014b; Das et al., 2016; Das and Mazumdar, 2018; Das et al., 2019; Nandi and Das, 2023b). The flow characteristic near the pier has been studied by Das et al., 2013; Das et al., 2014c; Das et al., 2017; Jaman et al., 2017; and Das et al., 2019. The extensive review of the literature has revealed a significant gap in research concerning spur dikes and their working principles. Spur dikes are mainly used for reducing the flow velocity and diverting the main channel flow (Oliveto and Hager, 2002; Kothyari et al., 2007). The scour depth at a spur dike mainly depends on its length, flow parameters, and sediment characteristics (Azamathulla et al., 2010; Azamathulla et al., 2008; Karna et al., 2015; Pandey et al., 2019; Singh et al., 2020).

This study aims to evaluate and compare formulas predicting scour depth around a spur dike, using experimental data from the last two decades. It aims to establish criteria for selecting the best formula, employing multi-attribute decision-making techniques such as CRITIC, Entropy, and AHP to determine weightage, PROMETHEE, and TOPSIS for ranking.

1.2 Spur Dike

A spur dike is a kind of transverse structure that is usually built in rivers or streams. It creates a barrier that modifies the watercourse's flow patterns by extending outward from the bank into the moving water. These structures have different functions such as-

Flow Direction: Spur dikes help regulate and direct the flow of water through channels. Water can be directed towards a desired direction by extending into the stream, which helps to control the movement of sediment and prevent bank erosion.

Bank Protection: Spur dikes are used to protect against bank erosion, which is the main purpose of bank protection. When water can't move freely, it has less power to wear away the land and make the banks weaker and more likely to collapse.

Enhancement of Habitat: Spur dikes create stable pools in turbulence-prone or disturbed streams. These pools give aquatic life a place to live and a haven, which enhances biodiversity and the health of the ecosystem in the watercourse.

Spur dikes are beneficial, but they also have the potential to upset the natural equilibrium of streams or rivers. These structures cause modifications in the dynamics of the flow, which in turn affects the patterns of sediment transport and velocity. This disturbance starts a process called scouring, in which the water's force erodes the watercourse's bed and banks near the dike's base.

Hydraulic engineers face a great deal of difficulty with the scouring process because it can jeopardize the stability of surrounding structures like embankments and bridge foundations. Thus, it is considered essential to precisely forecast and alleviate the consequences of local scour around spur dikes in order to guarantee the sustainable and safe design of hydraulic infrastructure in riverine environments.

1.3 Scouring Around Spur Dike

The significant localized erosion of sediments that happens when a liquid's erosive capacity surpasses the sediments' resistance to it is known as scour. The liquid's erosive capacity results from pressure fluctuations that occur during turbulent flows, and the sediments' inherent properties such as mass strength, dimension, internal friction, and shape and orientation, determine their capacity to withstand it. Erosion and scour are interchangeable terms. Only two types of scours, local scour and contraction scour are taken into consideration. Here is a description of these to help for better understand.

When a stream channel's flowing area is reduced or contracted either naturally or through the installation of spur dikes contraction scour happens. An increase in average velocity and bed shear stress are the outcomes of a contraction in the flowing area. More bed and side materials are displaced as a result of an increase in erosive forces in the contracted area. Until the stream reaches a relative equilibrium, the flow area grows as the bed elevation decreases, resulting in a drop in velocity and shear stress. This indicates that the quantity of scoured bed material that was removed from the flow area and moved into the area is equal.

A spur dike's foundational stream flow contraction may result from a natural decline in the stream channel's flow area or from other causes like

(1) Constrictions in the natural flow of streams.

(2) Bends in the banks that are naturally formed by sediment deposits.

(3) Debris in the river.

(4) Vegetation growth in the floodplain or channel.

(5) Flow with pressure.

The development of vortices at the base of spur dikes is the fundamental process underlying local scour. The collision of water fronts on the obstruction's surface at the upstream side and the significant acceleration of flow close to the dike's toe are the causes of

vortices. The rate of change in the scour bed is greater close to the spur dike foundation than it is farther away. A scour hole is formed around the structure's base as a result of this process. The horseshoe vortex's strength diminishes with increasing scour hole depth, slowing the rate at which sediment is transported from the base region.

The following variables have an impact on the local scour depth around the spur dike:

(1) Velocity of flow upstream.
(2) Depth of flow.
(3) The spur dike's width.
(4) Contraction ratio.
(5) The spur dike's length.
(6) Size and grade of bed particles.
(7) The spur dike's orientation angle.
(8) Spur dike's shape.
(9) Bed configuration.
(10) Debris and vegetation.

1.4 Classification of Scour

Scour refers to the erosion of earth material from a channel, whether it is stable or unstable. It occurs in proximity to various hydraulic structures such as spur dikes, and abutments near roads, riverbanks, and bridge piers, and is a critical consideration for hydraulic engineers.

1.4.1 Contraction Scour

The erosion of the land around the structures that resemble spurs occurs when the water flow is restricted by their presence. Dikes are commonly constructed at right angles to the river's edge to guide water, prevent erosion, and maintain the river course. However, they can also cause erosion downstream, like other hydraulic structures such as bridges or culverts, but with some distinctions in mechanisms and characteristics. This is how the process of contraction scour (Fig. 1.1) occurs around structures that resemble spurs.

Flow Contraction: Spur dikes cause the river flow to narrow as water goes around and between them. The narrowing of the channel causes the water to move faster and have more energy as it flows past the dikes.

*Acceleration and Turbulence***:** When flow encounters spur dikes, it speeds up, resulting in increased flow speeds in the area behind the dikes. When the water moves faster, it creates swirls and bumps that make the land wear away more quickly.

Sediment Transport: The faster the water moves after the dikes are built, the more sediment it can pick up and carry away, which can damage the riverbed and banks. When soil is washed away by water, it can make the riverbanks and nearby buildings less secure.

*Channel Morpho dynamics***:** The morpho dynamics of the river channel can be changed by contraction scour caused by spur dikes, which can influence how sediment moves, the shape of the river bed, and the overall shape of the channel as it flows downstream.

To prevent erosion caused by the contraction of the land, various measures can be taken around the dikes, such as:

Riverbank Stabilization: Using techniques like riprap or planting vegetation to secure the riverbanks located after the spur dikes, can help protect the bank from erosion.

*Flow deflectors or guide structures***:** They can be installed to redirect the flow of water away from areas that are susceptible to erosion and protect downstream locations.

*Aprons for Scouring***:** Building aprons or energy-absorbing structures after spur dikes to slow down water flow and absorb energy, which helps prevent erosion.

Monitoring and Maintenance: To maintain the stability and structural integrity of spur dikes, it is crucial to regularly assess the depth of scour and the movement of sediment, and promptly address any necessary repairs or maintenance.

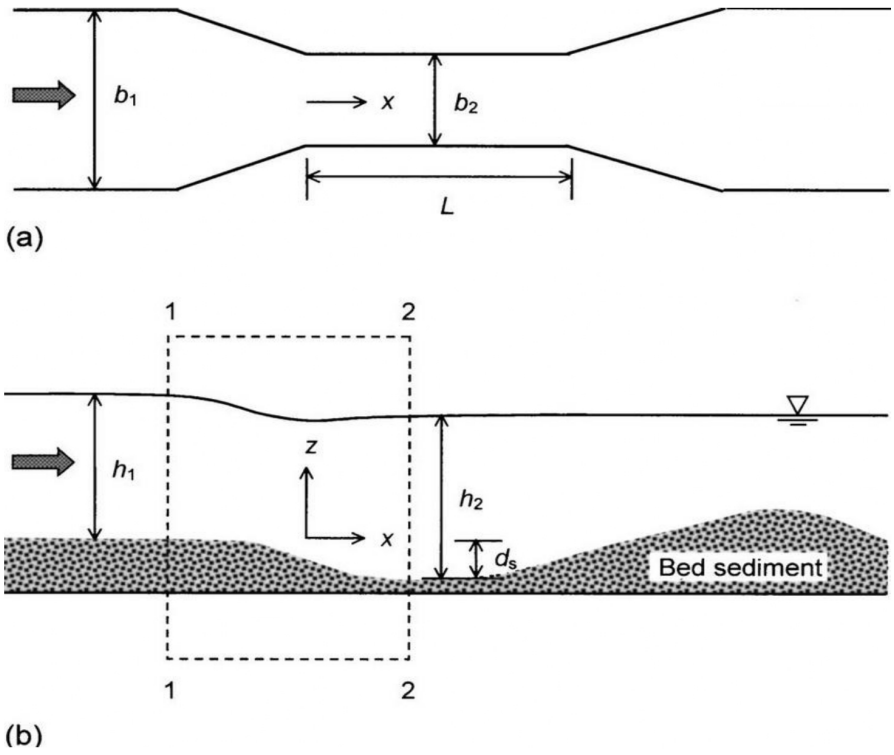

Fig. 1.1. Schema of a long rectangular channel contraction at equilibrium scour condition: **a** top view; and **b** side view (Dey, 2014).

1.4.2 Local Scour

The erosion that happens right next to and below the hydraulic structures is called local scour. Dike construction is usually done at right angles to the riverbank to guide water flow, manage sediment accumulation, and maintain river stability. Nevertheless, their existence can cause erosion in the immediate vicinity of the structures because of the intricate water movement and higher water speeds near and after the structures. This is how the erosion of the land around the dike structures occurs locally.

Flow Contraction and Acceleration: Spur dikes cause a reduction in the flow path width, resulting in an increase in flow speeds around and downstream of the structure. The riverbed and banks experience more erosion as the speed of the water increases.

Vortices and Turbulence: As the water moves around the sharp bend, it forms whirls and chaos behind it. In the rivers, turbulent flow can worsen erosion by removing sediment from the riverbed and banks.

Bed and Bank Erosion: When spur dikes are present in the rivers, the flow becomes faster and more chaotic, causing the riverbed and banks to lose sediment and create small holes or pits.

Undermining of Structure: When the ground around the dikes is eroded for a long time or very deeply, it can weaken the base of the structure, which can make it less safe and less able to stop water and soil from moving.

The following are possible mitigation strategies for local scour around spur dike structures:

Armour Protection: To prevent scour and stabilize the riverbed and banks, place erosion-resistant materials around the base of the spur dike, such as riprap or concrete armour units.

Toe Protection: To reduce the risk of undermining and stop erosion at the base of the spur dike, toe protection measures like grouted riprap or gabions should be installed.

Scour Aprons: Build scour aprons, also known as energy dissipators, downstream of the spur dike to minimize scour depth, dissipate energy, and lower flow velocities.

Hydraulic Modelling and Design: During the design phase, the possibility of local scour is evaluated using hydraulic modeling techniques, and suitable scour countermeasures are incorporated into the design of spur dike structures.

1.4.3 Live Bed Scour

Live bed scour at spur dikes is critical due to its potential to jeopardize the stability of river engineering structures and disrupt the hydraulic dynamics of the channel. This erosion phenomenon can result in structural damage, erosion, and safety risks downstream. Details regarding its definition, mechanism, characteristics, and mitigation strategies are provided below.

Definition: When sediment particles are entrained and carried by the flow around and downstream of the spur dike structure, live bed scour (Fig. 1.2), also referred to as sediment transport scour, takes place.

Mechanism: When flow velocities and sediment transport capacity are high enough to start sediment transport, live bed scour usually happens during high flow events. This kind of scour is typical in rivers and streams that are high in silt.

Features: Changes in bed morphology and channel geometry are caused by live bed scour, which is the erosion and transport of sediment from the riverbed and banks downstream of the spur dike. The eroded sediment can move downstream and deposit itself in places with slower-flowing water.

Mitigation: Installing scour aprons or energy dissipaters downstream of the structure can help minimize scour depth and erosion by reducing flow velocities and dissipating energy, which are two possible mitigation strategies for live bed scour around spur dike structures.

1.4.4 Clear Water Scour (CWS)

Clear water scour (CWS) at spur dikes is crucial, as it directly undermines the structural integrity of river engineering structures, posing risks of erosion, structural failure, and downstream safety concerns. Details on its definition, mechanism, characteristics, and mitigation strategies are elaborated below.

Definition: The erosion that happens right next to and below the hydraulic structures is called local scour (Fig. 1.2). Dike construction is usually done at right angles to the riverbank to guide water flow, manage sediment accumulation, and maintain river stability. Nevertheless, their existence can cause erosion in the immediate vicinity of the structures because of the intricate water movement and higher water speeds near and after the structures. This is how the erosion of the land around the dike structures occurs locally.

Mechanism: Spur dikes cause a reduction in the flow path width, resulting in an increase in flow speeds around and downstream of the structure. The riverbed and banks experience more erosion as the speed of the water increases.

Features: As the water moves around the sharp bend, it forms whirls and chaos behind it. In the rivers, turbulent flow can worsen erosion by removing sediment from the riverbed and banks. When spur dikes are present in the rivers, the flow becomes faster and more chaotic, causing the riverbed and banks to lose sediment and create small holes or pits.

Mitigation: When the ground around the dikes is eroded for a long time or very deeply, it can weaken the base of the structure, which can make it less safe and less able to stop water and soil from moving.

The following conditions are typical of clear water scour:

(1) Coarse bed material in streams;

(2) Flat gradient of the streams during low flow conditions;

(3) Local deposits of larger bed materials; and

(4) The areas along the banks or in vegetated channels.

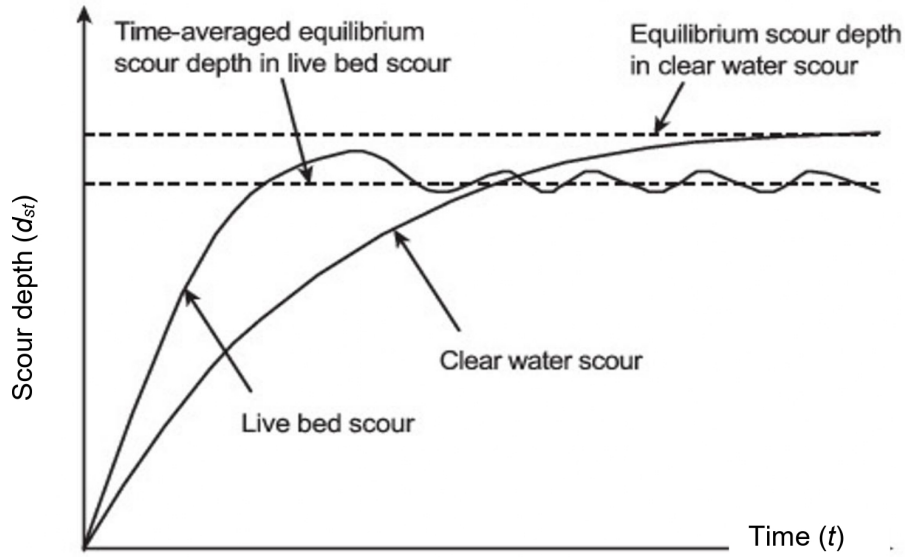

Fig. 1.2. Time development of Clearwater and live-bed scour (after Chabert and Engeldinger 1956).

Chapter 2
Review of Literatures

2.1 Literature Review

This thesis work primarily focuses on predicting the temporal scour depth around spur dikes and identifying the parameters that are highly influenced by the performance of spur dikes. Prior studies have attempted to comprehend and forecast the temporal scour depth surrounding spur dikes. Some of their contributions are discussed in more detail below:

The investigation on the effect of flow, spur-dike, and sediment characteristics on maximum scour depth was conducted by Garde (1961) in a non-recirculating flume measuring 0.61 m wide and 7.62 m long. It was determined that the influence on maximum scour depth is adequately represented by the Froude number (F_r) of the normal channel, opening ratio (e), angle of inclination of the spur-dike (Θ), and average drag coefficient (C_d) of sediment particles.

Experiments were conducted by Gill (1972), utilizing a flume measuring 0.76 m in width, 0.46 m in depth, and 12.2 m in length. Two different sizes of uniform sand were employed in the experiments. It was shown that a rather simple kinematic model for erosion of sand beds in a long contraction can be modified for application to erosion around spur dikes. The equilibrium depth of the scour depends on the size of the sand and the flow depth upstream of the location of the spur dike.

Copeland (1983) conducted tests on a model in a sand bed flume with a channel top width of approximately 2.4 m (8 feet) and an average depth of 0.07 m (0.24 feet). The flume had a length of 39.62 m (130 feet). Copeland proposed that, in addition to other factors, the coarse fraction of the bed material plays a significant role in influencing the scour depth around the spur dike.

Suzuki (1987) conducted experiments to examine the characteristics of local bed forms around a series of spur dikes in an alluvial bed with continuous sediment motion. Utilizing two different flumes-one measuring 0.5 m wide and the other 0.4 m wide-and uniform sand with a diameter of 0.6 mm, Suzuki observed that the local scour around the first spur dike resembled that of a single spur dike. Additionally, he noted that the depth depended on the flow depth d when the ratio d/W was less than 1.5.

Kuhnle (1997, 1998, 1999) conducted a series of experiments in a flume measuring 30 m in length, 1.2 m in width, and 0.6 m in height to investigate the volume of scour holes associated with spur dikes. These experiments involved varying the orientation angles of the spur dikes, overtopping flow height, and the contraction ratio. The findings revealed the following:

- There exists a positive correlation between the contraction ratio and flow depth with the volume of scour for a given elapsed time under steady flow conditions.
- The geometry of the scour hole was found to be influenced by the overtopping ratio.

- Among the three angles of spur dikes and two contraction ratios considered, 135° spur dikes exhibited the lowest value, 90° spur dikes showed an intermediate value and 45° had the highest bed erosion in the vicinity of a channel bank. Consequently, the volume of the scour hole was highest for the 135° spur dikes.

Ballio and Orsi (2001) used multiple series of experiments to study the time-dependent variation in scour depth for uniform sediment in clear-water scour conditions (CWS) surrounding bridges, abutments, and spur dikes. Local phenomena around bridge piers and abutments are generally considered to be similar; however, the presence of the incoming boundary layer on the side wall in the abutment case results in extra pressure gradients and, consequently, a more complex vortex pattern. Experimental data for bridge, abutments are relatively scarce in the literature, especially regarding the time evolution of scour. This study presents the results of several long-duration (3 days to 5 weeks) CWS laboratory tests around bridge abutments. The time evolution of the erosion process was analyzed with respect to local and global characteristic values (maximum, volume, hole shape). In particular, the effect of the constriction ratio (e) between the transversal obstacle dimension (b) and the flume width (W) was analyzed. In many practical situations, abutments (or piers or spur dikes) obstruct a significant portion of the channel, leading to an expected increase in scour effects due to the average acceleration caused by constriction around the obstacle. Measured values for maximum scour are poorly predicted by literature formulas. Scour depths are positively correlated with the constriction ratio, but increases are smaller than expected from literature indications. Experimental results by Ballio and Orsi (2001) indicated that models for bridge piers cannot be directly applied to abutments, spur dikes in particular, time scales for the latter are significantly larger than for piers.

Experiments involving rectangular shaped singular and multiple spur dikes were conducted by Oliveto and Hager (2002). Significant attention has been devoted to scour related to bridge hydraulics in the past decade, encompassing its relationship to flood hydrology and hydraulic processes alongside steady flow. A research study on bridge pier and abutment scour, based on a large dataset collected at ETH Zurich, Switzerland, was presented in their paper. In total, six different sediments were tested, including three uniform sediments. Additionally, a wide range of scour elements were considered, spanning from 1 to 60% of the channel width (W), with flow depths (d) ranging from 1 to approximately 40% of the channel width. The agreement of his scour equation with both the data and the literature data was considered sufficient in terms of river engineering accuracy, provided limitations relating to hydraulic, granulometric, and geometrical parameters were satisfied.

Coleman et al. (2003) investigated time-dependent scour depth variation with several series of experiments for uniform sediment under clear-water conditions near vertical wall abutments. Each combination of flow, rectangular shaped abutment, and sediment parameters underwent analysis, including the change in maximum local scour depth from plane-bed to equilibrium conditions over time. Differences in scour rates and depths were observed based on flow and sediment parameters, particularly for short ($d/l > 1$) and long ($d/l < 1$) abutments. They proposed a time-dependent scour equation. It was concluded temporal scour depth increases with an increase in V/V_c ratio. For the same value of V/V_c temporal scour depth increases with the decrease in d/l ratio.

Kothyari et al. (2007) modified the approach of Oliveto and Hager (2002) on the basis of the difference between F_d and $F_{d\beta}$, where $F_{d\beta}$ is the densimetric particle Froude number for the inception of scour at element (spur dikes). He took into account rectangular shaped single and multiple spur dikes. Several experiments were conducted in a 1 m wide VAW, ETH Zurich, Switzerland, scour channel. Gravel with a median particle size D_{50} of 4.3 mm and a sediment gradation (σ) of 2.35 made up the bed sediment. In the case of a single spur dike, taking into account two different angles: 45°, and 90°. In the case of multiple spur dikes, taking into account three different angles: 60°, 90° and 120°. Kothyari et al. also concluded that the erosion rate mainly depends on the difference between the starting point of the total bed shear stress and the critical bed shear stress and proposed a new method to calculate the temporal variation in erosion depth around the spur dike in non-viscous sediments. They also examined huge scour data near abutments and spur dikes and proposed the following relationship to estimate the dimensionless temporal scour depth near un-submerged spur dikes. when the channel section is rectangular and straight in plain, viscous effects of fluid are less corresponding to approach flow depth $d \geq 50$ mm, $D_{50} \geq 0.80$ mm for $\rho_s > 2.65$ kg/m^3.

Yanmaz and Kose (2007) studied the properties of scour holes surrounding vertical wall rectangular shaped abutments in clear water with consistent bed materials in relation to time. Further relationships were looking into the surface area and volume of the scour holes surrounding abutments in relation to time. Useful information for the preliminary design of abutment footings and the placement details of armoring counter-measures, such as riprap, provided by the findings of those studies. A 30 m long, 1.25 m wide, and 1 m deep rectangular channel was used for a number of tests 1 to 23. The length of the abutment was 12.5 cm for tests 1 to 10 and 20 to 21, and 10 cm for tests 11 to 19 and 22 to 23. gravel that, for tests 1 to 19, had a median particle size D_{50} of 1.8 mm, and for tests 20 to 23, 0.9 mm. The non-cohesive sand bed sediment had a sediment gradation of 1.3, and the discharge flow was Q = 0.08 m^3/sec (constant) and V/V_c <1 with a geometric standard deviation of roughly 1·40. Additional relations were also derived for the time-dependent volume and surface area of the scour holes around abutments.

Nasrollahi et al. (2008) took into account with rectangular shaped singular spur dike. They studied the local scour of spur dikes using physical model tests and found that the scour hole characteristics of spur dikes are related to Froude number, spur dike permeability, the ratio of water depth to dike length, and the ratio of river channel width to dike length. A single spur dike was erected in each experiment at a 90° angle to the direction of the main flow. A number of tests 1 to 14 were carried out in a rectangular channel 12 m long, 2 m wide, and 0.6 m deep and Unsubmerged spur dike circumstances. Gravel with a median particle size D_{50} of 1.3 mm and a sediment gradation of 1.3 made up the non-cohesive sand bed sediment and Discharge of flow Q = 0.08 m^3/sec (constant) and V/V_c <1.

Karami et al. (2012a) took into account multiple spur dikes in rectangular shape. Multiple spur dikes were erected in each experiment at a 90-degree angle to the direction of the main flow. The time variation of scour around the first spur dike in a series of spur dikes was experimentally examined under different values of (V/V_c) and four sizes of sediment bed materials. It was found that the highest percentage of scouring (d_{st}/d_{se} = 70–90%) occurred during the initial times of scouring (t/T = 20%). Sediments were deposited between each two spur dikes due to a decrease in velocity. The location of maximum scour depth was

consistently observed near the upper corner of the first spur dike. The average upstream slope of the scour hole was found to be near the angle of repose of sediment particles (θ). Several tests S1 to S8 and G1 to G3 were carried out in a rectangular channel 14 m long, 1.0 m wide, and 1 m deep and Un submerged spur dike circumstances. Gravel with a median particle size D_{50} of 0.19 mm for S1 and S2 and 0.91 mm for S3 to S5, 1 mm for S6 to S8 and 3 mm for G1 to G3 and a sediment gradation of 1.28, 1.38,1.39 and 1.37 respectively made up the bed sediment and approach flow depth d varied and V/V_c <1,

Karami et al. (2012b) investigated the scour phenomenon around rectangular shape multiple spur dikes using both experimental and numerical methods. Tests were conducted in a rectangular channel with gravel bed sediment and varying flow intensities (V/Vc). The high-resolution laser bed-profiler (LBP) measured scour geometry. The computational fluid dynamics (CFD) model SSIIM 2.0, employing the finite-volume method and the k-e turbulence model with RNG extensions, simulated sediment transport. Results showed rapid scour development initially, with around 80% occurring within the first 20% of equilibrium time. Increasing the velocity ratio increased scour depth and volume around spur dikes, particularly the last one. The average upstream slope of the scour hole matched the angle of repose of sediment particles, and the first and last spur dikes experienced the maximum scour depth. Different vortex formations were observed influencing scour hole depth.

Research was conducted by Pandey et al. (2014a) to investigate the scour and flow behavior around rectangular shape single and multiple spur dikes. Six experiments were conducted, comprising three runs for single spur dikes and three runs for multiple spur dikes under clear water scouring over fine sand with a mean diameter of 0.27 mm. The experiments took place in a rectangular channel measuring 24 m in length, 1.0 m in width, and 0.50 m in depth. The working section of the flume was positioned 13.7 meters downstream from the flume entrance and measured 3.9 m × 1.0 m × 0.40 m. Partially submerged spur dikes with a transverse length of 10 cm were selected for the experiments.

An investigation was carried out by Pandey et al. (2014b) into the temporal variation of scour around a single spur dike and the effect of multiple spur dikes on the scour phenomenon. Nine experiments were conducted, comprising three runs for a single spur dike and six runs for multiple spur dikes under clear-water scouring over fine sand with a mean diameter of 0.27 mm, standard deviation of 1.23, and specific gravity of 2.65, for three different discharge rates, namely 0.0159 m^3/sec, 0.0188 m^3/sec, and 0.0210 m^3/sec. He observed that the maximum scour depth typically occurs at the nose of the spur dike. Additionally, he noted that the maximum scour depth is generally lower in cases involving multiple spur dikes compared to those with a single spur dike. The experiments were conducted in a rectangular channel measuring 24 m in length, 1.0 m in width, and 0.50 m in depth. The working section of the flume commenced 13.7 m downstream from the flume entrance and measured 3.9 m × 1.0 m × 0.40 m. Partially submerged spur dikes with a transverse length of 20 cm and a thickness of 2.5 mm were selected for the experiments.

An investigation was conducted by Pandey et al. (2015) to assess the accuracy of existing equations for computing maximum scour depth, utilizing available data in the literature and data collected in their study through graphical and statistical performance indices. Additionally, three new relationships were proposed to estimate the maximum scour depth and maximum scour length upstream and downstream of the spur dike. Experiments

were conducted under clear-water scouring over fine sand with a mean diameter of 0.27 mm, standard deviation of 1.23, and specific gravity of 2.65 for three different discharge rates: 0.0159 m^3/sec, 0.0188 m^3/sec, and 0.0210 m^3/sec. They reached the conclusion that the Froude number of the spur dike significantly impacts both the equilibrium scour depth. Furthermore, he reiterated that the maximum scour depth consistently occurs at the upstream side and nose of the spur dike, accompanied by sediment deposition downstream due to erosive forces. The experiments took place in a rectangular channel measuring 24 m in length, 1.0 m in width, and 0.50 m in depth. The working section of the flume commenced 13.7 meters downstream from the flume entrance and measured 4.0 m × 1.0 m × 0.60 m. Impermeable spur dikes with a thickness of 2 mm and various transverse lengths of 6 cm, 8.5 cm, 10 cm, 12 cm, and 20 cm were utilized for the experiments.

Pandey et al. (2019) investigated the estimation of temporal scour depth variation around spur dikes. A total of 12 experiments were conducted, comprising six runs for a single spur dike and six runs for multiple spur dike under clear water scouring over fine sand with a mean diameter of 0.27 mm. The experiments were carried out for three different discharge rates: 0.0159 m^3/sec, 0.0188 m^3/sec, and 0.0210 m^3/sec, in a rectangular channel measuring 24 m in length, 1.0 m in width, and 0.50 m in depth. The working section of the flume commenced 13.7 m downstream from the flume entrance and measured 4.0 m × 1.0 m × 0.45 m. Partially submerged and impermeable spur dikes with transverse lengths of 10 cm and 20 cm and a thickness of 2 mm were selected for the experiments. He concluded that the maximum scour depth is typically situated at the noses of the spur dike, but in the case of equidistant three spur dikes, it was found to be located between the noses of the spur dike and the junction with the spur dike wall. Additionally, he determined that the maximum scour depth at the equilibrium stage increases with an increase in discharge and the transverse length of the spur dike.

The temporal fluctuation of scour around partially submerged spur dikes formed in cohesive sediment mixtures comprising clay-gravel and clay-sand-gravel mixes were investigated by Lodhi et al. (2017) in a number of laboratory studies. The two most significant cohesive sediment mixture characteristics that affect the depth of scour along rectangular shaped spur dikes are the percentage of clay and unconfined compressive strength (UCS). As the ratio of clay and UCS in the cohesive sediment mixtures rises, the depth of scour decreases. The temporal variation of depth around partially submerged spur dikes embedded in cohesive sediment mixtures in the wake of the spur dikes was proposed to be determined by a computational technique.

Khassaf and Abbas (2018) calculated the maximum scour depth around an L-shaped groyne in the current study using data from 56 laboratory experiments in which varying groyne numbers and spacing were employed as a kind of countermeasure to lessen scour around the groyne foundations. Within the study's limitations, the results demonstrated a discernible decrease in scour depth as the number of groynes increased as well as the distance between them. The scour depth increased as the flow depth, flow velocity, and Froude number increased for a constant number of groynes and their distances from one another. The scour depth decreased with increasing the number of groynes by approximately 3.33-30.2% for each increase in groyne count equal to one, and with increasing the distances between them by approximately 3.13-17% for each half of groyne length (0.5l) increase in these distances,

under constant hydraulic conditions. At the groyne nose on the upstream side, the maximum depth of scour was reached. Because it is the first groyne that the water collides with, maximum scour has been seen at that location.

Lodhi et al. (2018) carried out a number of experiments to examine the impact of cohesion on scour depth at the spur dike's wake zone using cohesive sediment mixtures combining clay-gravel and clay-sand-gravel. In the experiments, two different kinds of sediment mixtures were used. 1. A clay percentage ranging from 10 to 50% was combined by weight with fine gravel; 2. A clay percentage ranging from 10 to 50% was combined by weight with an equal amount of fine sand and fine gravel. It was discovered that the scouring process surrounding the rectangular spur dike differed noticeably between cohesive and cohesion less sediment mixtures that contained gravel-sized sediment. The scour pattern surrounding the spur dike resembled cohesiveness sediment when the clay concentration was less than 10% in the gravel-clay mixture and less than 20% in the gravel-sand-clay mixture. Since all tests were carried out in clear water, no sediment deposition happened in the spur dike's wake zone in cohesive sediment combinations.

In the study by Ning et al. (2019), the rectangular size of the spur dike group consisted of four spur dikes of identical length and regular spacing. The spur dike spacings were 2 l, 3 l, and 4 l mm in all three instances. D_{50} = 0.473 mm was used as the sediment's particle size. Re =16,585, the Reynolds number, and Fr = 0.28, the Froude number, were constants, as were the 0.00962 m^3/sec (9.62 l/s) of flow discharge, 1/1000 channel slope, 40 cm of channel width, 9 cm of flow depth, 0.267 m/sec of flow velocity, and 1900 kg/m^3 (1.9 gm/cm^3) of sediment density. He concluded that the maximum scour depth is typically found near the head of the first spur dike. As the spacing between spur dikes increases, the shielding effect of the first spur dike diminishes. In terms of velocity, he concluded that the maximum velocity in the main flow zone is twice that of the approach flow velocity in a fixed bed, while it aligns approximately with the incoming velocity during equilibrium scouring. The maximum turbulent energy is predominantly located in the backflow area of the fourth spur dike in a fixed bed, whereas in a movable bed, it peaks at the head of the second spur dike. Additionally, shear stress decreases as scouring progresses. These findings suggest potential practical applications for understanding and manipulating spur dike spacing in real rivers.

Pandey et al. (2019) estimated the maximum scour depth under equilibrium conditions and identified the parameters influencing it in a sand-gravel mixture bed. They conducted 32 experiments under clear-water conditions in a rectangular channel measuring 24 m in length, 1.0 m in width, and 0.25 m in depth. The test section was situated 12 meters from the entrance of the flume and measured 4.0 m × 1.0 m × 0.25 m. Each experiment had a duration of 20 hours. Four different rectangular spur dikes, made of 5 mm thick cast iron plates and having transverse lengths of 6.0 cm, 9.0 cm, 11.5 cm, and 14.0 cm, were utilized in the experiments. The study revealed that the non-dimensional maximum equilibrium scours depth increases with the critical velocity ratio (V/V_c), water depth-armour particle ratio (d/d_a), Froude number for sediment mixture (F_{rsm}), and water depth-spur dike length ratio (d/l), while it decreases with an increase in the armour particle-spur dike length ratio (d_a/l).

Pandey et al. (2020) investigated to estimate the maximum scour depth around rectangular spur dikes in sand-gravel mixes, Pandey et al., (2020) devised a temporal scour depth equation. They concluded that the dimensional temporal scour depth variation increases

with an increase in the threshold velocity ratio, the densimetric Froude number (F_d) of the bed surface sediment mixture, the flow shallowness (defined as the ratio of the approach flow depth (d), to the transverse length of the spur dike (l), and the flow depth-particle size ratio. Additionally, he concluded that the temporal scour depth variation in the sediment mixture was influenced by the non-uniformity of sediment and decreased with an increase in the non-uniformity of the sediment mixture. The key contribution of this study was that it treats sand-gravel mixes like movable beds. 32 clear-water trial runs were conducted in a rectangular channel measuring 24 m in length, 1.0 m in width, and 0.50 m in depth. The working test portion was located 12 m from the flume entrance and measured 4.0 m × 1.0 m × 0.4 m. Every trial had a 20-hour duration.

Masood et al. (2021) examined the geometry of scour holes surrounding non-submerged, impermeable spur dikes under clear water scour circumstances (V/V_c =0.61). On the two physically created bend models, several spur dikes with a rectangular shape were built at various angles, including severe and gentle bends within an open rectangular channel. The sediments in the channel bed have an average diameter of 0.71 mm (D_{50}) and the slope is consistent. The experimental execution of multiple spur dikes was found to be more efficient in reducing scour in a channel bend.

Farshad et al. (2022) took into account rectangular singular spur dike. 9 runs were conducted in the case of a singular spur dike for steady flow and 27 runs were conducted in the case of a singular spur dike for unsteady flow, taking into account three different angles: 60°, 90°, and 120°. Several tests were carried out in a rectangular channel 10 m long, 0.76 m wide, and 0.60 m deep and Un submerged spur dike circumstances. Gravel with a median particle size D_{50} of 0.8 mm and a sediment gradation of 1.22 made up the bed sediment. For steady flow, depth of flow (d) = 0.202 m, discharge of flow (Q)=0.05 m^3/sec (50 l/s) and time taken to reach temporal scour depth (t)=3600 sec was constant, but for unsteady flow, these parameters were varied. He concluded that the orientation angle of the spur dike had no significant effect on scour depth, particularly with impermeable spur dikes. However, the impact of orientation angle became more apparent with increased permeability, Spur dike permeability consistently influenced scour depth, with scouring reducing significantly as permeability increased. The percentage differences in maximum scour depth between impermeable spur dikes and various degrees of permeability ranged from 44% to 88%.

Alasadi et al. (2023) conducted all of the experiments with clear water flowing on a zero-flume bed in a subcritical steady state. The impact of the following critical parameters on the entire scouring process and the maximum depth of scour was demonstrated by a number of experiment sets (56 experiments): flow depth (d), flow velocity (V), Froude number (Fr), spur-dikes number (n), and distance between spur-dikes (S_s). The Froude number (Fr), flow depth (d), and mean approach velocity (V) of the flow all directly impacted the scour depths. The hydraulic conditions increase the scour depths when the number and distance of spur dikes remain constant. For a single V shaped spur-dike (n = 1), the scour depth will rise by approximately 80% when the water depth is increased from 16 to 26 mm, by approximately 30% when the water depth is increased from 26 to 36 mm, and by approximately 23% when the water depth is increased from 36 to 46 mm. The spur-dike nose at the upstream face had the deepest scour.

Patel and Kumar (2023) analyzed the flow behavior near the T-shaped spur dike field with 5%, 10%, and no seepage in experimentally. Analyzing the channel morphology with various discharges was the goal of the experiments. The findings show that the channels' bed elevation and scour depth are significantly altered by downward seepage movement. At the edge of the first spur dike facing the flow, the maximum scour depth is noted. The effect of seepage also accelerates the rate of scouring. The flow distribution is shifted close to the channel bed as a result of downward seepage. Nevertheless, attained some velocity close to the channel boundary, greatly increasing the rate of sediment transport. Extremely low velocity magnitudes of both positive and negative values were observed in the wake zone between the spur dikes. This demonstrates cross-stream circulation and secondary current generation within the loop. Near the channel's edge, the velocity, Reynolds shear stress, and turbulent kinetic energy magnitude all increase with an increase in seepage percentage. The purpose of this study was to examine how the hydro-morpho dynamics process near the spur dikes is affected by seepage that occurs downward. Three T-shaped spur dikes with different percentages of seepage—no seepage, 5% seepage, and 10% seepage—were the subject of the investigation. The variation in bed morphology, longitudinal profile, and temporal evolution of scour depth are also shown in this section for two distinct discharge rates, 0.023 m^3/s and 0.030 m^3/s, with and without downward seepage. In addition to these findings, the zone of spur dikes' turbulent flow properties under seepage and non-seepage circumstances were investigated, including stream wise velocity, Reynolds shear stress, and turbulent kinetic energy.

An investigation was conducted by Patel and Kumar (2024), focusing on three distinct spur dike shapes (T, L, and rectangular) under different seepage velocities (V_{S1} and V_{S2}) and a no-seepage condition. Nine experiments were conducted, comprising three runs for T-shaped spur dike, three for L-shaped spur dike, and three for a rectangular spur dike under clear-water scouring over fine sand with a mean diameter of 1.1 mm, a discharge of 0.023 m^3/sec, a geometric standard deviation of 1.03, and a sediment density of 2.65. The experiments took place in a rectangular channel measuring 17.2 m in length, 1.0 m in width, and 0.72 m in depth. Partially submerged and impermeable spur dikes with a transverse length of 12.6 cm were utilized for the experiments. Additionally, it was investigated that downward seepage intensified the motion of sediment particles, and increased seepage resulted in escalated particle detachment, leading to deeper scour depressions. The T-shaped spur dikes exhibited the lowest scour depths compared to the other shapes, both with and without seepage.

2.2 Research Gap

Various studies have explored methods to predict the temporal scour depth around a spur dike. Several researchers utilized their experimental data (Pandey et al. 2020) to validate it using formulas from 2-3 existing researchers (Oliveto and Hager, 2002; Kothyari et al. 2007). None of the researchers has developed a formula that combines data from all researchers and validates it against all the existing formulas. Likewise, none of the researchers has conducted

thorough statistical analyses to rank the formulas So, there is a notable gap in the existing literature: a lack of comprehensive reviews that compile all available literature data and formulas for conducting a thorough comparative analysis. This gap suggests a need for a study.

2.3 Need of the Study

The need for this study stems from several critical factors that highlight its importance in the present research landscape:

Addressing a Research Gap: The absence of comprehensive reviews that compile all available literature data and formulas for predicting temporal scour depth around a spur dike signifies a significant gap in the existing literature. Addressing this gap is crucial for advancing the understanding and predictive capabilities in this field.

Integration of Multiple Sources: Existing studies have primarily validated their findings using formulas from a limited number of researchers, neglecting the potential benefits of integrating data from various sources.

Lack of Comprehensive Formulas: Researchers have not developed formulas that combine data from all available studies and validate them against each other. This gap suggests a need for a more holistic approach to formula development.

Absence of Thorough Statistical Analyses: Despite the abundance of studies, there is a lack of comprehensive statistical analyses to rank the effectiveness of different formulas. This hinders the ability to identify superior formulas or discern trends across various conditions.

Need for Comprehensive Understanding: Given the critical importance of accurately predicting scour depth around a spur dike for infrastructure safety, there is a pressing need for a study that systematically gathers and evaluates existing research. Such a study would provide a comprehensive understanding of the predictive capabilities of different formulas and facilitate informed decision-making in engineering practices.

Advancing Research: By conducting a thorough comparative analysis of existing literature data and formulas, this study can identify gaps in knowledge, highlight areas for further research, and stimulate advancements in the field of hydraulic engineering. This, in turn, can lead to the development of innovative approaches and tools for predicting scour depth around a spur dike.

Chapter 3
Local Scour Characteristics Around Spur Dike

3.1 Local Scour Mechanism

Local scour around a spur dike is a significant concern in river engineering and hydraulic structure design. Spur dikes are built perpendicular to the riverbank to redirect flow, control erosion, and stabilize riverbanks. However, they can induce scouring due to the alteration of flow patterns around them. Here's a detailed explanation of the local scour mechanism around a spur dike, accompanied by a figure (Fig. 3.1a, b) illustrating the process.

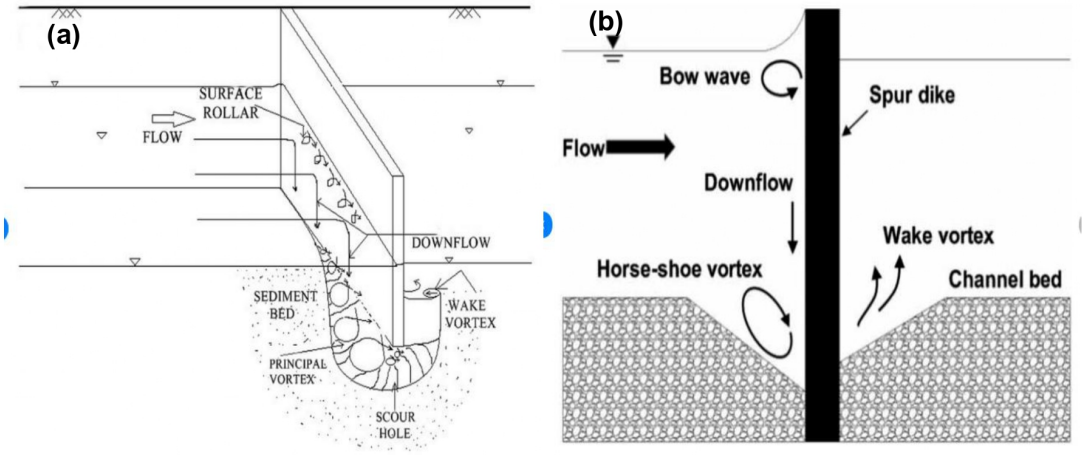

Fig. 3.1. (a) Diagrammatic representation of the flow processes around a spur dike (Pandey et al., 2018*a*), and **(b)** Flow pattern around a spur dike (Zhang and Nakagawa, 2008).

3.1.1 Flow Diversion

When the river flow encounters the spur dike, it divides into two streams: one flowing around the dike (main channel flow) and the other behind the dike (secondary flow or eddy).

3.1.2 Horseshoe Vortex Formation

As the flow passes the upstream end of the spur dike, a horseshoe vortex forms. This vortex is caused by the abrupt change in flow direction and velocity, resulting in intense swirling motion near the dike's nose.

The horseshoe vortex (Fig. 3.1b) is characterized by high velocities and turbulence, leading to sediment erosion at the base of the dike.

3.1.3 Down Flow Formation

Downstream of the spur dike, the flow accelerates, creating a region of down-flow (Fig. 3.1a, b) where sediment erosion can occur. The downward velocity gradient leads to the scouring of the riverbed.

The high-velocity down-flow can deepen the scour hole around the base of the dike, further compromising its stability.

3.1.4 Wake Vortex Formation

As flow continues downstream, a wake vortex forms in the lee of the spur dike. This vortex is characterized by recirculating flow and can further exacerbate scouring by trapping sediment particles.

The wake vortex (Fig. 3.1a, b) contributes to the scouring process by maintaining turbulence and sediment suspension, leading to continued erosion around the dike's base.

3.1.5 Scour Hole Formation

The combined effects of the horseshoe vortex, down-flow, and wake vortex result in the formation of a scour hole (Fig. 3.1a) around the base of the spur dike. Sediment erosion occurs due to the complex flow patterns, leading to the excavation of the riverbed.

The scour hole can compromise the stability of the dike foundation, potentially leading to structural failure if left unaddressed.

Local scour around a spur dike is a dynamic process influenced by complex flow interactions. Understanding the mechanisms involved is crucial for designing effective countermeasures to mitigate erosion and ensure the stability of hydraulic structures.

3.2 Classification of Spur Dikes

Classifying spur dikes helps predict scour depth, vital for erosion risk assessment and long-term structural stability. By understanding hydraulic behavior, accurate modelling of scour evolution enables proactive mitigation and sustainable riverbank management, streamlining decision-making and minimizing maintenance costs. Below are the descriptions detailing the classifications of spur dikes.

3.2.1 Classification of Spur Dikes Based on Permeability

Spur dikes are classified based on different criteria, including their construction methodology. They can be categorized as either permeable or impermeable as shown in Fig. 3.2. Permeable spurs allow water to pass through, reducing velocity, while impermeable spurs deflect flow entirely because they are solid structures (Uijttewaal, 2005).

Impermeable Spur Dikes: These spur dikes are designed to obstruct water flow completely, directing it away from vulnerable areas or controlling sediment deposition. Impermeable spur dikes are typically constructed using materials such as concrete or compacted soil, which do not allow water to pass through easily.

Permeable Spur Dikes: These spur dikes are designed to allow significant water flow through or around the structure without causing obstruction. They are typically constructed using porous materials such as vegetation, geotextiles, or rock-filled gabions with larger void spaces. Permeable spur dikes are often used in ecological restoration projects where maintaining natural hydrological processes is important.

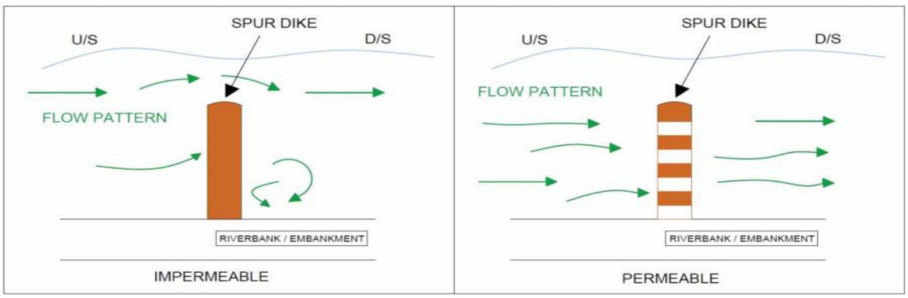

Fig. 3.2. Types of spurs based on construction methodology (Uijttewaal, 2005).

3.2.2 Classification of Spur Dikes Based on Submergence

Spur dikes can be classified based on various construction materials, including timber, wood, piles, rock, and concrete (Barkdoll et al., 2007; Dehghani et al., 2013). They are also categorized according to submergence conditions, which include fully and partially submerged types, as illustrated in Fig. 3.3.

Submerged Spur Dikes: These spur dikes are completely submerged under all flow conditions, including normal flow and flood events. While they may not provide visible above-water structures, they can still influence flow patterns and sediment transport beneath the surface. Fully submerged spur dikes are often used in locations where maintaining a natural appearance or minimizing obstruction to navigation is important.

Non-Submerged Spur Dikes: These spur dikes remain above the water level under normal flow conditions. They are designed to redirect flow, control sediment, and stabilize riverbanks without being fully submerged. Non-submerged spur dikes are typically effective in managing moderate flow conditions and are commonly used in river engineering projects.

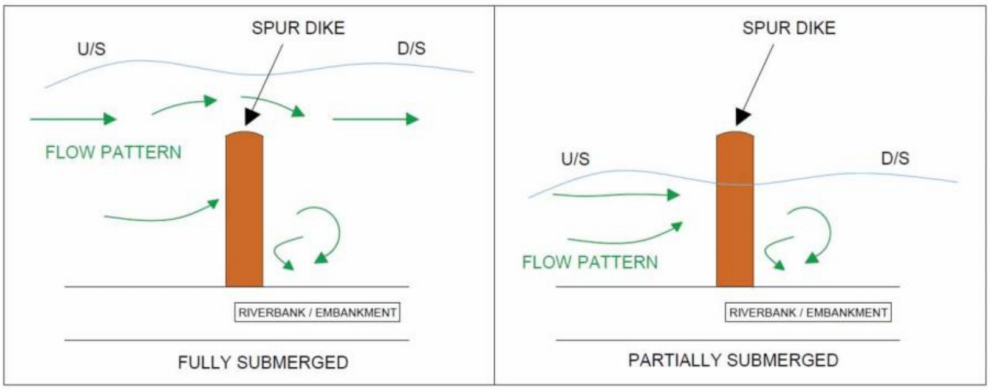

Fig. 3.3. Types of spurs based on submergence conditions (Uijttewaal, 2005).

Under fully submerged conditions, water flows over the top of the spurs, while in partially submerged spurs, the height of the spurs exceeds the water depth. Permeable spurs are typically favored for fully submerged conditions because water can pass through them without significantly affecting the structure. Conversely, solid impermeable spur dikes are used in non-submerged conditions due to the potential extreme impact of horizontal water pressure.

3.2.3 Classification of Spur Dikes Based on Angle of Inclination

Spur dikes are classified based on the action of stream flow, including attracting, repelling, and deflecting spurs, as depicted in Fig. 3.4. Attracting spurs are constructed with a downstream inclination typically ranging from 45° to 60°. This orientation reduces the impact of flow on the opposite riverbank by diverting flow towards the structure. Repelling spurs, on the other hand, feature an upstream inclination typically ranging from 60° to 80°. This orientation is employed to repel water flow away from the structure towards the opposite bank. Deflecting spurs are oriented at an angle of 90° with the bank and are commonly used for localized bank protection.

Attracting Spur Dikes: These spur dikes are oriented to attract flow towards specific areas, often to mitigate erosion or sedimentation concerns in targeted locations. They are typically installed at an angle or curve to guide flow towards the desired area, such as a riverbank undergoing erosion or a sediment deposition zone. Attracting spur dikes can help concentrate flow, enhancing sediment transport or promoting bank stability in critical areas.

Deflecting Spur Dikes: Deflecting spur dikes are designed to redirect flow away from vulnerable areas, such as eroding riverbanks or infrastructure. They are typically oriented perpendicular or at an angle to the flow direction, causing the flow to change direction upon encountering the structure. Deflecting spur dikes helps in controlling erosion by diverting flow away from sensitive areas or preventing sediment deposition by maintaining flow velocity.

Repelling Spur Dikes: These spur dikes are oriented to repel flow from specific areas, often to protect infrastructure or habitats from erosive forces or sedimentation. They are typically installed parallel or at an angle to the flow direction, creating flow resistance or

turbulence to discourage flow towards the protected area. Repelling spur dikes are effective in preventing scouring around bridges, protecting embankments, or maintaining clear channels in sensitive habitats**.**

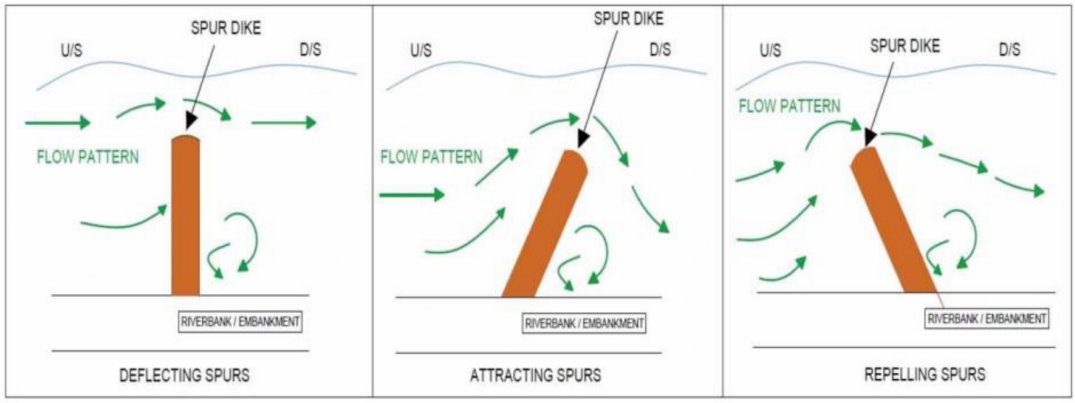

Fig. 3.4.Types of spurs based on the action of stream flow (Barkdoll et al., 2007).

3.2.4 Classification of Spur Dikes Based on Geometry

In terms of plan shape, spurs can be further classified as straight spurs or variations such as I-head, T-head, L-head, hockey-shaped, inverted hockey-shaped spurs, as well as straight spurs with pier head, wing, or tail spurs, as illustrated in Fig. 3.5.

Straight Spur Dike: Straight spur dikes extend directly outward from the riverbank into the channel in a linear fashion. They are typically used in locations where flow redirection is needed without significant curvature in the river channel. Straight spur dikes are relatively simple in design and construction, making them common in various river engineering applications.

T-Head Spur Dike: T-head spur dikes have a configuration resembling the letter "T", with a main structure extending outward perpendicular to the bank and a perpendicular extension at the end. The perpendicular extension helps in deflecting flow and guiding it away from the bank, reducing erosion and promoting sediment deposition along the structure. T-head spur dikes are effective in stabilizing riverbanks and controlling flow dynamics in areas with moderate to high flow velocities.

L-Head Spur Dike: L-head spur dikes have a configuration resembling the letter "L", with a main structure extending outward perpendicular to the bank and a shorter extension at the end.

The shorter extension provides some deflection of flow while minimizing obstruction to navigation or flow conveyance. L-head spur dikes are often used in locations where space or hydraulic conditions limit the length of the structure.

Hockey-Shaped Spur Dike: Hockey-shaped spur dikes have a curved configuration resembling the shape of a hockey stick, with a gradual curve extending outward from the bank.

The curved shape helps in gently redirecting flow around bends or meanders in the river channel, reducing erosion and promoting sediment deposition along the structure. Hockey-

shaped spur dikes are effective in stabilizing riverbanks and controlling flow dynamics in areas with pronounced curvature in the channel.

Inverted Hockey-Shaped Spur Dike: Inverted hockey-shaped spur dikes have a curved configuration similar to hockey-shaped spur dikes but with the curve facing upstream. This configuration is designed to create flow separation and induce sediment deposition on the upstream side of the structure while minimizing scouring on the downstream side. Inverted hockey-shaped spur dikes are effective in managing sediment transport and stabilizing riverbanks in locations with high sediment loads or variable flow conditions.

Wing or tail spur dikes: Wing or tail spur dikes are structural elements built perpendicular to the riverbank, resembling the wings or tails of birds. These formations are designed to deflect or redirect flow away from vulnerable areas, such as eroding banks or nearby structures. They are particularly effective in controlling sediment transport and stabilizing river channels by altering flow dynamics and reducing erosive forces along the banks. Wing or tail spur dikes are commonly utilized in river engineering projects to enhance flood protection, improve navigation, and promote ecological restoration.

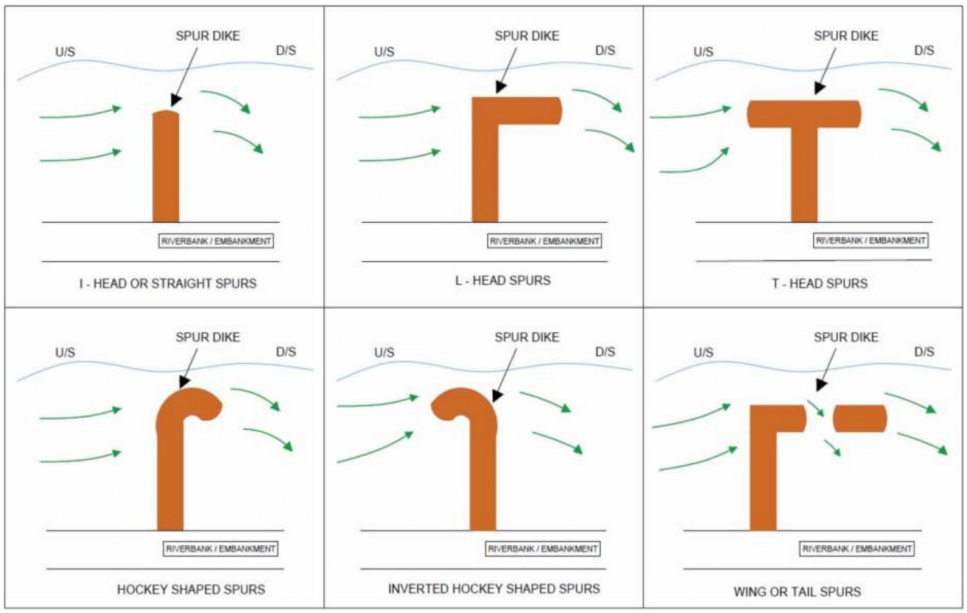

Fig. 3.5. Types of spurs based on appearance in plan (Przedwojski et al., 1995).

3.3 Classification of Scour Parameters

The classification of scour parameters around spur dikes involves identifying and categorizing the various factors that influence the erosion and scouring processes near these hydraulic structures. Here's a detailed description of the key scour parameters:

3.3.1 Spur Dike Properties

Classifying scour parameters based on spur dike properties is important for tailoring effective erosion mitigation strategies and designing resilient river engineering structures that account for specific site conditions and environmental factors. The characteristics of spur dikes, delineated below, encompass dimensions such as length, height, and thickness, as well as factors like orientation and material composition, all of which are pivotal in influencing their hydraulic behavior and susceptibility to scour.

Spur Dike Length (l): The length of the spur dike affects the extent of flow diversion and alteration, consequently impacting scour patterns. Longer spur dikes may induce larger scour holes.

Spur Dike Geometry: The shape of the spur dike, whether straight or curved, can influence flow patterns and scour mechanisms. Different shapes may lead to variations in scour depth and distribution.

Spacing between Spur Dikes (S_S)*:* When multiple spur dikes are installed in a series, the spacing between them affects flow patterns and scouring mechanisms. Closer spacing may lead to increased scour between dikes.

Spur Dike Orientation (θ): The angle at which the spur dike is positioned relative to the flow significantly influences flow patterns and scour mechanisms around the structure, impacting erosion and stability.

Degree of Permeability (φ): The degree of permeability of the spur dike material affects flow dynamics and scour patterns, with more permeable materials potentially reducing scour intensity by allowing water passage through the structure.

*Spur Dike Construction Materials***:** The choice of construction materials for the spur dike, such as concrete, riprap, or gabions, determines its resistance to erosion and scour, directly influencing the longevity and effectiveness of the structure in mitigating erosion risks.

3.3.2 Flume Properties

Flume Width (W): "Flume width" is crucial in hydraulic experiments, especially those studying sediment transport, flow dynamics, and channel morphology. It directly shapes water flow patterns, velocity distribution, and sediment transport capacity. Precise control and measurement of flume width are vital for reliable experimental outcomes and insights into river or stream behavior.

3.3.3 Bed Properties

Understanding bed properties on spur dikes is crucial as they directly impact sediment transport, scour processes, and the overall stability of river engineering structures, informing effective design and maintenance strategies.

Bed Material Size and Type (D_{50}): The size and type of sediment particles in the riverbed determine their susceptibility to erosion. Finer sediment particles are more easily entrained by flowing water, leading to increased scour.

Sediment Cohesion: Cohesive sediments tend to resist erosion more than non-cohesive sediments. The cohesion among sediment particles affects their stability and susceptibility to scour.

Geometric standard deviation (σ): A measure of sediment particle size distribution, that impacts scour depth and erosion potential around spur dikes. It helps characterize sediment properties, aiding in accurate scour prediction and mitigation strategies.

Relative density: indicating the compactness of sediment particles, influences scour depth and erosion patterns around spur dikes. Higher relative density often correlates with reduced scour potential due to greater particle stability and resistance to erosion.

3.3.4 Fluid Properties

Fluid properties on spur dikes are critical as they govern the density of fluid, kinematic viscosity, and sediment transport, directly influencing scour processes and the structural integrity of river engineering features.

Density of Fluid (ρ): The density of the fluid within the system plays a vital role in determining buoyancy forces, pressure gradients, and the fluid's ability to carry sediment, all of which impact the effectiveness of the spur dike in managing river dynamics.

Kinematic viscosity (v): Kinematic viscosity, reflecting the fluid's internal resistance to flow, affects the boundary layer development and shear stresses, influencing sediment transport rates and overall flow dynamics within the spur dike structure.

Acceleration due to gravity (g): The acceleration due to gravity remains a constant force influencing the behavior of fluid flow around and through the structure, affecting sediment transport and erosion patterns.

3.3.5 Flow Properties

Understanding flow properties on spur dikes is essential as they dictate the interaction between water and the structure, influencing scour depth, sediment transport, and structural stability, thus guiding effective design and maintenance approaches.

Flow Velocity (V): The velocity of water flow around the spur dike is a crucial parameter affecting scour depth. Higher velocities generally lead to increased erosion and scouring.

Critical Flow Velocity (V_c): Critical velocity is crucial for understanding and mitigating scour around spur dikes, dictating scour onset and guiding design for stability. Mitigation strategies involve adjusting dike parameters and flow conditions, while regular monitoring is essential for maintenance.

Flow Depth (d): The depth of flow upstream and downstream of the spur dike influences the energy of the flow, which in turn impacts scour potential. Greater flow depths can result in higher scour depths.

Flow Discharge (Q): The volume of water passing a point in a specified time, influences scour intensity and erosion patterns around spur dikes. Understanding flow discharge is crucial for accurately predicting and managing scour risks.

Sediment Transport Capacity: This parameter refers to the flow's ability to transport sediment particles. Higher sediment transport capacity increases the erosive potential of the flow, contributing to scouring around the spur dike.

Steady and Unsteady Flow: Scour processes can differ under steady flow conditions compared to unsteady flow conditions, such as during flood events. Unsteady flows may induce more rapid and unpredictable scouring.

Uniform and Non-Uniform Flow: Flow uniformity or non-uniformity affects the distribution of flow velocities and sediment transport, thereby influencing scour patterns. Non-uniform flows can lead to scour hotspots.

Froude Number (Fr): The Froude number, a dimensionless parameter comparing flow inertia to gravitational forces, characterizes flow regimes around spur dikes. It helps predict the occurrence of critical flow conditions leading to scour initiation or mitigation.

Reynolds Number (Re): Reynolds number, another dimensionless parameter comparing inertial to viscous forces, quantifies flow turbulence and boundary layer behaviour around spur dikes. It aids in assessing sediment transport capacity and scour potential under different flow conditions.

3.3.6 Time Properties

Time properties on spur dikes are crucial as they govern the evolution of scour processes over time, providing insights into the long-term stability and maintenance requirements of river engineering structures.

Temporal time (t_t): Temporal time refers to the duration over which changes in flow patterns or sediment deposition occurs, crucial for understanding the dynamic response of the system to external factors such as water flow variations or sediment loads.

Maximum time (t_m): Maximum time represents the point at which the system reaches its peak response or stability, indicating the time required for the system to adjust to significant changes in flow conditions or sediment transport rates.

Equilibrium time (t_e): Equilibrium time signifies the period when the system reaches a steady state, with flow and sediment dynamics stabilizing, essential for assessing the long-term effectiveness of spur dike structures in river management and erosion control strategies.

3.3.7 Scour Depth Properties

Scour depth properties on spur dikes are vital as they directly reflect the erosion susceptibility of structures, guiding risk assessment, maintenance scheduling, and structural design for optimal stability and safety.

Temporal Scour Depth (d_{st}): The variation of scour depth over time, is critical for assessing the dynamic behaviour and long-term stability of spur dikes. Monitoring temporal scour depth aids in understanding erosion trends and implementing timely maintenance measures.

Maximum Scour Depth (d_{sm}): The deepest point of scouring around the spur dike, influenced by all the aforementioned parameters. Maximum scour depth is a critical factor for evaluating the stability of the dike.

Equilibrium Scour Depth (d_{se}): The stable depth of scour around a spur dike under steady flow conditions, is essential for assessing the long-term stability and design adequacy of the structure. Understanding this parameter helps engineers ensure the dike's resilience against erosion over time.

Rate of Scour Development: The speed at which scour depth increases over time, influenced by flow characteristics and sediment properties. Understanding the rate of scour development is essential for assessing the long-term stability of the structure.

3.3.8 Structural Properties

Structural properties for spur dikes are essential as they determine the capacity to withstand hydraulic forces, influencing the longevity and reliability of river engineering structures in mitigating scour and ensuring overall stability.

Spur Dike Material: The material composition of the spur dike impacts its resistance to scour and erosion. Materials like concrete or riprap are commonly used for their durability.

Spur Dike Design: The design characteristics of the spur dike, including its cross-section and profile, influence flow patterns and scour mechanisms.

Toe Protection: The presence of protective measures (e.g., riprap, concrete aprons) at the base of the spur dike can mitigate scouring effects by dissipating energy and reducing erosion.

3.3.9 Environmental Properties

Environmental properties such as water temperature, turbulence, and vegetation are crucial for spur dikes as they influence flow patterns, sediment transport, and ecological interactions, ultimately impacting scour processes and structural performance.

Turbulence: The presence of turbulence in the flow, caused by natural or artificial factors, can enhance scouring around spur dikes. Turbulent flow conditions increase erosive forces.

Vegetation: Vegetation along the riverbank and within the flow field can influence flow patterns and sediment dynamics, affecting scour development. Vegetation can act as a buffer against erosion or enhance it depending on its characteristics.

Chapter 4
Collection of Data, Methods and Equations from Literatures

4.1 Experimental Procedures followed by Researchers

Research groups typically employ experimental procedures involving flume or field studies to investigate scour phenomena around spur dikes, incorporating varying flow conditions, sediment types, and structural configurations to gather data for analysis and model validation.

Ballio and Orsi (2001) filled partially a layer of sediments with a density of ρ_s = 15.7 kN/m^3 in a tilting hydraulic flume measuring 15 m in length and 1.0 m in width. D_{50} = 5.0 mm was the mean size diameter, and σ = 1.3 mm was the standard deviation. A plexiglass prism with dimensions of b = 0.10 m and l = 0.40 m made up the bridge's abutment, which was positioned midway along the flume. In the test, a smaller obstacle (b = 0.05 m, l = 0.20 m) was also utilized. The flow's depth varied between 0.092 and 0.183 m, and its velocity varied between 0.60 and 0.73 m/sec.

Oliveto and Hager (2002) conducted tests using two rectangular channels, one measuring 1.00 m in width and the other 0.50 m. The working section of the 11-meter-long 1 m channel had a length of approximately 5 m, with a glass wall on the left and a smooth steel wall on the right. For this reason, a plane bed was used for the majority of the tests. Three uniform sediments with grain sizes of 0.55, 3.3, and 4.8 mm and three mixtures with D_{50} = 5.3, 1.2, and 3.1 mm and σ = 1.43, 1.80, and 2.15, respectively, were among the six different sediments that were used. While the remaining sediment had ρ_s = 2650 kg/m^3, the uniform sediment with D_{50} = 3.3 mm had ρ_s = 1420 kg/m^3. The abutments that were utilized had widths of b = 0.05, 0.10, 0.20, 0.40 and 0.60 m and were always rectangular in plan. The water's surface was measured with a conventional point gauge to an accuracy of ±0.5–1 mm, depending on the local surface turbulence. With an accuracy of roughly 1%, the closed-loop water system in the channel had a maximum discharge of Q=0.130 m3/sec. An experiment's temporal beginning (t=0) was established at the onset of scour. In certain runs, additional measurements were obtained at times t=60, 180, 360, 600, 900, and 1200 sec, as well as over several days and even weeks.

Oliveto and Hager (2005) conducted tests using two rectangular channels, one measuring 1.00 m in width and the other 0.50 m. The working section of the 11-meter-long 1 m channel had a length of approximately 5 m, with a glass wall on the left and a smooth steel wall on the right. For this reason, a plane bed was used for the majority of the tests. Six distinct sediments were utilized: two mixtures for sediment mixture 3, with D_{50} = 3.1 mm and σ = 2.15, and three uniform sediments with grain sizes of 0.55, 3.3, and 4.8 mm. The uniform sediment with D_{50} = 3.3 mm had a density of ρ_s = 1420 kg/m^3, while the remaining sediment had ρ_s = 2650 kg/m^3. This was also the case for sediment mixture 4 with D_{50} = 4.3 mm and σ = 2.35. The abutments that were utilized had widths of b = 0.05 and 0.20 m and were always rectangular in plan. The water's surface was measured with a conventional point gauge to an accuracy of ±0.5–1 mm, depending on the local surface turbulence. With an accuracy of

roughly 1%, the closed-loop water system in the channel had a maximum discharge of Q=0.130 m^3/sec. An experiment's temporal beginning (t=0) was established at the onset of scour. In certain runs, additional measurements were obtained at times t=60, 180, 360, 600, 900, and 1200 sec, as well as over several days and even weeks.

Yanmaz and Kose (2007) used a 30 m long, 1.25 m wide, and 1.0 m deep flume for performing experiments. The geometric standard deviation of the bed materials was roughly 1.40, and their median sizes were 1.8 and 0.9 mm. The bed slope of the flume bed was 0.001, and the bed materials were layered 40 cm thick. Plexiglas abutment models with lengths of 12.5 cm and 10 cm and a constant width of 20 cm were tested to examine the impact of abutment size. Examines scour contours; experimental runs 6–10 and 15–19 were carried out for the abutments under test using a densimetric particle Froude number of 2.38. Scour contours were only acquired for this fixed F_d value. Due to the fundamental similarity of all local scouring situations, other values of F_d were not tested. To use point gauges to determine the contours of the scour hole around abutment models, experiments were stopped at 5, 20, 60, 100, and 150 minutes. Water was cautiously drained from the channel at the conclusion of each experiment to avoid changing the bed topography. Measurements were then taken in a grid system surrounding the abutment, which consisted of joints spaced 2 cm apart both along and across the channel. The bed was levelled after every run so that the experiment could continue for the next duration.

Karami et al. (2012a) used four flumes for each experiment. Each of the first three flumes measured 0.6, 1.3, and 1.5 m in width, 1 m in depth, and 30 m in length. The remaining flume was 14 m long, 1 m wide, and 1 m deep. The bed sediments used were uniform (σ<1.4), and composed of gravel and sand with a thickness of 0.35 m. Various V/V_c values were used in the experiments. In every trial, the clear water condition ($V/V_c<1$) was met.

The experiments were conducted by Karami et al. (2012b) in a 14 m long, 1 m wide, and 1 m deep rectangular-section flume. The glass flume's bed and sides were held up by a metal frame. In the flume, three 25 cm long spur dikes that were impermeable, exposed, and perpendicular to the direction of flow were placed. The initial spur dike was positioned 6.16 m away from the flume entrance, with a fixed distance between them equal to twice the spur dike's length. The approach flow depth (d) was always configured at 15 cm. Bed sediments (σ < 1.4) with a median size (D_{50}) of 0.91 mm and a thickness of 0.35 m were evenly distributed throughout the flume. 2.65 (specific gravity) and 1.38 (geometric standard deviation, σ). In each experiment, the clear water condition (V/V_c < 1) was met. A laser bed-profiler (LBP) was used to measure the variations in bed profile surrounding spur dikes, providing an accuracy of ± 0.1 mm in depth and ±1 mm in width.

Lodhi et al. (2017) utilized a fixed bed masonry flume with dimensions of 25 m in length, 1 m in width, and a depth of 0.30 m for conducting the experiments. The geometric standard deviations (σ) for clay, sand, and gravel were 2.16, 1.41, and 1.21 respectively, while their median sizes (D_{50}) were 0.0014 mm, 0.24 mm, and 2.7 mm, respectively. The sand and gravel had a relative density of 2.65. Before every experimental run, the prepared bed of sediment mixture was saturated for a full day. Thirty cohesive sediment mixture (clay-gravel and clay-sand-gravel) experiments with a partially submerged spur dike were carried out.

The two flume bed slopes that were used for the experiments were 0.003 and 0.005. A 4 m long, 1 m wide, and 0.6 m deep test section made up the flume. It began at the entrance

of the flume, 12 m downstream. Three distinct sizes of partially submerged spur dikes with transverse lengths of 6.1, 8.9, and 11.52 cm were employed. The spur dike stood 60 cm high. A metal sheet, 3 mm thick, was used to make the spur dikes. A single spur dike was erected in each experiment at a 90°-angle to the flow direction, 14 meters downstream from the flume entrance. Before the experiment began, the area surrounding the spur dike was covered with a 3mm transparent Perspex sheet to stop scouring. A pointer gauge with a flat bottom and an accuracy of ±1 mm was used to measure the temporal variation of scour at the wake region of the partially submerged spur dike.

Lodhi et al. (2018) aimed to investigate the impact of cohesive characteristics, including clay percentage, unconfined compressive strength, antecedent moisture content, and void ratio, on the scour depth in the wake region of spur dikes within cohesive sediment mixtures. The experiment material was clay that had been excavated 1.0 m below the surface of the earth. The median size of the clay particle was determined using the laser particle size analyzer. The geometric standard deviation σ for the same was 2.16, 1.41, and 1.21 for clay, sand, and gravel, respectively, and the median size was 0.0014 mm, 0.24 mm, and 2.7 mm. The sand and gravel had a relative density of 2.65. A 25.0 m long, 1.0 m wide, and 0.35 m deep fixed bed masonry flume served as the site for all laboratory tests.

The two flume bed slopes that were used for the experiments were 0.003 and 0.005. 12 meters downstream from the flume entrance was the test section of the 4 m long, 1 m wide, and 0.60 m deep flume. In each experiment, a single spur dike was positioned at a 90° angle to the flow direction in the groove on the side wall of the flume. An overhead tank helped to maintain the steady flow rate into the flume. A sharp-crowned weir placed at the downstream end of the flume was used to measure the discharge. The test section was filled with the cohesive sediment mixture up to the general flume bed level. Three distinct spur dikes with transverse lengths of 6.10 cm, 8.90 cm, and 11.52 cm as well as a height of 60 cm were employed in this study's experiments. A metal sheet, 3 mm thick, was used to make the spur dikes. A single partially submerged spur dike was erected in each experiment at a distance of 14 meters downstream from the flume entrance and at a 90° angle to the flow direction. To prevent scour around the spur dike before the flow in the flume reaches the predetermined condition, a transparent Perspex sheet, 3 mm thick, was used to cover the area. A pointer gauge with a flat bottom was used to measure the temporal variation of scour depth with an accuracy of ±1 mm.

Khassaf and Abbas (2018) utilized a 7.225 m long flume, featuring an inner section measuring 0.4 × 0.4 meters and is constructed with a metal frame with sides made of tempered (8 mm) glass. The flume consists of three sections. The first section is the 0.4 × 0.6 m cross section inlet tank, which is 1 m long. The working section, which is the second section, is 5.025 m long. The final section of the flume is a metal reservoir that is 1.2 × 1 × 0.625 m in length, width, and height, respectively, and is situated at the end of the flume. There were fifty-six distinct experiments carried out. The head and discharge are 10.5-20.5 m and 0.000833-0.00467 m^3/sec (0.833-4.67 l/sec), respectively. The L-shaped greenhouse, which measured 13 cm in length and 15 cm in net height, was constructed from 10 mm thick polystyrene foam material for all of the experiments. D_{50} has a mean diameter of 0.7 mm. The sand size σ had a geometric standard deviation of 1.31.

Ning et al. (2019) evaluated the effectiveness of the numerical model; three experimental cases were chosen. Four spur dikes with uniform spacing and equal length made up the spur dike group. In all three cases, the spacings of the spur dike were 2 l, 3 l, and 4 l. The entrance tank, fixed bed, movable bed, and sand recycling zone were all part of the 10 m long, 40 cm wide, and 50 cm deep flume channel. The 200 cm long fixed bed was made of coarse sand and gravel. The 400 cm long movable bed had 20 cm of sand covering it. A set of impermeable spur dikes was installed here, oriented perpendicular to the right side of the flume. To ensure they remained above water for the duration of the experiments, the spur dikes were designed to be 10 cm long, 1 cm thick, and 50 cm high. With each spur dike spaced equally apart, the first of the four was positioned 100 cm into the observation area. The chosen grain size for the sediment was D_{50} = 0.473 mm. 0.00962 m^3/sec (9.62 l/s) of flow discharge, 1/1000 channel slope, 40 cm of channel width, 9 cm of flow depth, 0.267 m/sec of flow velocity, and 1.9 gm/cm^3 of sediment density, Re = 16,585, the Reynolds number, and Fr = 0.28, the Froude number, were constant.

Pandey et al. (2020) carried out each experiment within a flume measuring 24 m in length, 1 m in width, and with a depth of 0.5 m. The working test section is located 12 m from the flume's inlet and measures 4 m × 1 m × 0.4 m. Every experiment was conducted in an environment with clear water scour. 50% sand (D_{50S} =0.27 mm, σ =1.22) and 50% gravel (D_{50g} =2.7 mm, σ =1.21) make up the first sediment mixture. 50% sand (D_{50S} =0.27 mm, σ =1.22) and 50% gravel (D_{50g} =3.1 mm, σ =1.18) make up the second sediment mixture. There were four vertical rectangular wall spur dikes used, with transverse length scales varying from 6,9,11.5, and 14 cm. Every experiment was conducted for the case of an unsubmerged spur dike. Until an equilibrium scour geometry was reached, the scour depth (d_{st}) was measured using a point gauge at various time intervals (t=1,3, 5,10,15,30, and 60 min up to several hours). Every experiment lasted for twenty hours. The spur dike was fixed vertically at the right side of the channel wall prior to the commencement of each experimental run.

Masood et al. (2021) conducted laboratory experiments on scour using a smooth rectangular flume channel measuring 20 m in length, 1 m in width, and with a depth of 0.75 m, equipped with a recirculating water facility. One-fifth of the channel width was calculated using the spur dike's length. Over the course of the entire experimental project, there were five spur dikes. Wooden spur dikes, both submerged and impermeable, were built at predetermined bend models, encompassing both gentle and steep bends. There were three equal sections cut out of the rectangular channel. The experimental work was conducted in the middle section. The middle section measured 6 m in length and had a fine sand bed of uniformly graded sediments with an average diameter (D_{50}) of 0.71 mm, which was 0.3 m thick. A standard deviation of σ 1.20 was observed, with a D_{50} of 0.71mm being employed in all the experiments. Every experiment was run for a duration of three hours.

Farshad et al. (2022) utilized a flume measuring 10 m in length, 0.76 m in width, and 0.60 m in depth. There were glass walls, inlet and outlet tanks in the flume. Tests were conducted 4.0 m from the inlet in a section of sediment recess. Sand with a median grain size of D_{50} = 0.8 mm and a relative density of 2.65 comprised the mobile bed. The sediment mixture's gradation, as indicated by the standard deviation σ = 0.5, was 1.22. Three permeability levels for a single unsubmerged spur dike were taken into consideration: 0% (i.e., an impermeable spur dike), 33%, and 66%. Additionally, three spur dike orientation

angles were taken into consideration: 60° for repelling alignment, 90° for deflecting alignment, and 120° for attractive alignment. To replicate an impermeable spur dike, a 0.5 m high by 10 mm thick Plexiglas plate was used. Brass rods, 0.5 m in height and 4 mm in diameter were fastened to the top and bottom Plexiglas plates. For the repelling, deflecting, and attractive alignments, the spur dike's effective length was always 20% of the flume width. Two categories—steady and unsteady flows were used for the experiments conducted for this study. Experiments with steady and unsteady flow were designed to guarantee clear-water scour regimes even after the hydrograph peak flow was attained.

In the study by Alasadi et al. (2023), the flume featured an inner cross-section of 0.4 × 0.4 m and a total length of 6.6 m. It was constructed with glass fiber for the sides and steel stiffeners for the mainframe. The two main components of the two flumes are the 5.6 m working section and the 1 m high upstream inlet tank. Erodible sediments measuring 0.1 m in depth and 2 m in length covered the middle portion of the working section. Wooden plates covered the other two sections of the operating section. To measure the entering discharge to the working section, a man-made rectangular weir with sharp crested edges, measuring 0.4 m in width and 0.25 m in height was positioned at the upstream flume section. A movable point gauge with ±1 mm accuracy is used to measure the scour depth both transversely and longitudinally above the operating section. Utilized a checkmark or V-shaped spur-dikes that are 13 cm long, 12 cm net high, and 10 mm thick. These are placed perpendicular to the direction of flow, and their length should be at least one-third of the flume's width. Polystyrene foam, which does not swell, was used to construct the models. They have experimented with three different configurations (double, triple, and single). The geometric standard deviation (σ) of sand was 1.31, with a median particle grain size D_{50} equal to 0.7 mm. A total of fifty-six experiment sets were conducted.

The flume, as described by Patel and Kumar (2023), spanned a length of 17.2 m and a width of 1 m. The seepage chamber beneath the sediment bed was 0.22 m deep, and the flume reached a depth of 0.72 m. The sand size D_{50} = 1.1 mm is used to prepare the bed. The channel features a glass wall on one side and a one-sided bank with a 45°slope. Three spur dikes in a row formed a spur dike zone according to the arrangement of the spur dikes. The spur dikes were T-shaped, partially submerged, and perpendicular to the bank. The projected length of each spur dike was 12.6 cm. The spur dikes rose to a total height of 28 cm, with 13 cm below the sediment bed and 15 cm above it. The wood-built spur dikes were situated 8.5 m upstream from the channel's terminus. Every experiment ran for twenty-four hours, or until the equilibrium condition was met. According to this study, the scour depth increased dramatically for the first 0–6 hours, then moderately for the next 6–18 hours, and then slightly for the next 18–24 hours. The scour depth changed by less than 1 mm over the course of 22–24 hours.

4.2 Literature Equations to Predict Temporal Scour

Existing literature offers equations to forecast temporal scour depth around spur dikes, incorporating parameters like flow velocity, sediment properties, and dike geometry for

informed erosion risk assessment and structural design. The following Table 4.1 presents literature sources along with empirical formulas.

Table 4.1. Empirical formulas derived by different research groups in the last two decades.

Literature	Equation
Oliveto and Hager (2002)	$\frac{d_{st}}{L_R} = 0.068 N \sigma^{-1/2} \mathrm{F_d}^{1.5} \log(T)$
Coleman et al. (2003)	$\frac{d_{st}}{d_{se}} = \exp\left\{-0.07\left(\frac{V}{V_c}\right)^{-1}\left\lvert\ln\left(\frac{t}{t_e}\right)\right\rvert^{3/2}\right\}$
Kothyari et al. (2007)	$\frac{d_{st}}{L_R} = 0.272\sigma^{-1/2}\left(\mathrm{F_d} - \mathrm{F_{d\beta}}\right)^{2/3}\log(T)$
Yanmaz and Kose (2007)	$\frac{d_{st}}{l} = 0.25\mathrm{F_d}^{0.85}\left(\frac{l}{d}\right)^{0.15}\left\{\log(T_s)\right\}^{0.6}$
Nasrollahi et al. (2008)	$\frac{d_{st}}{d_{se}} = \left(\frac{t}{t_e}\right)^{0.15}$
Karami et al. (2012a)	$\frac{d_{st}}{d_{se}} = \left(\frac{t}{T}\right)^{0.16}\left(\frac{V}{V_c}\right)^{-0.14}$
Karami et al. (2012b)	$\frac{d_{st}}{d_{se}} = \left[1-\exp\left\{-2.48\left(\frac{t}{T}\right)^{0.31}\right\}\right]\left(\frac{V}{V_c}\right)^{-0.10}$
Pandey et al. (2020)	$\frac{d_{st}}{L_R} = 0.02\left(F_{sm}\right)^{1.68}\left(\frac{l}{D_{50}}\right)^{0.28}\log(T)$

4.3 New Functional Relationship developed based on Literatures

Researchers developing formulas for predicting temporal scour depth around spur dikes use functional relationships based on variables like flow velocity, sediment characteristics and time. The following Table 4.2 illustrates the functional relationships utilised by various researchers in formulating their equations.

Table 4.2. Functional relationships considered by researchers to develop their formulas.

Serial Number	Literature	Function
1	Oliveto and Hager (2002)	$d_{st}/L_R = f\{\sigma, \mathrm{F_d}, \log(T)\}$
2	Coleman et al. (2003)	$d_{st}/d_{se} = f\{(V/V_c), \ln(t/t_e)\}$
3	Kothyari et al. (2007)	$d_{st}/L_R = f\{\sigma, \mathrm{F_d}, \mathrm{F_{d\beta}}, \log(T)\}$
4	Yanmaz and Kose (2007)	$d_{st}/l = f\{\mathrm{F_d}, (l/d), \log(T_s)\}$

5	Nasrollahi et al. (2008)	$d_{st}/d_{se} = f\,(t/t_e)$
6	Karami et al. (2012a)	$d_{st}/d_{se}=f\{(V/V_c),\ (t/T)\}$
7	Karami et al. (2012b)	$d_{st}/d_{se}=f\{(V/V_c),\ (t/T)\}$
8	Pandey et al. (2020)	$d_{st}/L_R=f\ \{F_{sm},\ (l/D_{50}),\ log(T)\}$
9	Present Study	$d_{st}/L_R=f\ \{(V^2/L_Rg),\ (V/V_c),\ (Vt/L_R),\ \Phi,\ (d/L_R),\ \sigma\}$

4.4 Temporal Scour Depth Formulas developed by Researchers

The d_{st} has been measured in many numerical and laboratory researches. Most of these studies were based on the results of controlled laboratory experiments. Several researchers have provided formulas in computing d_{st} around spur dikes (Oliveto and Hager (2002) as OH; Coleman et al. (2003) as CO; Yanmaz and Kose (2007) as YK; Kothyari et al. (2007) as KO; Nasrollahi et al. (2008) as NA; Karimi et al. (2012*a*, *b*) as KM and KB; and Pandey et al. (2020) as PY. For different flow parameters and bed materials, it was necessary to compute d_{st} around spur dikes. Various researchers have also used the above-mentioned formulas to compute the d_{st} based on their laboratory test results. The most promising formulas for computing d_{st} were compared by taking one or more formulas from the literatures and analyzed by different researchers with their developed formulas. Such short bibliography studies for the period from 2002 to 2023 are shown in Table 4.3.

Table 4.3. Evaluation of d_{st} computing formulas used by different researchers.

Researchers who analyzed the time -dependent formulas	Formulas evaluated in the present study							
	Olivet o and Hager (2002)	Colema n et al. (2003)	Kothyar i et al. (2007)	Yanma z and Kose (2007)	Nasrolla hi et al. (2008)	Karami et al. (2012a)	Karami et al. (2012b)	Pandey et al. (2020)
Kothyari et al. (2007)	Yes	–	–	–	–	–	–	–
Yanmaz and Kose (2007)	Yes	Yes	–	–	–	–	–	–
Nasrollahi et al. (2008)	Yes	–	–	–	–	–	–	–
Karami et al. (2012a)	Yes	Yes	–	Yes	–	–	–	–
Lodhi et al. (2017)	Yes	–	Yes	–	–	–	–	–
Lodhi et al. (2018)	Yes	–	Yes	–	Yes	–	–	–
Pandey et al. (2020)	Yes	–	Yes	–	Yes	–	–	–
Farshad et al. (2022)	Yes	–	–	–	–	–	–	Yes

Patel and Kumar (2023)	–	–	–	–	–	–	–	Yes
Present Study	Yes	Yes	Yes	Yes	Yes	Yes	Yes	Yes

Note: "–'' indicates "not considered.'

4.5 Datasets selected for Present Study

In the current study, the performance of each predictor in terms of d_{st} around spur dikes is analyzed using data from laboratory experiments from various sources, including a predictor for the time evolution of scour. For this analysis, data from 16 different research groups over two decades namely Nasrollahi et al. (2008) as NS, Karimi et al. (2012a, b) as KM and KB respectively, Pandey et al. (2014a,b) as PA and PB respectively, Pandey et al. (2015) as PD, Lodhi et al. (2017,18) as LO and LD respectively, Khassaf and Abbas (2018) as KA, Pandey et al. (2019) as PN, Pandey et al. (2020) as PY, Masood et al. (2021) as MA, Farshad et al. (2022) as FS, Patel and Kumar (2023) as PK, Alasadi et al. (2023) as AS and Pandey et al. (2019) as PI have been collected for the development of new formula as well as comparison of 8 literature formulas.

Data screening has been conducted to compare 9 equations for the CWS condition. Table 4.4 and Table 4.5 list the experimental ranges that are selected for the construction of the equation and comparison are covered by the range of their dimensional parameters and dimensionless parameters respectively.

Table 4.4. Sources of information for the full selected d_{st} data series and pertinent experimental ranges.

Literature	#	l (m)	L_R (m)	V (m/s)	V_C (m/s)	d (m)	g (m/s^2)	σ	Φ	t (hr)	d_{st} (m)
AS	56	0.13-0.13	0.07-0.09	0.15-0.22	0.23-0.28	0.02-0.05	9.81-9.81	1.31-1.31	0-0	4.00-4.00	0.003-0.045
PK	48	0.13-0.13	0.11-0.12	0.25-0.33	0.36-0.38	0.07-0.10	9.81-9.81	1.23-1.23	0-100	0.0420-23.96	0.02-0.08
FS	45	0.15-0.15	0.16-0.16	0.35-0.35	0.36-0.36	0.20-0.20	9.81-9.81	1.22-1.22	0-66	0.13-1.00	0.10-0.17
MA	70	0.20-0.20	0.21-0.21	0.33-0.33	0.49-0.49	0.23-0.23	9.81-9.81	1.20-1.20	0-0	0.003-3.014	0.0002-0.107
PY	99	0.12-0.12	0.11-0.11	0.28-0.41	0.45-0.45	0.09-0.11	9.81-9.81	1.23-1.23	0-0	0.04-16.58	0.01-0.13
PN	30	0.12-0.12	0.11-0.11	0.41-0.41	0.46-0.46	0.11-0.11	9.81-9.81	1.21-1.21	0-0	0.03-19.97	0.01-0.13
KA	68	0.13-0.13	0.07-0.07	0.15-0.22	0.24-0.24	0.02-0.02	9.81-9.81	1.31-1.31	0-0	0.24-6.02	0.003-0.043
LD	5	0.06-0.12	0.08-0.12	0.50-0.59	0.60-0.61	0.12-0.13	9.81-9.81	1.21-1.21	0-0	14.00-16.00	0.09-0.15
LO	36	0.12-0.12	0.11-0.12	0.41-0.55	0.60-0.61	0.11-0.13	9.81-9.81	1.21-1.21	0-0	0.40-36.07	0.003-0.197
PD	15	0.06-0.20	0.07-0.16	0.16-0.21	0.25-0.25	0.10-0.10	9.81-9.81	1.23-1.23	0-0	10.00-10.00	0.05-0.14
PA	67	0.10-0.10	0.10-0.10	0.16-0.21	0.25-0.25	0.10-0.10	9.81-9.81	1.23-1.23	0-0	0.03-7.04	0.02-0.11
PB	36	0.20-0.20	0.16-0.16	0.16-0.21	0.25-0.25	0.10-0.10	9.81-9.81	1.23-1.23	0-0	0.07-7.04	0.03-0.14
KM	62	0.25-0.25	0.21-0.21	0.23-0.35	0.36-0.37	0.15-0.15	9.81-9.81	1.38-1.38	0-0	0.02-50.28	0.02-0.33
KB	102	0.25-0.25	0.21-0.21	0.24-0.35	0.37-0.37	0.15-0.15	9.81-9.81	1.38-1.38	0-0	0.09-50.15	0.02-0.33
NS	49	0.25-0.5	0.20-0.32	0.42-0.427	0.43-0.43	0.13-0.13	9.81-9.81	1.30-1.30	0-70	0.31-30.73	0.02-0.32
PI	144	0.10-0.20	0.10-0.16	0.16-0.21	0.25-0.25	0.10-0.10	9.81-9.81	1.23-1.23	0-0	0.06-7.02	0.02-0.14
Total	932	0.06-0.50	0.06-0.32	0.15-0.59	0.23-0.61	0.02-0.23	9.81-9.81	1.21-1.38	0-70	0.003-50.28	0.0002-0.33

Note: # indicates the number of datasets considered in selected literature.

Table 4.5. Sources of information for the full selected d_{st}/L_R data series and pertinent experimental ranges.

Literature	#	d_{st}/L_R	V^2/L_Rg	V/V_c	Vt/L_R	Φ	d/L_R	σ
AS	56	0.042-0.537	0.033-0.071	0.622-0.911	28189.464-45152.327	0-0	0.247-0.500	1.31-1.31
PK	48	0.132-0.684	0.058-0.101	0.682-0.898	450.584-255481.256	0-10	0.701-0.852	1.23-1.23
FS	45	0.055-1.029	0.074-0.074	0.950-0.950	944.561-7556.485	0-66	1.230-1.230	1.22-1.22
MA	70	0.001-0.508	0.054-0.054	0.684-0.684	19.878-17219.304	0-0	1.101-1.101	1.20-1.20
PY	99	0.125-1.122	0.080-0.150	0.610-0.90	330.090-214695.990	0-0	0.850-0.980	1.23-1.23
PN	30	0.110-1.120	0.150-0.150	0.900-0.900	378.610-258588.810	0-0	0.980-0.980	1.21-1.21
KA	68	0.04-0.607	0.033-0.071	0.622-0.911	1844.548-67626.795	0-0	0.297-0.297	1.31-1.31
LD	5	1.043-1.247	0.218-0.360	0.827-0.976	244583.892-346400.999	0-0	1.028-1.622	1.21-1.21
LO	36	0.027-1.661	0.150-0.260	0.687-0.904	5151.664-603221.129	0-0	0.981-1.056	1.21-1.21
PD	15	0.490-1.140	0.020-0.060	0.630-0.830	36058.940-106272.520	0-0	0.630-1.410	1.23-1.23
PA	67	0.223-1.051	0.026-0.045	0.630-0.840	143.099-52861.331	0-0	1.000-1.000	1.23-1.23
PB	36	0.210-0.870	0.020-0.030	0.630-0.840	266.510-33307.680	0-0	0.630-0.630	1.23-1.23
KM	62	0.090-1.590	0.030-0.060	0.630-0.960	90.670-300460.860	0-0	0.710-0.710	1.38-1.38
KB	102	0.080-1.550	0.030-0.060	0.650-0.950	463.790-298569.590	0-0	0.710-0.710	1.38-1.38
NS	49	0.072-0.999	0.056-0.093	0.980-1.000	1505.967-148794.309	0-70	0.401-0.640	1.30-1.30
PI	144	0.200-1.380	0.020-0.040	0.630-0.840	212.610-53010.810	0-0	0.630-1.000	1.23-1.23
Total	932	0.001 -1.661	0.016-0.36	0.610-1.000	19.878-603221.129	0-70	0.247-1.622	1.21-1.38

Note: # indicates the number of datasets considered in selected literature.

Chapter 5
Objectives and Methodology

5.1 Research Objectives

The erosion of riverbanks due to high flow in rivers is a common occurrence, posing a significant challenge for civil engineers, particularly in densely populated cities worldwide, including India. Protecting riverbanks is imperative, and spur dikes serve as a simple yet effective solution to mitigate erosion. These structures not only help maintain suitable depths for navigation but also control river meandering.

When spur dikes are installed in flowing streams, scouring occurs around their foundations. Failure to consider scouring during the dike's design can result in structural failure while overestimating scouring leads to uneconomical designs. Therefore, this thesis aims to predict the temporal scour depth formula around the spur dike. By identifying the various parameters influencing scour depth, spur dikes can be designed properly to prevent failure. The objectives involve a comprehensive review of recent literature to identify and compile temporal scour depth formulas for spur dikes. These formulas will be evaluated against literatures data to assess accuracy and applicability across varying conditions. The research aims to uncover trends in scour depth dynamics over time and refine selected formulas through validation, weightage and ranking analyses among various literature formulas. Ultimately, the goal is to provide actionable recommendations for researchers to select and apply the most effective temporal scour depth formula, enhancing the safety of hydraulic infrastructure amidst evolving challenges. Furthermore, a comparison will be made between our results and those obtained by previous researchers, providing additional insights into the effectiveness of the proposed methodology.

5.2 Research Methodology

This methodology offers a comprehensive framework for predicting temporal scour depth formulas for spur dikes, covering various essential stages in hydraulic engineering research. It begins with meticulous data collection from reputable sources, followed by rigorous analysis to extract relevant information. Subsequently, predictive models are developed and validated to ensure accuracy and reliability. Evaluation techniques are then employed to assess the effectiveness of the models. By encompassing data collection, analysis, model development, validation, and evaluation, this approach ensures a comprehensive and systematic methodology (Fig. 5.1) for advancing scour depth prediction in hydraulic engineering.

Literature Collection: The initial step involved a thorough search across reputable databases such as Scopus, Google, and Google Scholar to compile a diverse range of papers relevant to spur dikes. From these sources, researchers extracted both formulated equations and raw data, for subsequent analysis.

Preliminary Screening: Raw data underwent a rigorous screening process to select clear water scour data, ensuring the quality and relevance of the dataset. Additionally, eight researchers' formulas were identified for further investigation.

Parameter Identification: Key parameters such as spur dike dimensions (length, height, thickness), time-related scour depth, time, fluid properties (density, kinematic viscosity), hydraulic factors (acceleration due to gravity, depth of flow, flow velocity, critical flow velocity), geometric factors (spur dike orientation angle, degree of permeability, median diameter of sediment, sediment density), and flow characteristics (Reynolds number, Froude number, Geometric Standard Deviation) were identified. This step ensured a comprehensive understanding of the variables affecting scour depth.

Dimensionless Framework: Dimensionless analysis was conducted to reduce the number of parameters involved in the study of spur dike scour depth. This process involved transforming the dimensional parameters into dimensionless forms using relevant scaling parameters. By doing so, the analysis aimed to simplify the model and improve its generalizability across different conditions. This technique allowed researchers to focus on the essential characteristics influencing scour depth while minimizing the complexity of the model.

Dimensionality Reduction: Thirteen dimensionality reduction methods (Gamma Statistics test, Pearson Correlation coefficient, Spearman's rho correlation coefficient, Kendall's tau b correlation coefficient, PCA, Discriminant Analysis, Line of least squares regression, Enter, Forward, Backward, Removed, Stepwise regression and Subset regression) were applied to streamline the parameters further, with the optimal reduction technique determined using weighted mean percentage, Subset regression, and PCA methods. This step aimed to refine the model and improve its efficiency.

Data Visualization: Graphical representations were utilized to validate the collected data against empirical formulas, ensuring the correctness and consistency of the dataset and providing visual insights into the relationship between variables.

Model Development: Eighty percent of the training data was randomly selected from the preliminary screening data. Nonlinear regression analysis, utilizing the Levenberg-Marquardt and Gauss-Newton methods, was employed to predict the formula. The developed formula was then validated using the remaining 20% of testing data. This process aimed to predict the formula with high accuracy and reliability.

Comparison and Evaluation: The predicted formula was compared with eight literature empirical formulas using data from the preliminary screening. Weightage percentages of parameters for statistical metrics (R^2, RMSE, NSE, MBE) (section 5.3) were calculated using CRITIC, Entropy, and AHP methods to assess model performance comprehensively.

Ranking and Comparison: Finally, researchers' formulas and the developed formula (present study formula) were ranked using PROMETHEE and TOPSIS methods, providing insights into their effectiveness and suitability relative to each other. This step facilitated the selection of the most promising temporal scour depth formula for spur dikes, contributing to advancements in hydraulic engineering research.

5.3 Statistical Influencing Parameters

Statistical analysis is used to evaluate the provided accuracy of the literature formulas and newly predicted formulas. Various cost and beneficial criteria are used to assess how well the estimated and observed d_{st} values agree. Now, the following formulas, are given in Eqs. 5.1–5.4, have been used to define the various performance indices such as R^2, RMSE, NSE and MBE. Here, $(d_{st}/L_R)_o$ is the observed values and $(d_{st}/L_R)_c$ is the computed and, n represents the total number of input samples.

Coefficient of Determination (R^2)

R-squared is a statistical measure of how well the regression line approximates the real data points. It ranges from 0 to 1 (Legates et al., 1999), where 0 indicates the model fails to explain any of the variability of the response data around its mean, 1 indicates the model perfectly explains all the variability of the response data around its mean and $0<R^2<1$ indicates the model explains some proportion of the variability in the response data around its mean. The closer R^2 is to 1, the better the model fits the data. The formula is (Eq. 5.1):

$$R^2 = \left\{ \frac{\sum_{i=1}^{n} \left\{ \left(\frac{d_{st}}{L_R}\right)_{oi} - \overline{\left(\frac{d_{st}}{L_R}\right)_o} \right\} \left\{ \left(\frac{d_{st}}{L_R}\right)_{ci} - \overline{\left(\frac{d_{st}}{L_R}\right)_c} \right\}}{\left[\sum_{i=1}^{n} \left(\left(\frac{d_{st}}{L_R}\right)_{oi} - \overline{\left(\frac{d_{st}}{L_R}\right)_o} \right)^2 \right]^{0.5} \sum_{i=1}^{n} \left\{ \left(\frac{d_{st}}{L_R}\right)_{ci} - \overline{\left(\frac{d_{st}}{L_R}\right)_c} \right\}^2} \right\}^2 \quad (5.1)$$

Root Mean Square Error (RMSE)

RMSE is a measure of the differences between values predicted by a model or an estimator and the observed values. It is calculated by taking the square root of the average of the squared differences between the predicted and observed values. RMSE values typically range from 0 to infinity (Willmott, 1981), with lower values indicating better model performance. The formula is (Eq. 5.2)

$$RMSE = \sqrt{\sum_{i=1}^{n} \frac{\left\{ \left(\frac{d_{st}}{L_R}\right)_{ci} - \left(\frac{d_{st}}{L_R}\right)_{oi} \right\}^2}{n}} \quad (5.2)$$

Nash–Sutcliffe Model Efficiency Coefficient (NSE)

NSE compares the modeled data to the observed data, considering both the mean and variance of the data. The values typically range from negative infinity to 1 (Nash and Sutcliffe, 1970), with higher values indicating better model performance and negative values suggesting the model performs worse than a simple mean prediction. The formula is (Eq. 5.3)

$$\mathrm{NSE} = 1 - \frac{\sum_{i=1}^{n}\left\{\left(\frac{d_{st}}{L_R}\right)_{oi} - \left(\frac{d_{st}}{L_R}\right)_{ci}\right\}^2}{\sum_{i=1}^{n}\left\{\left(\frac{d_{st}}{L_R}\right)_{oi} - \overline{\left(\frac{d_{st}}{L_R}\right)_{o}}\right\}^2} \tag{5.3}$$

Mean Bias Error (MBE)

The MBE quantifies the average difference between predicted and observed values, providing insight into the model's tendency to overestimate or underestimate. MBE values range from negative to positive infinity (Legates et al., 1999), with 0 indicating perfect agreement between predictions and observations. Positive values indicate a tendency to overestimate, while negative values suggest underestimation. The formula is (Eq. 5.4)

$$\mathrm{MBE} = \sum_{i=1}^{n} \frac{\left\{\left(\frac{d_{st}}{L_R}\right)_{ci} - \left(\frac{d_{st}}{L_R}\right)_{oi}\right\}}{n} \tag{5.4}$$

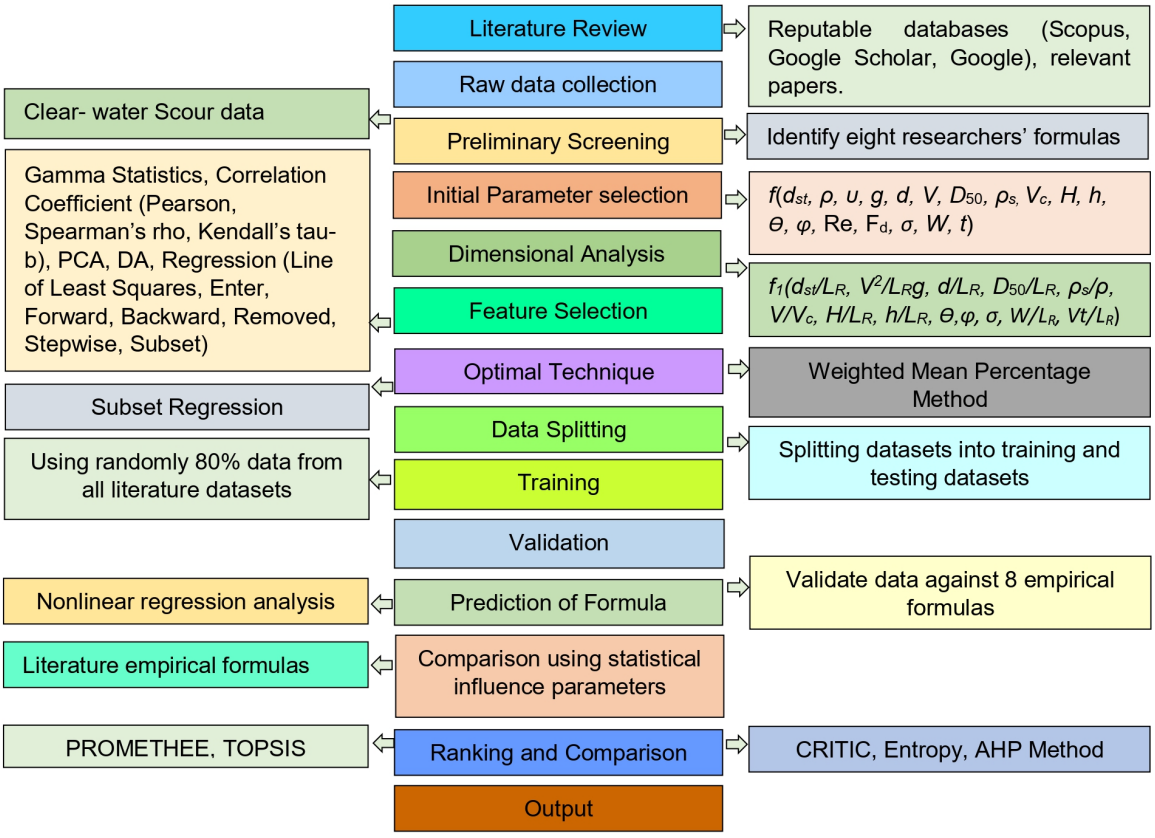

Fig. 5.1. The flowchart showing the methodology adopted for the present study.

Chapter 6
Dimensional Analysis

6.1 Dimensional Framework

Dimensionless analysis on spur dikes involves scaling down physical parameters like length, velocity, and discharge to non-dimensional numbers such as Froude or Reynolds numbers, facilitating model testing and generalization of results across different scales and conditions. The following details are provided below.

6.1.1 Analyses of Scouring Parameters

The magnitude which interests the designer in determining the Spur dike Scouring depth is the temporal depth to be reached by the scouring process. For this reason, the quantitative study will be limited to the temporal depth d_{st} reached by the scour hole around the spur dike after sufficient temporal time (t) has elapsed to reach the temporal. d_{st} is measured below ambient bed level.

Limiting the study to the case of the unsubmerged spur dike in a river whose flow is assumed to be steady and uniform, there are many parameters which may influence the scouring phenomenon:

Variables characterizing the fluid:

- g acceleration due to gravity,
- ρ density of fluid,
and - v kinematic viscosity of the fluid.

Variables characterizing the bed material:

- ρ_s density of the sediment,
- σ Geometric standard deviation/sediment gradation,
- D_{50} Median grain size.

Variables characterizing the flow:

- d depth of approach flow,
- V mean velocity of flow,
- V_c flow velocity,
- Re Reynolds number, and
- F_d Densimetric Froude number.

Variable characterizing the Flume property:

- W Width of the flume.

Variables characterizing the Spur dike:

-l its length,
-H its height.
-h its thickness
-Θ its angle and
-φ its permeability.

6.1.2 Ratio-Based Analysis

Temporal scour depth d_{st} grows over time t (Eq. 6.1) can be a function of

$$f\left(d_{st},\rho,\nu,g,d,V,D_{50},\rho_s,V_c,l,H,h,\theta,\varphi,\mathrm{Re},F_d,\sigma,W,t\right)=0 \tag{6.1}$$

where, d_{st} is scour depth at any instant of time t and the dimension of d_{st} is $\left[L\right]$ or $\left[M^0L^1T^0\right]$

ρ is fluid density for flow which has a dimension of $\left[ML^{-3}\right]$ or $\left[M^1L^{-3}T^0\right]$

v is kinematic viscosity for flow which has a dimension of $\left[L^2T^{-1}\right]$ or $\left[M^0L^2T^{-1}\right]$

g is the gravitational acceleration which has a dimension of $\left[LT^{-2}\right]$ or $\left[M^0L^1T^{-2}\right]$

d is approach flow depth; the dimension of d is $\left[L\right]$ or $\left[M^0L^1T^0\right]$

V is approach flow velocity and the dimension is $\left[LT^{-1}\right]$ or $\left[M^0L^1T^{-1}\right]$

D_{50} is the median diameter of sediment which also has an also dimension of length $\left[L\right]$ or $\left[M^0L^1T^0\right]$

ρ_s is sediment density having a dimension similar to the dimension of ρ is $\left[ML^{-3}\right]$ or $\left[M^1L^{-3}T^0\right]$

V_c is critical flow velocity having a dimension the same as approach flow velocity $\left[LT^{-1}\right]$ or $\left[M^0L^1T^{-1}\right]$

l is the spur dike length which has a dimension of $\left[L\right]$ or $\left[M^0L^1T^0\right]$

H is the spur dike height which has a dimension of $\left[L\right]$ or $\left[M^0L^1T^0\right]$

h is the spur dike thickness which has a dimension of $\left[L\right]$ or $\left[M^0L^1T^0\right]$

θ is the spur dike orientation angle which has a dimension of $\left[M^0L^0T^0\right]$

φ is the spur dike degree of permeability which has a dimension of $\left[M^0L^0T^0\right]$

Re is the Reynolds number which has a dimension of $\left[M^0L^0T^0\right]$

F_d is the densimetric Froude number which has a dimension of $\left[M^0L^0T^0\right]$

π is sediment gradation or geometric standard deviation with a dimension of $\left[M^0L^0T^0\right]$

W is the width of the channel which has a dimension of $\left[L\right]$ or $\left[M^0L^1T^0\right]$

t is time to develop d_{st} is a dimension of time only which is equal to $\left[T\right]$ or $\left[M^0L^0T^1\right]$

For dimensionless analysis here we have considered the Buckingham π theorem method, but not considered the Rayleigh method as a number of variables of more than three (3) or four (4). Here $\theta, \varphi, R_e, F_d, \sigma$ already dimensionless. Here we have also considered the repeating variable as *l*, *V* and ρ, where *l* is the geometric property, *V* is the flow property and ρ is the fluid property. Here total number of parameters, *n* = 14 and the number of independent parameters, *m* = 3. Therefore, we will get a total $\left(n-m=14-3=11\right)$ i.e. 11 π terms as follows

$$f_1\left(\pi_1, \pi_2, \pi_3, \cdots\cdots\cdots, \pi_{n-m}\right)=0$$

$$\text{So, } f_1\left(\pi_1, \pi_2, \pi_3, \cdots\cdots\cdots, \pi_{11}\right)=0$$

After considering the repeating variable in the above stated way the pi $\left(\pi\right)$ term looks like the below:-

$\pi_1 = l^{a1}V^{b1}\rho^{c1}d_{st}$; $\pi_2 = l^{a2}V^{b2}\rho^{c2}\nu$; $\pi_3 = l^{a3}V^{b3}\rho^{c3}g$; $\pi_4 = l^{a4}V^{b4}\rho^{c4}d$; $\pi_5 = l^{a5}V^{b5}\rho^{c5}D_{50}$; $\pi_6 = l^{a6}V^{b6}\rho^{c6}\rho$; $\pi_7 = l^{a7}V^{b7}\rho^{c7}V_C$; $\pi_8 = l^{a8}V^{b8}\rho^{c8}H$; $\pi_9 = l^{a9}V^{b9}\rho^{c9}h$; $\pi_{10} = l^{a10}V^{b10}\rho^{c10}W$; $\pi_{11} = l^{a11}V^{b11}\rho^{c11}t$

1. Now for the first π terms we can write-

$$\pi_1 = l^{a1}V^{b1}\rho^{c1}d_{st}$$

From this π_1 term, we deduce that the dimensions of mass, length, and time must equate to zero, yielding

$$M^0L^0T^0 = \left(M^0L^1T^0\right)^{a1}\left(M^0L^1T^{-1}\right)^{b1}\left(M^1L^{-3}T^0\right)^{c1}\left(M^0L^1T^0\right)$$

Equating the left and right-side power of *M*, *L* and *T* on either side we get the value of *a*1, *b*1 and *c*1 and by putting this value in the above π term we get Eq. (6.2) where the first non-dimensional term is represented as $\pi_1 = l^{-1}V^0\rho^0 d_{st}$

So,

$$\pi_1 = \frac{d_{st}}{l} \tag{6.2}$$

2. Similarly we can write 2nd π term as

$$\pi_2 = l^{a2}V^{b2}\rho^{c2}\nu$$

From this π term, we conclude that the dimensions of mass, length, and time must balance to zero, resulting in

$$M^0L^0T^0 = \left(M^0L^1T^0\right)^{a2}\left(M^0L^1T^{-1}\right)^{b2}\left(M^1L^{-3}T^0\right)^{c2}\left(M^0L^2T^{-1}\right)$$

Equating the power of M, L and T on either side we get the value of $a2$, $b2$ and $c2$ and by putting this value in the above π term we get (Eq. 6.3) the 2nd non-dimensional term as

$$\pi_2 = l^{-1}V^{-1}\rho^0\upsilon \text{ so } \pi_2 = \frac{\upsilon}{lV} \tag{6.3}$$

3. Similarly we can write 3rd π term as

$$\pi_3 = l^{a3}V^{b3}\rho^{c3}g$$

From this π term, we conclude that the dimensions of mass, length, and time must balance to zero, resulting in

$$M^0L^0T^0 = \left(M^0L^1T^0\right)^{a3}\left(M^0L^1T^{-1}\right)^{b3}\left(M^1L^{-3}T^0\right)^{c3}\left(M^0L^1T^{-2}\right)$$

Equating the power of M, L and T on either side we get the value of $a3$, $b3$ and $c3$ and by putting this value in the above π term we get (Eq. 6.4) the 3rd non-dimensional term as $\pi_3 = l^1V^{-2}\rho^0 g$, so,

$$\pi_3 = \frac{l\,\mathrm{g}}{V^2} \tag{6.4}$$

4. Similarly we can write the 4th π term as

$$\pi_4 = l^{a4}V^{b4}\rho^{c4}d$$

From this π term, we deduce that the dimensions of mass, length, and time must equate to zero, yielding

$$M^0L^0T^0 = \left(M^0L^1T^0\right)^{a4}\left(M^0L^1T^{-1}\right)^{b4}\left(M^1L^{-3}T^0\right)^{c4}\left(M^0L^1T^0\right)$$

Equating the power of M, L and T on either side we get the value of $a4$, $b4$ and $c4$ and by putting this value in the above π term we get (Eq. 6.5) the 4th non-dimensional term as $\pi_4 = l^{-1}V^0\rho^0 d$, so,

$$\pi_4 = \frac{d}{l} \tag{6.5}$$

5. Similarly we can write the 5th π term as-

$$\pi_5 = l^{a5}V^{b5}\rho^{c5}D_{50}$$

From this π term, we deduce that the dimensions of mass, length, and time must equate to zero, yielding

$$M^0L^0T^0 = \left(M^0L^1T^0\right)^{a5}\left(M^0L^1T^{-1}\right)^{b5}\left(M^1L^{-3}T^0\right)^{c5}\left(M^0L^1T^0\right)$$

Equating the power of M, L and T on either side we get the value of $a5$, $b5$ and $c5$ and by putting this value in the above π term we get (Eq. 6.6) the 5th non-dimensional term as $\pi_5 = l^{-1}V^0\rho^0 D_{50}$, so,

$$\pi_5 = \frac{D_{50}}{l} \tag{6.6}$$

6. Similarly we can write the 6th π term as

$$\pi_6 = l^{a6}V^{b6}\rho^{c6}\rho$$

From this π term, we deduce that the dimensions of mass, length, and time must equate to zero, yielding

$$M^0L^0T^0 = \left(M^0L^1T^0\right)^{a6}\left(M^0L^1T^{-1}\right)^{b6}\left(M^1L^{-3}T^0\right)^{c6}\left(M^1L^{-3}T^0\right)$$

Equating the power of *M*, *L* and *T* on either side we get the value of *a*6, *b*6 and *c*6 and by putting this value in the above π term we get (Eq. 6.7) the 6th non-dimensional term as $\pi_6 = l^0 V^0 \rho^{-1} \rho_s$, so,

$$\pi_6 = \frac{\rho_s}{\rho} \tag{6.7}$$

7. Similarly we can write the 7th π term as-

$$\pi_7 = l^{a7} V^{b7} \rho^{c7} V_C$$

From this π term, we deduce that the dimensions of mass, length, and time must equate to zero, yielding

$$M^0 L^0 T^0 = \left(M^0 L^1 T^0\right)^{a7} \left(M^0 L^1 T^{-1}\right)^{b7} \left(M^1 L^{-3} T^0\right)^{c7} \left(M^0 L^1 T^{-1}\right)$$

Equating the power of *M*, *L* and *T* on either side we get the value of *a7, b7* and *c7* and by putting this value in the above π term we get (Eq.6.8) the 7th non-dimensional term as $\pi_7 = l^0 V^{-1} \rho^0 V_C$, so,

$$\pi_7 = \frac{V_c}{V} \tag{6.8}$$

8. Similarly we can write the 8th π term as-

$$\pi_8 = l^{a8} V^{b8} \rho^{c8} H$$

From this π term, we deduce that the dimensions of mass, length, and time must equate to zero, yielding

$$M^0 L^0 T^0 = \left(M^0 L^1 T^0\right)^{a8} \left(M^0 L^1 T^{-1}\right)^{b8} \left(M^1 L^{-3} T^0\right)^{c8} \left(M^0 L^1 T^0\right)$$

Equating the power of *M*, *L* and *T* on either side we get the value of *a8, b8* and *c8* and by putting this value in the above π term we get (Eq. 6.9) the 8th non-dimensional term as $\pi_8 = l^{-1} V^0 \rho^0 H$, so,

$$\pi_8 = \frac{b}{l} \tag{6.9}$$

9. Similarly we can write the 9th π term as-

$$\pi_9 = l^{a9} V^{b9} \rho^{c9} h$$

From this π term, we deduce that the dimensions of mass, length, and time must equate to zero, yielding

$$M^0 L^0 T^0 = \left(M^0 L^1 T^0\right)^{a9} \left(M^0 L^1 T^{-1}\right)^{b9} \left(M^1 L^{-3} T^0\right)^{c9} \left(M^0 L^1 T^0\right)$$

Equating the power of *M*, *L* and *T* on either side we get the value of *a*9, *b*9 and *c*9 and by putting this value in the above π term we get (Eq. 6.10) the 9th non-dimensional term as $\pi_9 = l^{-1} V^0 \rho^0 h$, so,

$$\pi_9 = \frac{h}{l} \tag{6.10}$$

10. Similarly we can write the 10th π term as-

$$\pi_{10} = l^{a10} V^{b10} \rho^{c10} W$$

From this π term, we deduce that the dimensions of mass, length, and time must equate to zero, yielding

$$M^0L^0T^0 = \left(M^0L^1T^0\right)^{a10}\left(M^0L^1T^{-1}\right)^{b10}\left(M^1L^{-3}T^0\right)^{c10}\left(M^0L^1T^0\right)$$

Equating the power of M, L and T on either side we get the value of $a10$, $b10$ and $c10$ and by putting this value in the above π term we get (Eq. 6.11) the 10th non-dimensional term as

$$\pi_{10} = l^{-1}V^0\rho^0 W \text{, so } \pi_{10} = \frac{W}{l} \tag{6.11}$$

11. Similarly we can write the 11th π term as-

$$\pi_{11} = l^{a11}V^{b11}\rho^{c11}t$$

From this π term, we deduce that the dimensions of mass, length, and time must equate to zero, yielding

$$M^0L^0T^0 = \left(M^0L^1T^0\right)^{a11}\left(M^0L^1T^{-1}\right)^{b11}\left(M^1L^{-3}T^0\right)^{c11}\left(M^0L^0T^1\right)$$

Equating the power of M, L and T on either side we get the value of $a11$, $b11$ *and* $c11$ and by putting this value in the above π term we get (Eq. 6.12) the 16th non-dimensional term as $\pi_{11} = l^{-1}V^1\rho^0 t$, so $\pi_{11} = \dfrac{Vt}{l}$ (6.12)

Now the dimensionless group will be in the following form (Eq. 6.13) -

$$f_1(\pi_1, \pi_2, \pi_3, \cdots\cdots\cdots, \pi_{11}) = 0$$

$$f_1\left(\frac{d_{st}}{l}, \frac{\nu}{lV}, \frac{lg}{V^2}, \frac{d}{l}, \frac{D_{50}}{l}, \frac{\rho_s}{\rho}, \frac{V_c}{V}, \frac{H}{l}, \frac{h}{l}, \theta, \varphi, R_e, F_d, \sigma, \frac{W}{l}, \frac{Vt}{l}\right) = 0 \tag{6.13}$$

By re-arranging the above dimensionless group we can write the above equation as follows (Eq. 6.14)

$$\frac{d_{st}}{l} = f_2\left(\frac{lV}{\nu}, \frac{V^2}{l\mathrm{g}}, \frac{d}{l}, \frac{D_{50}}{l}, \frac{\rho}{\rho_s}, \frac{V}{V_c}, \frac{H}{l}, \frac{h}{l}, \theta, \varphi, \mathrm{Re}, F_d, \sigma, \frac{W}{l}, \frac{Vt}{l}\right) \tag{6.14}$$

Now Reynolds number and Froude number can be neglected so we can neglect the following terms- Re, $\mathrm{F_d}$

Hence, the non-dimensional group is reduced to the following form (Eq. 6.15)-

$$\frac{d_{st}}{l} = f_1\left(\frac{lV}{\nu}, \frac{V^2}{lg}, \frac{d}{l}, \frac{D_{50}}{l}, \frac{\rho}{\rho_s}, \frac{V}{V_c}, \frac{H}{l}, \frac{h}{l}, \theta, \varphi, \sigma, \frac{W}{l}, \frac{Vt}{l}\right) \tag{6.15}$$

Since both "l" and "L_R" represent the same unit, we can easily convert "l" to "L_R".
Now, the final dimensionless group is reduced to the following form (Eq. 6.16) -

$$\frac{d_{st}}{L_R} = f_1\left(\frac{L_R V}{\nu}, \frac{V^2}{L_R g}, \frac{d}{L_R}, \frac{D_{50}}{L_R}, \frac{\rho_s}{\rho}, \frac{V}{V_c}, \frac{H}{L_R}, \frac{h}{L_R}, \theta, \varphi, \sigma, \frac{W}{L_R}, \frac{Vt}{L_R}\right) \tag{6.16}$$

6.2 Classification of Dimensional Parameters

Reynolds Number (L_RV/ν): The ratio L_RV/ν represents the ratio that could be as a form of Reynolds number, where L_RV serves as the characteristic length scale multiplied by velocity.

In this case, the ratio $L_R V/v$ could be seen as a modified Reynolds number with a characteristic length scale adjusted by velocity. The Re characterizes the ratio of inertial forces to viscous forces in a fluid flow and is defined as:

Re= $L_R V/v$; Where: L is a characteristic length scale, V is a characteristic velocity, ν is the kinematic viscosity of the fluid.

Froude Number ($V^2/L_R g$): The expression $V^2/L_R g$ represents the ratio of the square of velocity V to the product of a characteristic length scale L_R and the acceleration due to gravity g. This ratio is often referred to as the Froude number (Fr) in fluid mechanics and naval architecture. The Froude number is a dimensionless parameter used to characterize the relative importance of inertial forces to gravitational forces in a fluid flow. It is particularly significant in analyzing open-channel flow, such as rivers, canals, and estuaries, where the behavior of the flow is influenced by both inertia and gravity.

The formula for the Froude number (Fr) is:

$Fr^2= V^2/L_R g$; Where: V is the velocity of the fluid, L_R is a characteristic length scale (such as the depth of the flow in open-channel flow), and g is the acceleration due to gravity.

The Froude number helps classify flow regimes in open-channel flow as subcritical (Fr <1), critical (Fr =1), or supercritical (Fr >1). These classifications have important implications for flow behavior and stability.

Length Scale Ratio (d/L_R): The ratio d/L_R typically represents the ratio of a characteristic dimension d to a reference or characteristic length scale L_R. This ratio might be referred to as the length scale ratio., and thus can be considered a dimensionless quantity.

Median Grain Size ratio (D_{50}/L_R): The ratio D_{50}/L_R typically represents the ratio of a characteristic particle diameter D_{50} to a reference or characteristic length scale L_R . In sedimentology and hydraulics, D_{50} often represents the median particle diameter, which is the diameter below which 50% of the particles by weight are smaller.

Relative density (ρ_s/ρ): The ratio ρ_s/ρ, where ρ_s is the density of a substance or material, and ρ is the density of a reference substance or material, is commonly referred to as the specific gravity or relative density of the substance with respect to the reference material.

Velocity Scale Ratio (V/V_c): The ratio V/V_c can represent the relative velocity of a fluid flow compared to a critical velocity V_c . This term is used in fluid mechanics or aerodynamics when comparing velocities to a characteristic velocity scale within the flow field. Since V/V_c has no units, it can also be classified as a dimensionless quantity, representing a velocity normalized by a characteristic scale.

Height Ratio (H/L_R): The ratio H/L_R, where H is the height of a structure (spur dike) or system and L_R is a characteristic length scale. This ratio can simply be referred to as the height ratio. It indicates how the height of the structure or system compares to the reference length scale. It can be classified as a dimensionless parameter, providing information about the geometry or configuration of a system relative to a reference length scale.

Thickness Ratio (h/L_R): The ratio h/L_R, can be referred to as the thickness ratio, indicating the ratio of the actual thickness h to a characteristic length scale L_R . It provides information about how the thickness of the spur dike compares to the reference length scale. It can be classified as a dimensionless parameter, providing information about the geometry or configuration of the spur dike relative to a reference length scale.

Width Ratio (W/L_R): The ratio W/L_R, can be referred to as the width ratio, indicating the ratio of the actual width W to a characteristic length scale L_R . It provides information about how the width of the flume compares to the reference length scale. It can be classified as a dimensionless parameter, providing information about the geometry or configuration of the flume relative to a reference length scale.

Tangential Velocity Ratio (Vt/L_R): The ratio Vt/L_R represents the ratio of the tangential velocity Vt to the characteristic length scale L_R . It indicates how the tangential velocity magnitude compares to the reference length scale. It can be considered a dimensionless parameter. It offers insights into the velocity distribution or characteristics of the flow relative to a reference length scale.

6.3 Dimensionless Parameters taken by Research Groups

Different research groups utilize dimensional parameters (Table 6.1) to devise empirical equations for estimating scour depth at spur dikes, aiming to capture the complex hydraulic processes and geometric factors influencing scour development. These dimensional terms often incorporate flow characteristics, sediment properties, and geometric features of the spur dike to enhance predictive accuracy across diverse hydraulic conditions.

Table 6.1. The dimensionless terms used by different research groups to develop the empirical formulas for computing scour depth at spur dike.

Research group	Dimensionless parameters taken to develop empirical relationship																
	L_RV/υ	V^2/L_Rg	d/L_R	D_{50}/L_R	ρ_S/ρ	V/V_C	H/L_R	h/L_R	θ	$\emptyset$	σ	W/L_R	Vt/L_R	F_d	F_r	F_{sm}	T
Alasadi et al. (2023)	×	×	×	×	×	✓	×	×	×	×	×	×	×	×	✓	×	×
Farshad et al. (2022)	×	×	✓	✓	×	✓	×	×	✓	✓	✓	×	×	✓	×	×	×
Pandey et al. (2020)	×	×	×	✓	×	×	×	×	×	×	×	×	×	×	×	✓	✓
Pandey et al. (2019)	×	×	✓	✓	×	×	×	×	×	×	×	×	×	×	×	✓	×
Khassaf and Abbas (2018)	×	×	×	×	×	✓	×	×	×	×	×	×	×	×	✓	×	×
Karimi et al. (2012a)	×	×	×	×	×	✓	×	×	×	×	✓	×	×	✓	✓	×	×
Karimi et al. (2012b)	×	×	×	×	×	✓	×	×	×	×	×	×	×	×	✓	×	×
Nasrollahi et al. (2008)	×	×	✓	✓	×	×	×	×	×	×	×	✓	×	×	✓	×	×
Kothyari et al. (2007)	×	×	×	×	×	×	×	×	×	×	✓	×	×	✓	×	×	✓
Yanmaz and Kose (2007)	×	×	✓	×	×	×	×	×	×	×	×	×	×	✓	×	×	✓
Coleman et al. (2003)	×	×	✓	×	×	✓	×	×	×	×	×	×	×	×	×	×	×
Oliveto and Hager (2002)	×	×	×	×	×	×	×	×	×	×	✓	×	×	✓	×	×	✓

Note: '×' indicates "not considered".

Chapter 7
Analysis of Parameters Using Feature Selection

7.1 Feature Selection

The goal of dimensionality reduction techniques is to reduce a dataset's feature or variable count while maintaining important information. Moreover, over fitting and model complexity are reduced. Every technique has advantages and disadvantages, and which one to use will depend on the specific characteristics of the dataset as well as the analysis's objectives. This investigation aimed to analyse the optimal dimensionality reduction techniques to reduce dimensionless parameters around spur dikes. The following lists some typical methods for reducing dimensionality

7.1.1 Gamma Statistic Test (GST)

Goodman and Kruskal introduced the gamma correlation coefficient, a measure of rank correlation. It assesses the similarity in the orderings of data when ranked according to different quantities, particularly useful with tied ranks (Siegel and Castellan, 1988). It calculates the cross-tabulated data's strength of association when both variables are measured at the ordinal level (Goodman and Kruskal, 1979). The gamma statistic is calculated as (Eq. 7.1):

$$Gamma(G) = \frac{N_{con} - N_{dis}}{N_{con} + N_{dis}}, \text{ or } Gamma(G) = \frac{P_{con} - P_{dis}}{P_{con} + P_{dis}} \tag{7.1}$$

where, N_{con}, is the number of concordant pairs; N_{dis}, is the number of discordant pairs. This statistic can be seen as a maximum likelihood estimator; P_{con} and P_{dis} represent the likelihood that a randomly chosen pair of observations will be ranked in the same or opposite order, respectively.

This statistic ranges from -1 to +1 (Kampen and Swyngedouw, 2000). A gamma of +1 signifies perfect positive association (all pairs are concordant), (-1) implies perfect negative association (all pairs are discordant), and (0) indicates no association (random relationship between variables). If the G value 0.00-0.10: Negligible correlation, similarly, 0.10-0.20: Weak,0.20-0.40: Moderate,0.40-0.60: Relatively strong,0.60-0.80: Strong and 0.80-1.00: Very strong correlation (Rea and Parker, 1992).

Table 7.1. Correlation for Goodman and Kruskal's gamma statistics test.

#	L_RV/ν		V^2/L_Rg		d/L_R		D_{50}/L_R		V/V_C		H/L_R		h/L_R		Θ		φ		σ		W/L_R		Vt/L_R	
	G	p	G	p	G	p	G	p	G	p	G	p	G	p	G	p	G	p	G	p	G	p	G	p
d_{st}/L_R	0.06	0	0.02	0.30	0.01	0.66	-0.01	0.57	0.12	0	-0.12	0.00	-0.29	0.00	-0.03	0.82	-0.45	0.00	0.15	0.00	0.06	0.01	0.36	0.00
L_RV/ν			0.49	0.00	0.25	0.00	0.24	0.00	0.56	0	0.31	0.00	-0.04	0.05	0.00	1.00	0.21	0.00	-0.35	0.00	0.01	0.78	0.19	0.00
V^2/L_Rg					0.37	0.00	0.70	0.00	0.68	0	0.76	0.00	0.23	0.00	0.00	1.00	0.26	0.00	-0.44	0.00	0.22	0.00	0.33	0.00
d/L_R							0.17	0.00	0.25	0	0.26	0.00	0.20	0.00	0.00	1.00	0.06	0.44	-0.62	0.00	0.25	0.00	0.08	0.00
D_{50}/L_R									0.46	0	0.85	0.00	0.30	0.00	0.00	1.00	-0.02	0.64	-0.25	0.00	0.20	0.00	0.40	0.00
V/V_C											0.52	0.00	0.07	0.01	0.00	1.00	0.26	0.00	-0.30	0.00	0.21	0.00	0.30	0.00
H/L_R													0.45	0.00	0.00	1.00	0.19	0.00	-0.52	0.00	0.36	0.00	0.36	0.00
h/L_R															0.00	1.00	-0.10	0.11	-0.45	0.00	0.03	0.31	0.03	0.23
Θ																	0.00	1.00	0.00	1.00	0.00	1.00	0.00	1.00
φ																			0.04	0.34	-0.26	0.00	-0.25	0.00
σ																					-0.41	0.00	-0.14	0.00
W/L_R																							0.26	0.00
Vt/L_R																								

Note: G - Gamma**,** p – Significant**,** #-Parameters; In the given Table 7.1, the parameters Θ and W/L_R are excluded based on their p-values being greater than 0.05 in relation to L_RV/υ. Similarly, regarding V^2/L_Rg, H/L_R is omitted due to its strong positive association with V^2/L_Rg indicated by a G value of 0.762. Additionally, Θ is excluded as its p-value exceeds 0.05. Likewise, in the context of d/L_R, parameters Θ and φ are omitted for the same reason. For D_{50}/L_R, H/L_R is disregarded given its G value of 0.851, and Θ and φ are omitted due to their p-values exceeding 0.05. Similarly, in the case of h/L_R, parameters Θ, φ, W/L_R, and Vt/L_R are excluded due to their p-values exceeding 0.05, although Vt/L_R is retained as it is deemed an important parameter. Hence, the dimension-less group was reduced to the following form (Eq. 7.2) -

$$\frac{d_{st}}{L_R} = f_1\left(\frac{L_RV}{\nu}, \frac{V^2}{L_Rg}, \frac{d}{L_R}, \frac{D_{50}}{L_R}, \frac{V}{V_c}, \frac{h}{L_R}, \sigma, \frac{Vt}{L_R}\right) \tag{7.2}$$

7.1.2 Pearson Correlation Coefficient (PCC)

The Pearson correlation coefficient is a statistical measure used to evaluate the linear correlation between two datasets. It ranges between -1 and +1, representing the strength and direction of the linear relationship (Pearson, 1895). A -1 or +1, with a negative or positive direction, respectively, indicates strong strength. When the strength and direction are 0, there is no correlation. Pearson correlation coefficient, given a pair of random variables (X, Y), the formula for ρ (Eq. 7.3) is

$$\rho_{X,Y} = \frac{\mathrm{cov}(X,Y)}{\sigma_X \sigma_Y} \tag{7.3}$$

where, cov (X, Y) is the covariance between X and Y. σ_X and σ_Y are the standard deviations of X and Y, respectively.

Table 7.2. Correlation for Pearson correlation coefficient.

#	d_{st}/L_R	L_RV/ν	V^2/L_Rg	d/L_R	D_{50}/L_R	V/V_C	H/L_R	h/L_R	θ	φ	σ	W/L_R	Vt/L_R
d_{st}/L_R	1												
L_RV/ν	0.06*	1											
V^2/L_Rg	0.04	0.51**	1										
d/L_R	0.10**	0.25**	0.54**	1									
D_{50}/L_R	0.11**	0.28**	0.81**	0.43**	1								
V/V_C	0.14**	0.68**	0.82**	0.36**	0.54**	1							
H/L_R	-0.11**	0.46**	0.84**	0.33**	0.66**	0.71**	1						
h/L_R	-0.37**	-0.04	-0.13**	-0.06*	-0.16**	-0.22**	0.07*	1					
θ	-0.01	0.00	0.00	0.00	0.00	0.00	0.00	0.00	1				
φ	-0.26**	0.25**	-0.11**	0.04	-0.16**	0.14**	0.09**	-0.02	0.00	1			
σ	0.18**	-0.02	-0.43**	-0.64**	-0.42**	-0.22**	-0.36**	-0.14**	0.00	-0.02	1		
W/L_R	0.13**	-0.09**	0.51**	0.51**	0.57**	0.28**	0.32**	-0.41**	0.00	-0.18**	-0.60**	1	
Vt/L_R	0.38**	0.34**	0.68**	0.34**	0.54**	0.55**	0.56**	-0.14**	0.00	-0.11**	-0.23**	0.36**	1

Note: *. Correlation is significant at the 0.05 level (2-tailed); **. Correlation is significant at the 0.01 level (2-tailed). The correlation values from Table 7.2 between V^2/L_Rg and D_{50}/L_R, V/V_c, and H/L_R are 0.81, 0.82, and 0.84 respectively, indicating strong correlations. Consequently, D_{50}/L_R and H/L_R are excluded from consideration. But V/V_c is considered as an important parameter. Although the correlation coefficient θ is zero, but it lacks significance (>0.05), thus θ is also disregarded. Hence, the dimension-less group was reduced to the following form (Eq. 7.4) -

$$\frac{d_{st}}{L_R} = f_1\left(\frac{L_RV}{\nu}, \frac{V^2}{L_Rg}, \frac{d}{L_R}, \frac{V}{V_c}, \frac{h}{L_R}, \varphi, \sigma, \frac{W}{L_R}, \frac{Vt}{L_R}\right) \tag{7.4}$$

7.1.3 Spearman's rho Correlation Coefficient (SRCC)

The Spearman's rank correlation coefficient (r_s) (Spearman, 1904) is used to evaluate the strength and direction of a monotonic relationship between two variables. SRCC does not presuppose a linear relationship, in contrast to the Pearson correlation. Instead, it measures how well observations in one variable correspond to the level of observations in another variable. It has a range of -1 to +1, where a perfect inverse relationship is represented by a value of -1, a perfect direct relationship by a value of +1, and no monotonic relationship by a value of 0. SRCC can be calculated using the following formula (Eq. 7.5):

$$\rho = 1 - \frac{6\sum D^2}{N(N^2-1)} \tag{7.5}$$

where D is the rank difference between the corresponding variables, and N is the number of observations.

Table 7.3. Correlation for Spearman's rho correlation coefficient.

#	d_{st}/L_R	L_RV/ν	V^2/L_Rg	d/L_R	D_{50}/L_R	V/V_c	H/L_R	h/L_R	θ	φ	σ	W/L_R	Vt/L_R
d_{st}/L_R	1												
L_RV/ν	0.08**	1											
V^2/L_Rg	0.10**	0.62**	1										
d/L_R	0.03	0.41**	0.54**	1									
D_{50}/L_R	0.07*	0.33**	0.86**	0.30**	1								
V/V_C	0.18**	0.71**	0.74**	0.38**	0.46**	1							
H/L_R	-0.21**	0.46**	0.70**	0.38**	0.61**	0.61**	1						
h/L_R	-0.35**	0.06*	0.25**	0.26**	0.23**	0.18**	0.61**	1					
θ	-0.01	0.00	0.00	0.00	0.00	0.00	0.00	0.00	1				
φ	-0.24**	0.13**	0.08**	0.03	-0.04	0.16**	0.16**	-0.01	0.00	1			
σ	0.14**	-0.41**	-0.56**	-0.77**	-0.32**	-0.34**	-0.52**	-0.50**	0.00	0.03	1		
W/L_R	0.12**	-0.08**	0.36**	0.38**	0.33**	0.17**	0.18**	-0.10**	0.00	-0.15**	-0.42**	1	
Vt/L_R	0.52**	0.27**	0.48**	0.14**	0.49**	0.37**	0.39**	0.02	0.00	-0.12**	-0.17**	0.31**	1

Note: **"**"-** Correlation is significant at the 0.01 level (2-tailed); *. Correlation is significant at the 0.05 level (2-tailed). Reduced D_{50}/L_R in the above Table 7.3 and the correlation value between D_{50}/L_R and V^2/L_Rg is 0.86. Likewise, since σ and d/L_R correlation value is -0.77, also reduced. Although the correlation coefficient θ is zero, but it lacks significance (>0.05), thus θ is also disregarded. In a similar vein, reduced φ, as the significance level >0.05. Hence, the dimensionless group was reduced to the following form (Eq. 7.6) -

$$\frac{d_{st}}{L_R} = f_1\left(\frac{L_RV}{\nu}, \frac{V^2}{L_Rg}, \frac{d}{L_R}, \frac{V}{V_c}, \frac{H}{L_R}, \frac{h}{L_R}, \frac{W}{L_R}, \frac{Vt}{L_R}\right) \tag{7.6}$$

7.1.4 Kendall's tau-b Correlation Coefficient (KCC)

KCC is a non-parametric test used to measure the similarity between two variables. Unlike Pearson correlation, it does not mean that the relationship between variables is linear but rather measures correlations as consistent and inconsistent pairs. Specifically, the coefficient measures the difference between the number of pairs that are concordant and discordant (Kendall, 1938). It is used when data is sorted rather than measured on an interval or ratio scale and this coefficient is robust to outliers and small samples. Kendall's tau-b adjusts for tied ranks by using the following formula (Eq. 7.7).

$$\text{Kendall's } \tau = \frac{c-d}{c+d} \tag{7.7}$$

where, c is the number of concordant pairs and d is the number of discordant pairs. Kendall's tau-b correlation coefficient ranges from -1 to +1. A value of -1 indicates a negative correlation, a value of 0 indicates no correlation and a value of +1 indicates a positive correlation. A p-value less than 0.05 indicates a significant correlation, while a p-value greater than 0.05 indicates no significant correlation.

Table 7.4. Correlation for Kendall's tau-b correlation coefficient.

#	d_{st}/L_R	L_RV/ν	V^2/L_Rg	d/L_R	D_{50}/L_R	V/V_c	H/L_R	h/L_R	θ	φ	σ	W/L_R	Vt/L_R
dst/L_R	1												
L_RV/ν	0.08**	1											
V^2/L_Rg	0.08**	0.45**	1										
d/L_R	0.03	0.27**	0.40**	1									
D_{50}/L_R	0.04*	0.18**	0.68**	0.20**	1								
V/V_C	0.13**	0.54**	0.57**	0.25**	0.32**	1							
H/L_R	-0.16**	0.31**	0.57**	0.24**	0.57**	0.47**	1						
h/L_R	-0.25**	-0.00	0.16**	0.18**	0.16**	0.12**	0.46**	1					
θ	-0.01	0.00	0.00	0.00	0.00	0.00	0.00	0.00	1				
φ	-0.19**	0.11**	0.07**	0.02	-0.03	0.14**	0.15**	-0.01	0.00	1			
σ	0.09**	-0.33**	-0.42**	-0.60**	-0.23**	-0.26**	-0.41**	-0.41**	0.00	0.02	1		
W/L_R	0.09**	-0.07**	0.23**	0.28**	0.29**	0.12**	0.18**	-0.03	0.00	-0.12**	-0.36**	1	
Vt/L_R	0.36**	0.18**	0.34**	0.10**	0.35**	0.26**	0.29**	0.02	0.00	-0.09**	-0.12**	0.21**	1

Note: **. Correlation is significant at the 0.01 level (2-tailed); *. Correlation is significant at the 0.05 level (2-tailed). Since the correlation coefficient θ is zero from Table 7.4, but it lacks significance (>0.05), thus θ is also disregarded. In the same manner, reduced h/L_R and φ, as the significance greater than 0.05. Hence, the dimension-less group was reduced to the following form (Eq. 7.8) -

$$\frac{d_{st}}{L_R} = f_1\left(\frac{L_RV}{\nu}, \frac{V^2}{L_Rg}, \frac{d}{L_R}, \frac{D_{50}}{L_R}, \frac{V}{V_c}, \frac{H}{L_R}, \sigma, \frac{W}{L_R}, \frac{Vt}{L_R}\right) \tag{7.8}$$

Table 7.5. Weighted mean percentage for gamma statistics, and correlations.

Frequency Range	*	Avg. of Freq.	GST #	GST **	GST ##	PCC #	PCC **	PCC ##	SRCC #	SRCC **	SRCC ##	KCC #	KCC **	KCC ##
0.00-0.19	Negligible	0.1	68	4.02		76	4.5		76	4.5		90	5.33	
0.20-0.39	Weak	0.3	56	9.94		34	6.04		38	6.75		40	7.1	
0.40-0.59	Moderate	0.5	22	6.51		28	8.28		24	7.1		22	6.51	
0.60-0.79	Relatively strong	0.7	8	3.31	31.8	12	4.97	33.9	16	6.63	32.9	4	1.66	27.5
0.80-1.00	Very strong	0.9	15	7.99		19	10.12		15	7.99		13	6.92	
			169			169			169			169		

Note: *-Descriptions, # -Number of Frequency (Freq.), **- Individual Weighted (%), ##-Weighted Mean (%)

7.1.5 Principal Component Analysis (PCA)

PCA is a statistical technique that transforms correlated feature observations into linearly uncorrelated features through orthogonal transformation. The PCA are the newly altered features. It's widely used in predictive modelling and exploratory data analysis. PCA reduces dimensionality by considering variance, which indicates a good split between classes. It begins by computing the dataset's covariance matrix to understand relationships between variables. The matrix is then decomposed into eigenvalues and eigenvectors. Higher eigenvalue components absorb more variance and are retained, while lower ones are eliminated. PCA is linear and utilized in data preprocessing, visualization, and exploratory analysis. Data is transformed into a new coordinate system to identify principal components capturing the most variation (Camdevyren et al., 2005).

Table 7.6. Rotated component matrix for principal component analysis (PCA).

#	Component	
	1	2
V/V_c	0.892	0.158
$V^2/L_R g$	0.835	0.488
$L_R V/v$	0.808	-0.199
H/L_R	0.801	0.315
Vt/L_R	0.664	0.314
D_{50}/L_R	0.601	0.570
W/L_R	0.107	0.864
σ	-0.072	-0.847
d/L_R	0.267	0.720

Note: #- parameters

PCA are independent linear combination of input variables Lu et al. (2003). Acceptable KMO and Bartlett's test values are >0.70 and P-values <0.05, respectively.

In the above technique (Table 7.6), the value of Kaiser–Meyer–Olkin (KMO) and Bartlett's test is 0.791, i.e. > 0.7 and p-value < 0.05. The eigenvalue for the first two components and the rest seven components is > 1 and < 1 respectively. For the total variance explained, the cumulative % is 72.062 and for the rotated component matrix, the eigenvalue of % of the variance is 53.786 (maximum). Hence, the dimension-less group was reduced to the following form (Eq. 7.9)-

$$\frac{d_{st}}{L_R} = f_1\left(\frac{L_R V}{\nu}, \frac{V^2}{L_R g}, \frac{d}{L_R}, \frac{D_{50}}{L_R}, \frac{V}{V_c}, \frac{H}{L_R}, \sigma, \frac{W}{L_R}, \frac{Vt}{L_R}\right) \tag{7.9}$$

7.1.6 Discriminant Analysis (DA)

Discriminant Analysis (DA) is used when the dependent variable is categorical and the predictor or the independent variable is interval in nature (Fisher, 1936). It aims to create discriminant functions, which are linear combinations of independent variables that accurately differentiate between categories of the dependent variable. DA helps assess differences among groups based on predictor variables and evaluates classification accuracy. Interpretation involves examining Wilk's Lambda, where lower values (0 to 1) indicate higher significance, values close to 0 suggest better discrimination, and an F-test with a p-value < 0.05 is considered significant.

For Discriminant Analysis: Eigen Value:0.32, Wilk's Lambda:0.76, Chi-square value:324.15,p-value:0.00, Proportion of variance Explained (%):100.00, Cumulative proportion of variance Explained (%):100.00 and Canonical Correlation: 0.49.

In this analysis, 90.9% of originally grouped cases were correctly classified. Cross-validation is done only for those cases in the analysis. In cross-validation, each case is classified by the functions derived from all cases other than that case 89.9% of cross-validated grouped cases were correctly classified (Table 7.7).

Table 7.7. Structure matrix for discriminant analysis.

Parameters	Vt/L_R	h/L_R	σ	V/V_c	D_{50}/L_R	d/L_R	L_RV/ν	φ	V^2/L_Rg	W/L_R	H/L_R	θ
Function	0.42	-0.27	0.22	0.22	0.19	0.17	0.16	-0.16	0.07	0.06	-0.05	0.00

The dimension-less group was reduced to the following form (Eq. 7.10)-

$$\frac{d_{st}}{L_R} = f_1\left(\frac{L_R V}{\nu}, \frac{V^2}{L_R g}, \frac{d}{L_R}, \frac{V}{V_c}, \frac{h}{L_R}, \theta, \varphi, \sigma, \frac{W}{L_R}, \frac{Vt}{L_R}\right) \tag{7.10}$$

Table 7.8. Weighted mean percentage for PCA and Discriminant analysis.

Frequency	*	Avg. of Frequency	PCA			DA		
			#	**	##	#	**	##
0.00-0.19	Negligible variable	0.1	2	2.22		8	6.67	
0.20-0.39	Weak variable	0.3	1	3.33		3	7.5	
0.40-0.59	Moderate variable	0.5	0	0	61.11	1	4.17	18.33
0.60-0.79	Relatively strong variable	0.7	2	15.56		0	0	
0.80-1.00	Very strong variable	0.9	4	40		0	0	
Total number of Frequency			9			12		

7.1.7 Line of Least Squares Regression (LSR)

The LSR method (Legendre, 1805) is a form of regression analysis used to determine the placement of a best-fit line among data points. It starts with plotting data on a graph with two variables. This linear method aims to create a line that minimizes the sum of squared errors between observed and predicted values. Equations for the best-fit line can be generated using computer software, providing coefficients (Table 7.9) and summary outputs for analysis, explaining variable dependence.

Note: UC-Unstandardized Coefficients, SC-Standardized Coefficients, C- Constant; SE-Std. Error; t- Ratio of the estimated coefficient to its standard error for Table 7.9.

Table 7.9. Coefficients for line of least squares regression.

Parameters	UC		SC	t	p
	B	SE	β		
C	-2.67	0.29		-9.34	0.00
$L_R V/v$	1.65×10^{-07}	0.00	0.01	0.47	0.64
$V^2/L_R g$	-3.52	0.16	-1.73	-22.41	0.00
d/L_R	0.56	0.03	0.48	16.40	0.00
D_{50}/L_R	15.73	1.21	0.47	13.05	0.00
V/V_c	1.39	0.08	0.74	17.09	0.00
H/L_R	0.02	0.01	0.13	3.14	0.00
h/L_R	-1.00	0.12	-0.22	-8.22	0.00
Θ	0.00	0.00	-0.01	-0.45	0.65
$\emptyset$	-0.01	0.00	-0.43	-18.67	0.00
σ	1.46	0.17	0.26	8.39	0.00
W/L_R	0.00	0.01	0.02	0.41	0.68
Vt/L_R	1.2×10^{-06}	0.00	0.63	24.88	0.00

Model summary: R:0.78, R-square: 0.61, Adjusted R Square:0.60, Std. Error of the Estimate:0.21, R Square Change:0.61, Sig. F Change:0.00**;** Predictors: (Constant), Vt/L_R, Θ, φ, h/L_R, σ, L_RV/ν, D_{50}/L_R, d/L_R, H/L_R, W/L_R, V/V_c, V^2/L_Rg and Dependent Variable: d_{st}/L_R

In the above model summary, it was found that (Eq. 7.11),

$$\frac{d_{st}}{L_R} = f_1\left(\frac{L_RV}{\nu}, \frac{V^2}{L_Rg}, \frac{d}{L_R}, \frac{D_{50}}{L_R}, \frac{V}{V_c}, \frac{H}{L_R}, \frac{h}{L_R}, \theta, \varphi, \sigma, \frac{W}{L_R}, \frac{Vt}{L_R}\right) \tag{7.11}$$

From coefficient Table 7.9, it has been seen that the p-value of L_RV/υ, Θ and W/L_R are greater than 0.05, so the dimension-less group was reduced to the following form (Eq. 7.12) -

$$\frac{d_{st}}{L_R} = f_1\left(\frac{V^2}{L_R\,\mathrm{g}}, \frac{d}{L_R}, \frac{D_{50}}{L_R}, \frac{V}{V_c}, \frac{H}{L_R}, \frac{h}{L_R}, \varphi, \sigma, \frac{Vt}{L_R}\right) \tag{7.12}$$

Table 7.10. Weighted mean percentage for line of least squares regression.

Frequency Range		Avg. of Frequency	Frequency	Individual Weighted (%)	Weighted Mean (%)
0.00-0.39	Negligible variable	0.2	6	10	
0.40-0.79	Weak variable	0.6	5	25	
0.80-1.19	Moderate variable	0.1	0	0	50
1.20-1.59	Relatively strong variable	1.395	0	0	
1.60-2.00	Very strong variable	1.8	1	15	
	Total frequency		12		

7.1.8 Enter Regression Analysis (ER)

Linear regression technique for variable selection in which each variable in a block is entered in a single step. This is an appropriate test when dealing with a small set of measured variables and the researcher cannot know which independent variable will produce the best predictor. Each predictor variable is weighted because it is entered after all other independent variables and is weighted according to its contribution to the estimate of the variance of the mean predicted by the other variables entering the model (Montgomery et al., 2012). Variables with the largest R^2 and lowest p value of less than 0.05 were included in the model and considered significant.

Table 7.11. Coefficient for entering regression analysis.

Parameters	UC		SC	t	p
	B	SE	β		
C	-2.68	0.20		-13.16	0
V^2/L_Rg	-3.51	0.16	-1.72	-22.53	0
d/LR	0.57	0.03	0.48	16.72	0
D_{50}/LR	15.79	1.19	0.47	13.28	0
V/VC	1.40	0.07	0.75	18.85	0
H/LR	0.02	0.01	0.13	3.13	0
h/LR	-1.02	0.10	-0.22	-10.51	0
Ø	-0.01	0.00	-0.43	-19.28	0
σ	1.44	0.14	0.26	10.04	0
Vt/LR	1.20×10^{-6}	0.00	0.63	24.94	0

Model summary**:** R:0.78, R-square: 0.61, Adjusted R Square:0.60, Std. Error of the Estimate:0.21, Durbin-Watson:0.44; Predictors: (Constant), Vt/L_R, φ, h/L_R, σ, V/V_C, d/L_R, D_{50}/L_R, H/L_R, V^2/L_Rg. In the above model summary (Table 7.11), it was found that (Eq. 7.13)

$$\frac{d_{st}}{L_R} = f_1\left(\frac{V^2}{L_R\,\mathrm{g}}, \frac{d}{L_R}, \frac{D_{50}}{L_R}, \frac{V}{V_c}, \frac{H}{L_R}, \frac{h}{L_R}, \varphi, \sigma, \frac{Vt}{L_R}\right) \tag{7.13}$$

7.1.9 Forward Regression Analysis (FR)

Forward regression is a linear regression method in which variables are added to the model one by one according to their contribution to improving model fit. It starts with a null model and adds predictions at each step to ensure the best improvement in model fit. This process continues until there is no further improvement in model fit or until stopping is complete (Efroymson,1960). Forward regression is useful when dealing with multiple potential predictors to identify the most likely predictors of different outcomes. Variables with a P value less than 0.05 were considered significant had a larger R^2 and were included in the model.

Table 7.12. Coefficient for forward regression analysis.

Parameters	UC		SC	t	Sig.
	B	*SE*	*β*		
C	-2.68	0.2		-13.16	0
Vt/L_R	1.2 × 10-06	0	0.63	24.94	0
H/L_R	0.02	0.01	0.13	3.13	0
h/L_R	-1.02	0.1	-0.22	-10.51	0
φ	-0.01	0	-0.43	-19.28	0
V^2/L_Rg	-3.51	0.15	-1.72	-22.53	0
V/V_C	1.4	0.07	0.75	18.85	0
d/L_R	0.56	0.03	0.48	16.72	0
D_{50}/L_R	15.79	1.19	0.47	13.28	0
σ	1.44	0.14	0.26	10.04	0

Model summary: R: 0.78, R-square: 0.61, Adjusted R Square:0.60, Std. Error of the Estimate:0.21, R Square Change:0.03, Sig. F Change:0.00; Predictors: (Constant), Vt/L_R, H/L_R, h/L_R, φ, V^2/L_Rg, V/V_c, d/L_R, D_{50}/L_R, σ

In the above model summary (Table 7.12), it was found that (Eq. 7.14),

$$\frac{d_{st}}{L_R} = f_1\left(\frac{V^2}{L_R\,\mathrm{g}}, \frac{d}{L_R}, \frac{D_{50}}{L_R}, \frac{V}{V_c}, \frac{H}{L_R}, \frac{h}{L_R}, \varphi, \sigma, \frac{Vt}{L_R}\right) \tag{7.14}$$

7.1.10 Backward Regression Analysis (BR)

Backward regression (Table 7.13) is a variable selection method where all variables are initially included in the model, then sequentially eliminated based on their partial correlation with the dependent variable. The variable with the smallest partial correlation is removed first, and this process continues until no variables meet the removal criteria (Efroymson,1960). Variables with the highest R^2 and low p-values (<0.05) are considered significant and retained in the model.

Table 7.13. Coefficient for backward regression analysis.

Parameters	UC		SC	t	p
	B	*SE*	*β*		
C	-2.68	0.20		-13.16	0
V^2/L_Rg	-3.51	0.16	-1.72	-22.53	0
d/L_R	0.56	0.03	0.48	16.72	0
D_{50}/L_R	15.79	1.19	0.47	13.28	0
V/V_c	1.40	0.07	0.75	18.85	0
H/L_R	0.02	0.01	0.13	3.13	0
h/L_R	-1.02	0.10	-0.22	-10.51	0
φ	-0.01	0.00	-0.43	-19.28	0
σ	1.44	0.14	0.26	10.04	0
Vt/L_R	0.00	0.00	0.63	24.94	0

Model summary: Removed: L_RV/υ, Θ, W/L_R; R: 0.78, R-square: 0.61, Adjusted R Square:0.60, Std. Error of the Estimate:0.21, R Square Change:0.00, Sig. F Change:0.65; Predictors: (Constant), Vt/L_R, φ, h/L_R, σ, D_{50}/L_R, d/L_R, H/L_R, V/V_c, V^2/L_Rg

In the above model summary (Table 7.13), it was found that (Eq. 7.15),

$$\frac{d_{st}}{L_R} = f_1\left(\frac{V^2}{L_R\,\mathrm{g}}, \frac{d}{L_R}, \frac{D_{50}}{L_R}, \frac{V}{V_c}, \frac{H}{L_R}, \frac{h}{L_R}, \varphi, \sigma, \frac{Vt}{L_R}\right) \tag{7.15}$$

7.1.11 Removed Regression Analysis (RR)

Removed regression is a technique that involves removing variables from a regression model. It starts with all variables in the model and removes one variable at each step. Variables selected for removal are generally those that contribute least to the model based on criteria such as their partial correlation with the dependent variable. This process continues to repeat until no other variables

complete the removal process. The remaining variables in the model are considered significant and are retained. This approach helps simplify the model by eliminating unnecessary variables and improving its interpretability and prediction accuracy (Efroymson, 1960). The variables that are considered significant and included in the model are those with the largest R^2 and low P-values less than 0.05.

Table 7.14. Coefficient for removed regression analysis.

Parameters	UC		SC	t	p
	B	*SE*	*β*		
C	-2.68	0.20		-13.16	0
V^2/L_Rg	-3.51	0.16	-1.72	-22.53	0
d/L_R	0.57	0.03	0.48	16.72	0
D_{50}/L_R	15.79	1.19	0.47	13.28	0
V/V_c	1.40	0.07	0.75	18.85	0
H/L_R	0.02	0.01	0.13	3.13	0
h/L_R	-1.02	0.10	-0.22	-10.51	0
φ	-0.01	0.00	-0.43	-19.28	0
σ	1.44	0.14	0.26	10.04	0
Vt/L_R	0.00	0.00	0.63	24.94	0

Model summary: R: 0.78, R-square: 0.61, Adjusted R Square: 0.60, Std. Error of the Estimate: 0.21, Predictors: (Constant), Vt/L_R, φ, h/L_R, σ, V/V_c, d/L_R, D_{50}/L_R, H/L_R, V^2/L_Rg

In the above model summary (Table 7.14), it was found that (Eq. 7.16),

$$\frac{d_{st}}{L_R} = f_1\left(\frac{V^2}{L_R\,\mathrm{g}}, \frac{d}{L_R}, \frac{D_{50}}{L_R}, \frac{V}{V_c}, \frac{H}{L_R}, \frac{h}{L_R}, \varphi, \sigma, \frac{Vt}{L_R}\right) \tag{7.16}$$

7.1.12 Stepwise Regression Analysis (SWR)

At each step, if the probability of F is small enough, enter the independent variable that is not included in the equation and has the smallest value of F. The F variable that is already in the equal regression will be removed if its probabilities are large enough. This method ends when there are no more variables available to include or exclude. This method combines forward and backward regression to add and remove predictors based on their contribution to the model to avoid incomplete models (Efroymson, 1960). The model included variables with the largest R^2 and low p values (less than 0.05) that were considered statistically significant.

Model summary: R:0.78, R-square: 0.61, Adjusted R Square:0.60, Std. Error of the Estimate:0.21, R Square Change:0.03, Sig. F Change:0.00**;** Predictors: (Constant), Vt/L_R, H/L_R, h/L_R, φ, V^2/L_Rg, V/V_c, d/L_R, D_{50}/L_R, σ

In the above model summary (table 7.15), it was found that (Eq. 7.17),

$$\frac{d_{st}}{L_R} = f_1\left(\frac{V^2}{L_R\,\mathrm{g}}, \frac{d}{L_R}, \frac{D_{50}}{L_R}, \frac{V}{V_c}, \frac{H}{L_R}, \frac{h}{L_R}, \varphi, \sigma, \frac{Vt}{L_R}\right) \tag{7.17}$$

Table 7.15. Coefficient for stepwise regression analysis.

Parameters	UC		SC	t	Sig.
	B	*SE*	*β*		
C	-2.68	0.20		-13.16	0
Vt/L_R	0.00	0.00	0.63	24.94	0
H/L_R	0.02	0.01	0.13	3.13	0
h/L_R	-1.02	0.10	-0.22	-10.51	0
φ	-0.01	0.00	-0.43	-19.28	0
V^2/L_Rg	-3.51	0.16	-1.72	-22.53	0
V/V_c	1.40	0.07	0.75	18.85	0
d/L_R	0.57	0.03	0.48	16.72	0
D_{50}/L_R	15.79	1.19	0.47	13.28	0
σ	1.44	0.14	0.26	10.04	0

Table 7.16. Weighted mean percentage for regression analysis.

Enter, Forward, Backward, Removed, Stepwise Regression					
Frequency Range	Description	Avg. of Frequency	Frequency	Individual Weighted (%)	Weighted Mean (%)
0.00-0.39	Negligible variable	0.2	3	6.67	
0.40-0.79	Weak variable	0.6	5	33.33	
0.80-1.19	Moderate variable	0.1	0	0.00	60
1.20-1.59	Relatively strong variable	1.395	0	0.00	
1.60-2.00	Very strong variable	1.8	1	20.00	
	Total Frequency		9		

7.1.13 Subset Regression Analysis (SSR)

The best subsets regression command involves examining all the models for all possible combinations of predictor variables and determining the best set of predictors for each subset size based on predefined criteria such as the Akaike Information Criterion (AIC) or Bayesian Information Criterion (BIC) (Doe and Smith, 2020). It can be used alternatively in place of the stepwise regression techniques. The best subsets regression is also known as all possible subsets' regression. This method command selects the subset of predictors at each step that fits best, based on the criterion of having the largest R^2.

Model summary: Predictors: V^2/L_Rg, d/L_R, D_{50}/L_R, V/V_c, H/L_R, h/L_R, φ, σ, Vt/L_R; Akaike Information Criterion (AIC): 3676.14; Schwarz Bayesian Criterion (SBC): -3625.39; Mallows' Cp: 7.5; Difference between Cp and Nr of Parameters: 2.5; Std. Error of the Estimate: 0.21; R^2:0.61 and Adj.R^2:0.60

In the above Model summary, it was found that (Eq. 7.18),

$$\frac{d_{st}}{L_R} = f_1\left(\frac{V^2}{L_R\,g}, \frac{d}{L_R}, \frac{D_{50}}{L_R}, \frac{V}{V_c}, \frac{H}{L_R}, \frac{h}{L_R}, \varphi, \sigma, \frac{Vt}{L_R}\right) \tag{7.18}$$

Table 7.17. Weighted mean percentage for subset regression analysis.

Frequency Range	Description	Avg. of frequency	Frequency	Individual weighted %	Weighted Mean (%)
0.00-0.19	Negligible variable	0.1	3	2.5	
0.20-0.39	Weak variable	0.3	0	0	
0.40-0.59	Moderate variable	0.5	0	0	70.00
0.60-0.79	Relatively strong variable	0.7	0	0	
0.80-1.00	Very strong variable	0.9	9	67.5	
	Total Frequency		12		

7.1.14 Mandatory and Additional Components Contributing to Dimensional Parameters

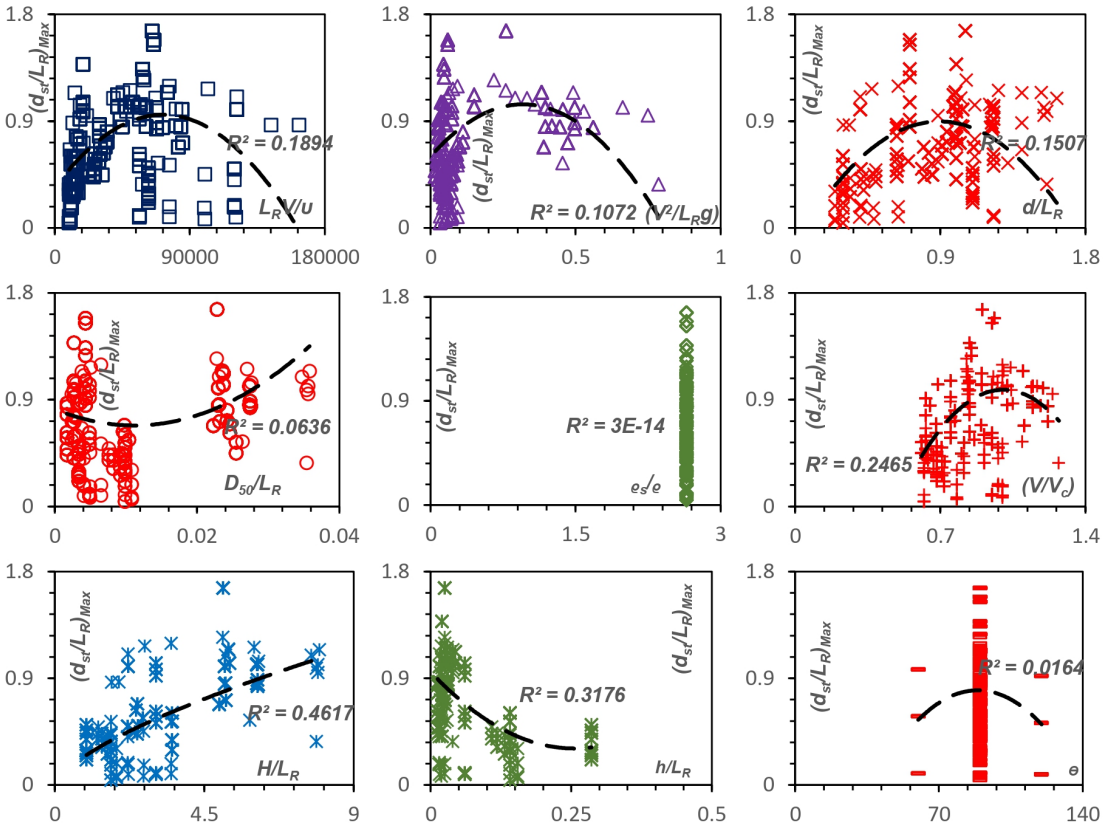

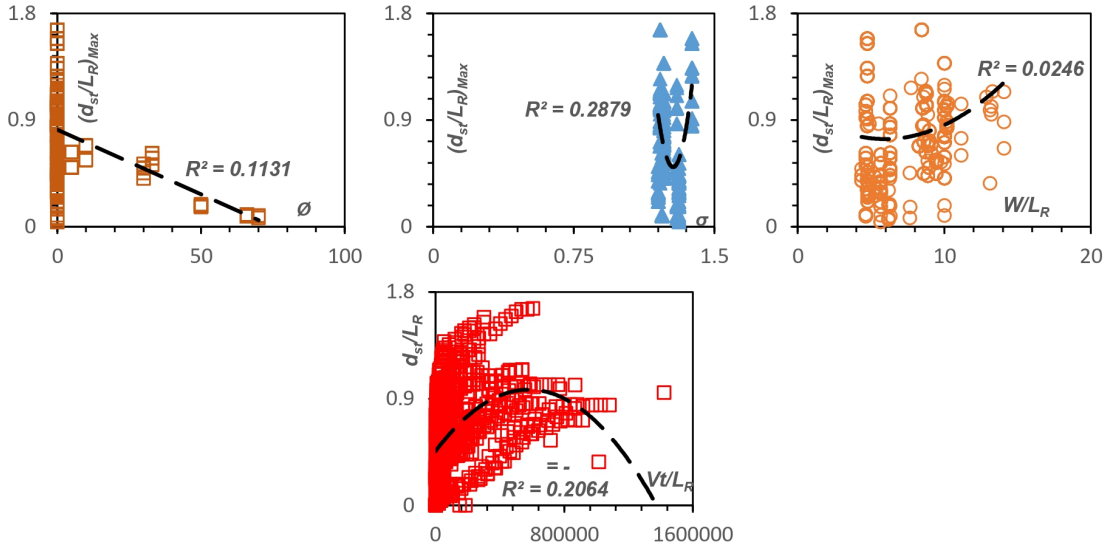

Fig. 7.1. Non-dimensional parameter graphs for all literature data against $(d_{st}/L_R)_{max}$.

After analyzing Fig.7.1, several observations stand out. For L_RV/v, the figure displays a moderate trend with some constant vertical lines, while R^2 indicates it as the strongest parameter. Conversely, for $V^2/L_R\,g$, there's no constant vertical line, making it the strongest parameter both visually and in terms of R^2 value. Similarly, d/L_R shows a moderate trend with constant vertical lines but ranks strongest based on R^2. D_{50}/L_R exhibits a moderate pattern with constant lines but is the weakest based on R^2. ρ_s/ρ is the weakest parameter as it only shows constant vertical lines in the figure and has a low R^2 value. Moving on, V/V_c emerges as the strongest parameter due to the absence of constant vertical lines and a high R^2 value. H/L_R and h/L_R exhibit moderate trends with constant vertical lines but rank strongest according to R^2 values. Conversely, Θ is the weakest parameter, showing constant vertical lines and a low R^2 value. φ and σ similarly rank weakest due to constant vertical lines, although their R^2 values are strong. W/L_R displays a moderate trend with constant lines and a weak R^2 value. Finally, Vt/L_R stands out as the strongest parameter, supported by both its visual representation and high R^2 value, without any constant vertical lines.

So, as per the Fig. 7.1, visualization: Strongest: $V^2/L_R\,g$, V/V_c, Vt/L_R; Moderate: L_RV/v, d/L_R, D_{50}/L_R, H/L_R, h/L_R, W/L_R; Weakest: ρ_s/ρ, Θ, φ, σ.

Similarly, as per the value of R^2: Strongest: L_RV/v, $V^2/L_R\,g$, d/L_R, V/V_c, H/L_R, h/L_R, φ, σ, Vt/L_R; Weakest: D_{50}/L_R, ρ_s/ρ, Θ, W/L_R.

Now combining strength: Strongest: $V^2/L_R\,g$, V/V_c, Vt/L_R; Weakest: ρ_s/ρ, Θ; Strongest and Moderate: L_RV/v, d/L_R, H/L_R, h/L_R; Strongest & Weakest: φ, σ; Moderate and Weakest: D_{50}/L_R, W/L_R.

The following Table 7.18 represents the summary of the all-dimensionality reduction techniques.

Table 7.18. Ultimate summary: fundamental and supplemental components for dimensional parameters.

Dimensionality Reduction Techniques	Additional Components								Mandatory Components
Gamma statistics test	$L_R V/\nu$	D_{50}/L_R	h/L_R	σ	–	–	–	–	
Pearson correlation coefficient	$L_R V/\nu$	–	h/L_R	σ	φ	W/L_R	–	–	
Spearman's rho correlation coefficient	$L_R V/\nu$	–	h/L_R	–	–	W/L_R	H/L_R	–	
Kendall's tau-b correlation coefficient	$L_R V/\nu$	D_{50}/L_R	–	σ	–	W/L_R	H/L_R	–	
Principal component analysis	$L_R V/\nu$	D_{50}/L_R	–	σ	–	W/L_R	H/L_R	–	$V^2/L_R g$,
Discriminant analysis	$L_R V/\nu$	–	h/L_R	σ	φ	W/L_R	–	Θ	d/L_R,
Line of least squares regression	–	D_{50}/L_R	h/L_R	σ	φ	–	H/L_R	–	V/V_c,
Enter regression analysis	–	D_{50}/L_R	h/L_R	σ	φ	–	H/L_R	–	Vt/L_R
Forward regression analysis	–	D_{50}/L_R	h/L_R	σ	φ	–	H/L_R	–	
Backward regression analysis	–	D_{50}/L_R	h/L_R	σ	φ	–	H/L_R	–	
Removed regression analysis	–	D_{50}/L_R	h/L_R	σ	φ	–	H/L_R	–	
Stepwise regression analysis	–	D_{50}/L_R	h/L_R	σ	φ	–	H/L_R	–	
Subset regression analysis	–	D_{50}/L_R	h/L_R	σ	φ	–	H/L_R	–	

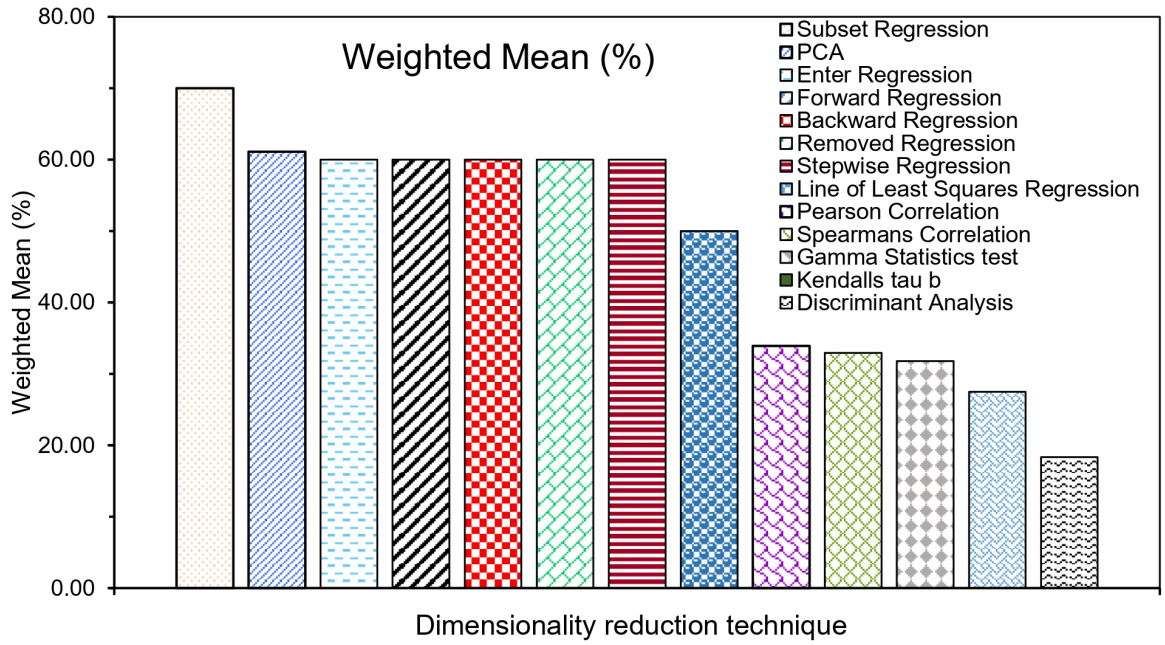

Fig 7.2. Weighted Mean (%) for different dimensionality reduction techniques.

7.1.15 Identify Optimal Technique using Weighted Mean Percentage Method

The Weighted Mean Percentage method (Fig. 7.2) determines the optimal technique by assigning weights (Tables 7.5, 7.8, 7.10, 7.16 and 7.17) to methods or criteria based on their perceived importance. In this analysis of scour depth prediction for spur dikes, Subset Regression emerges as the most influential technique (70%), followed by PCA (61.2%). Subset Regression selects predictor variables effectively, particularly beneficial for complex datasets, while PCA aids in identifying patterns. Conversely, Discriminant Analysis has the lowest weighted mean percentage (18.33%), suggesting limited suitability for scour depth prediction due to mismatched assumptions or dataset characteristics. This insight encourages researchers to seek more appropriate methods for improving scour prediction models in hydraulic engineering applications.

Chapter 8
Results and Discussion

8.1 Literature Data Compared to Empirical Formulas

To ensure the accuracy of data collected from Scopus and Google Scholar, a comprehensive comparison was conducted between all literature datasets and empirical formulas used for calculating scour depth in Spur dikes. This rigorous analysis aimed to evaluate how well the empirical formulas align with the literature data, providing insights into their accuracy and applicability across different scenarios. Empirical formulas proposed by Pandey et al. (2020), Karimi et al. (2012a, b), Nasrollahi et al. (2008), Kothyari et al. (2007), Yanmaz and Kose (2007), Coleman et al. (2003), and Oliveto and Hager (2002) were employed for this comparison.

By scrutinizing the agreement or discrepancies between the predicted scour depths and the actual measurements from the literature, researchers could ascertain the reliability and limitations of each formula. This thorough examination facilitated the identification of which empirical formula performed optimally for various datasets. Furthermore, it provided valuable guidance for selecting appropriate models in practical applications related to spur dike scour depth prediction.

Overall, this verification process upheld the integrity of the dataset, ensuring confidence in its reliability for further research and analysis in the field. It served as a crucial step in validating the accuracy of data obtained from literature sources and enhancing our understanding of spur dike scour depth prediction methodologies.

In Fig. 8.1 and Fig. 8.9a, the equation of Pandey et al. (2020) was applied to all data. It was observed that Pandey et al.'s data fell within the ±30% perfect agreement line (PAL) range, along with some data points from Masood, Khassaf, and Lodhi. However, the majority of literature data did not entirely fall within this threshold. Pandey et al. (2020) emerged as the most suitable data, while Alasadi et al. (2023), Patel and Kumar (2023), Farshad et al. (2022), Ning et al. (2019), and even Pandey et al. (2014a, 2014b) represented the least fitting literature data. Consequently, this formula was not deemed suitable for all types of data.

Similarly, in Fig. 8.2 and Fig. 8.9b, all data were analyzed using the equation of Karimi et al. (2012a). It was observed that the majority of literature data, including Karimi et al. (2012a), fell within the ±30% PAL, except for Alasadi et al. (2023), Patel and Kumar (2023), Masood et al. (2021), and Nasrollahi et al. (2008). Some data points from Khassaf and Abbas (2018), and Lodhi et al. (2018, 2017), also fell within the ±30% PAL range. Karimi et al. (2012a) emerged as the best-fitting data, while Alasadi et al. (2023) represented the least accurate literature data. Hence, this formula's application appeared to be nearly appropriate for all data types.

In a similar vein, Fig. 8.3 and Fig. 8.9c, applied the equation of Karimi et al. (2012b) to all datasets. It was illustrated that the majority of literature data, including Karimi et al. (2012b), aligned within the ±30% PAL range, except for Alasadi et al. (2023) and Patel and Kumar (2023). Some data points from Lodhi et al. (2018, 2017), and Nasrollahi et al. (2008), fell within the ±30% PAL range. Karimi et al. (2012 a, b), and Pandey et al. (2014b) emerged as the most suitable data,

while Alasadi et al. (2023) and Patel and Kumar (2023) represented the least accurate literature data. Hence, the application of these formulas appeared to be nearly suitable for all data types.

Similarly, in Fig. 8.4 and Fig. 8.9d, all data underwent analysis using the equation of Nasrollahi et al. (2008). Literature data from Pandey, Farshad, Ning, and Karimi fell within the ±30% PAL, except for Alasadi, Patel and Kumar, and Masood. Additionally, some data points from Khassaf, Lodhi, and Nasrollahi also fell within the ±30% PAL range. Karimi et al. (2012a) emerged as the most suitable data, whereas Alasadi, Patel and Kumar, and Masood represented the least accurate literature data. Consequently, this formula's application was deemed not nearly suitable for all data types.

Similarly, in Fig. 8.5 and Fig. 8.9e, all data were subjected to the equation of Kothyari et al. (2007). The figure revealed that the majority of literature data of Pandey et al. (2014a) aligned within the ± 30% PAL, except for Patel & Kumar, Karimi, and Nasrollahi. Some data points from Alasadi, Farshad, Pandey, Khassaf, and Lodhi fell within the ±30% PAL range. Pandey et al. (2014a) emerged as the most suitable data, while Patel and Kumar represented the least accurate literature data. Consequently, this formula's application was deemed not appropriate for all data types.

Similarly, in Fig. 8.6 and Fig. 8.9f, all data were analyzed using the equation of Yanmaz and Kose (2007). The figure showed that the literature data of Pandey and Karimi fell within the ±30% PAL, except for Alasadi, Masood, and Khassaf. Some data points from Patel, Farshad, Ning, Lodhi, and Nasrollahi fell within the ± 30% PAL range. Pandey et al. (2019) and Karimi et al. (2012a) emerged as the most fitting data, while Alasadi, Masood, and Khassaf represented the least accurate literature data. Consequently, this formula's application was not appropriate for all data types.

Similarly, in Fig. 8.7 and Fig. 8.9g, all data were analyzed using the equation of Coleman et al. (2003). The figure indicated that the majority of literature data of Pandey et al., Ning et al. (2019), and Karimi et al. (2012a, b) fell within the ± 30% PAL, except for the data from Alasadi et al. (2023) and Patel and Kumar (2023). Some data points from Farshad et al. (2022), Khassaf and Abbas (2018), Lodhi et al. (2018, 2017), and Nasrollahi et al. (2008) fell within the ±30% PAL range. Ning et al. (2019) and Karimi et al. (2012a, b) emerged as the most fitting data, while the literature data from Alasadi et al. (2023) and Patel and Kumar (2023) represented the least accurate. Consequently, the application of this formula was deemed unsuitable for all types of data.

Similarly, in Fig. 8.8 and Fig. 8.9h, all data were analyzed using the equation of Oliveto and Hager (2002). The figure indicated that the majority of literature data of Pandey et al. (2019) and Karimi et al. (2012a, b) fell within the ±30% PAL, except for the remaining literature data. Some data points from Pandey et al. (2020) and Khassaf and Abbas (2018) fell within the ±30% PAL range. Pandey et al. (2019) emerged as the most fitting data, while the majority of the remaining literature data represented the least accurate data. Consequently, this formula's application was not appropriate for all data types.

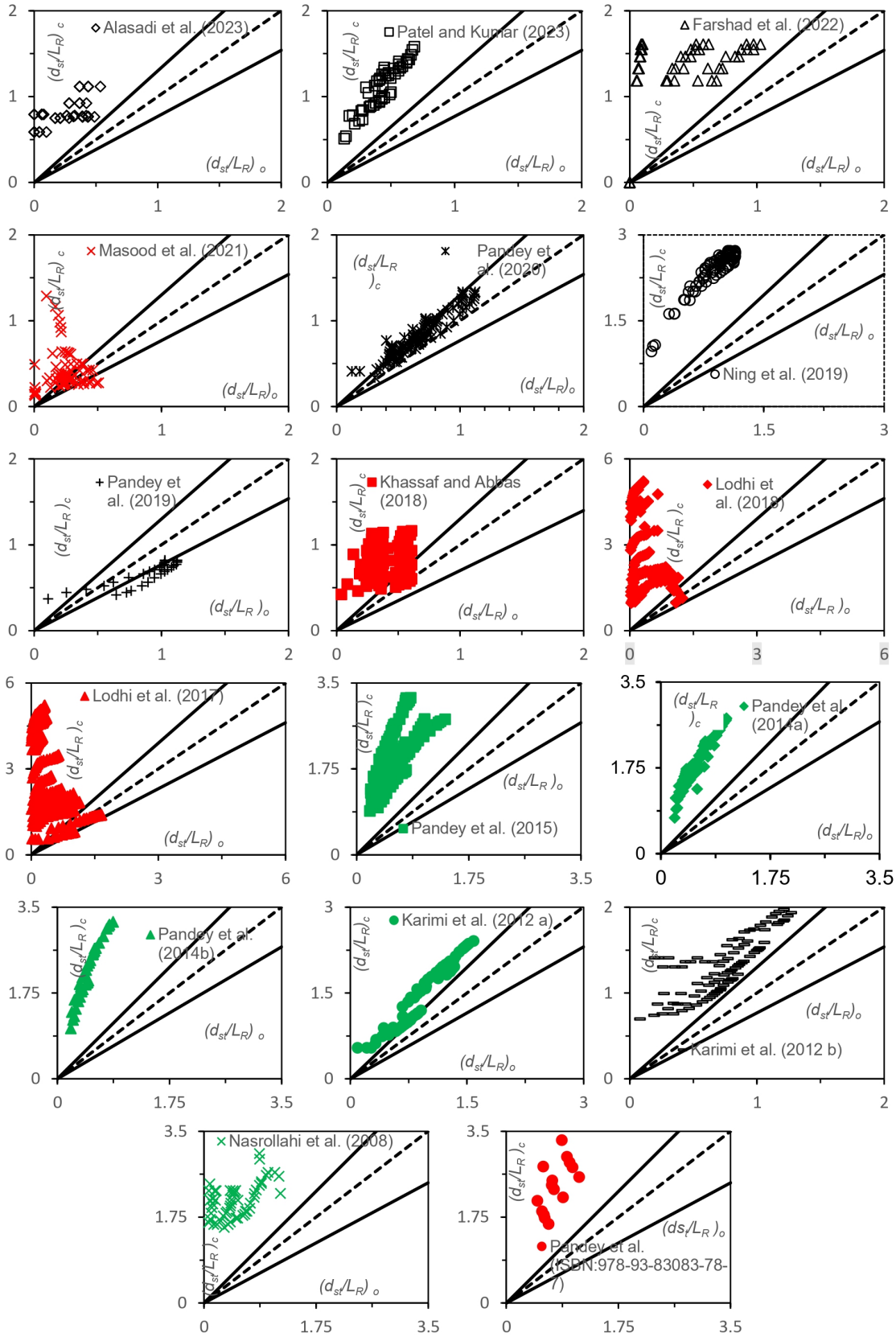

Fig. 8.1. Comparison of all literature data against the empirical formula of Pandey et al. (2020).

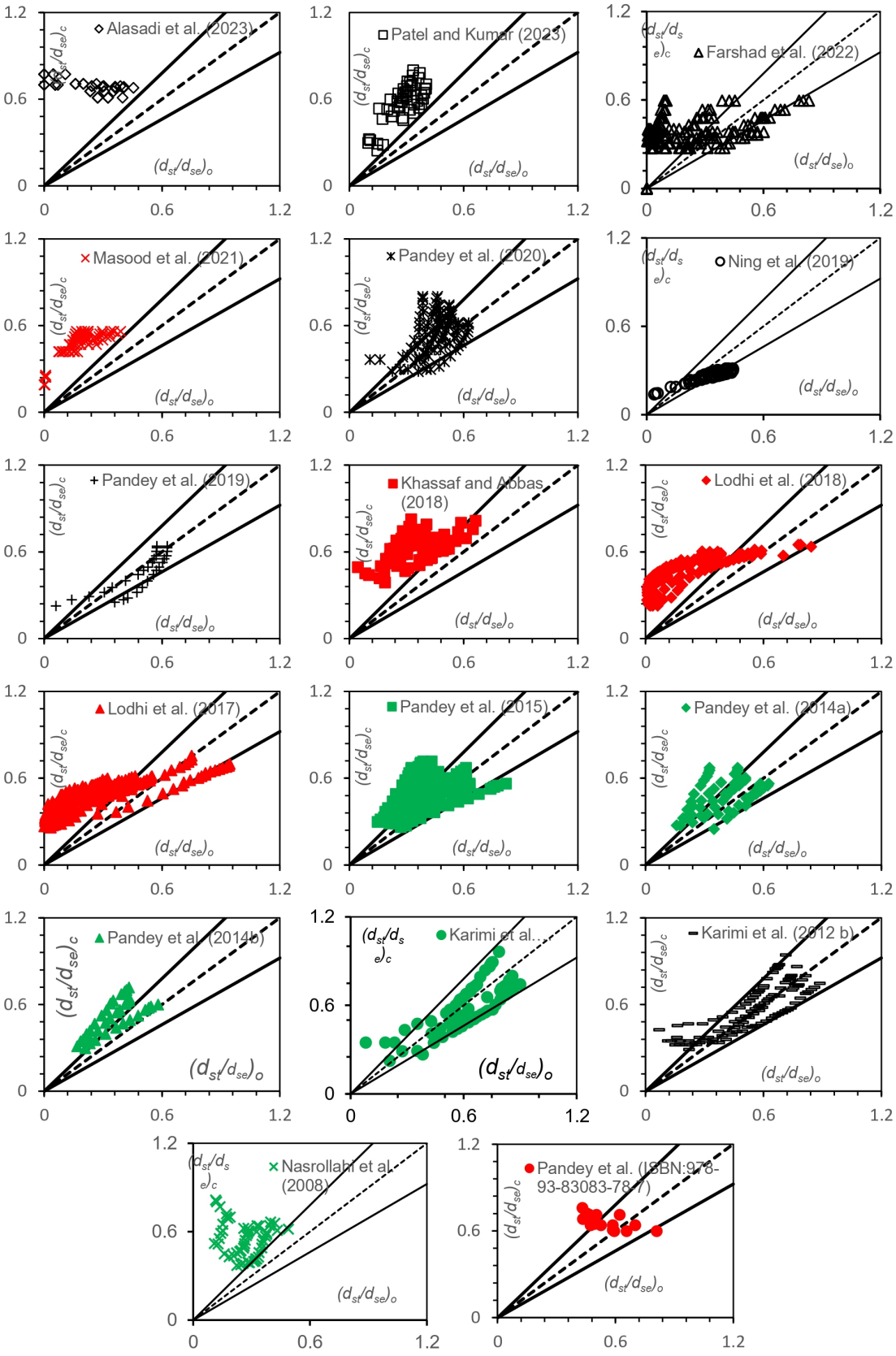

Fig. 8.2. Comparison of all literature data against the empirical formula of Karimi et al. (2012a).

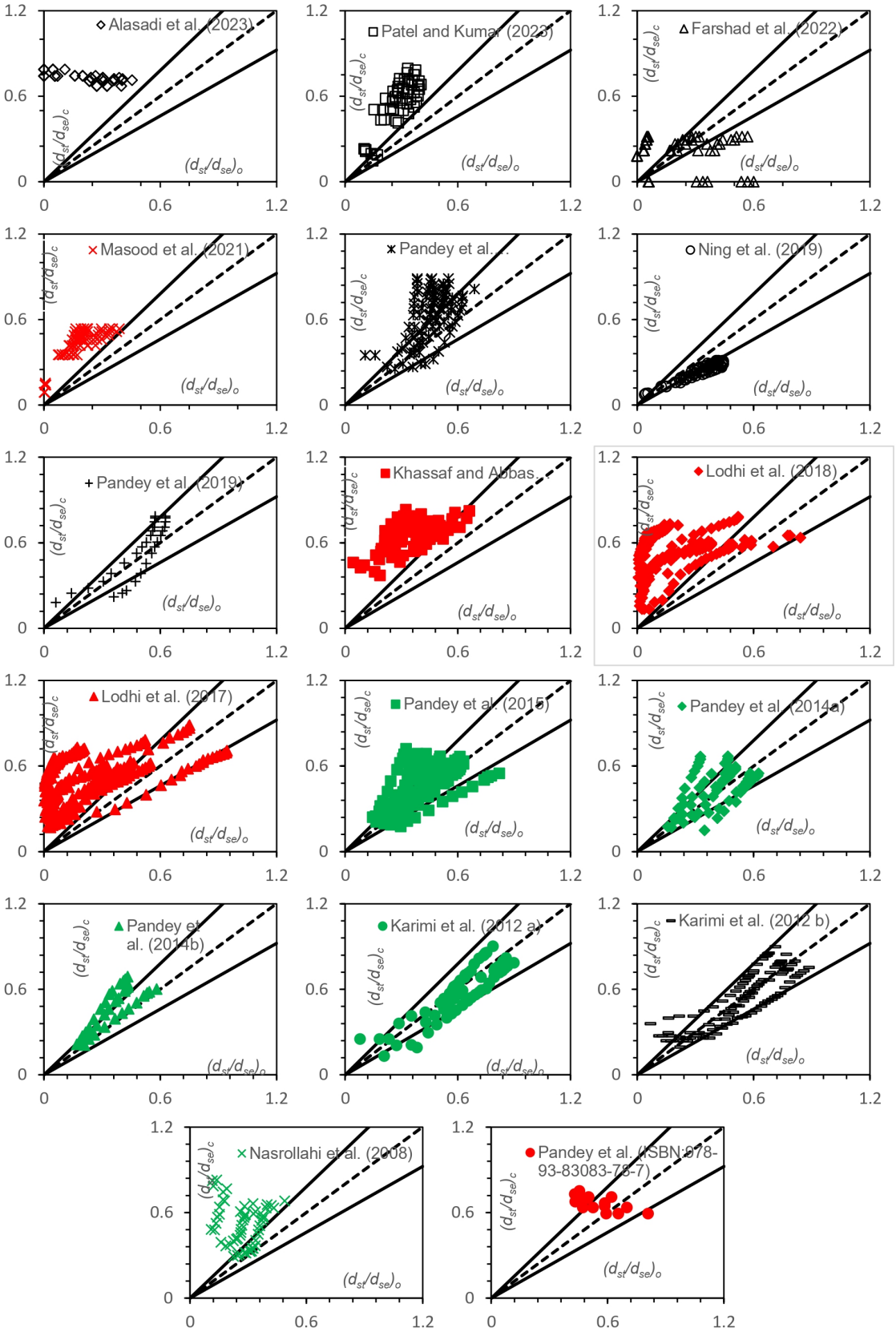

Fig. 8.3. Comparison of all literature data against the empirical formula of Karimi et al. (2012b).

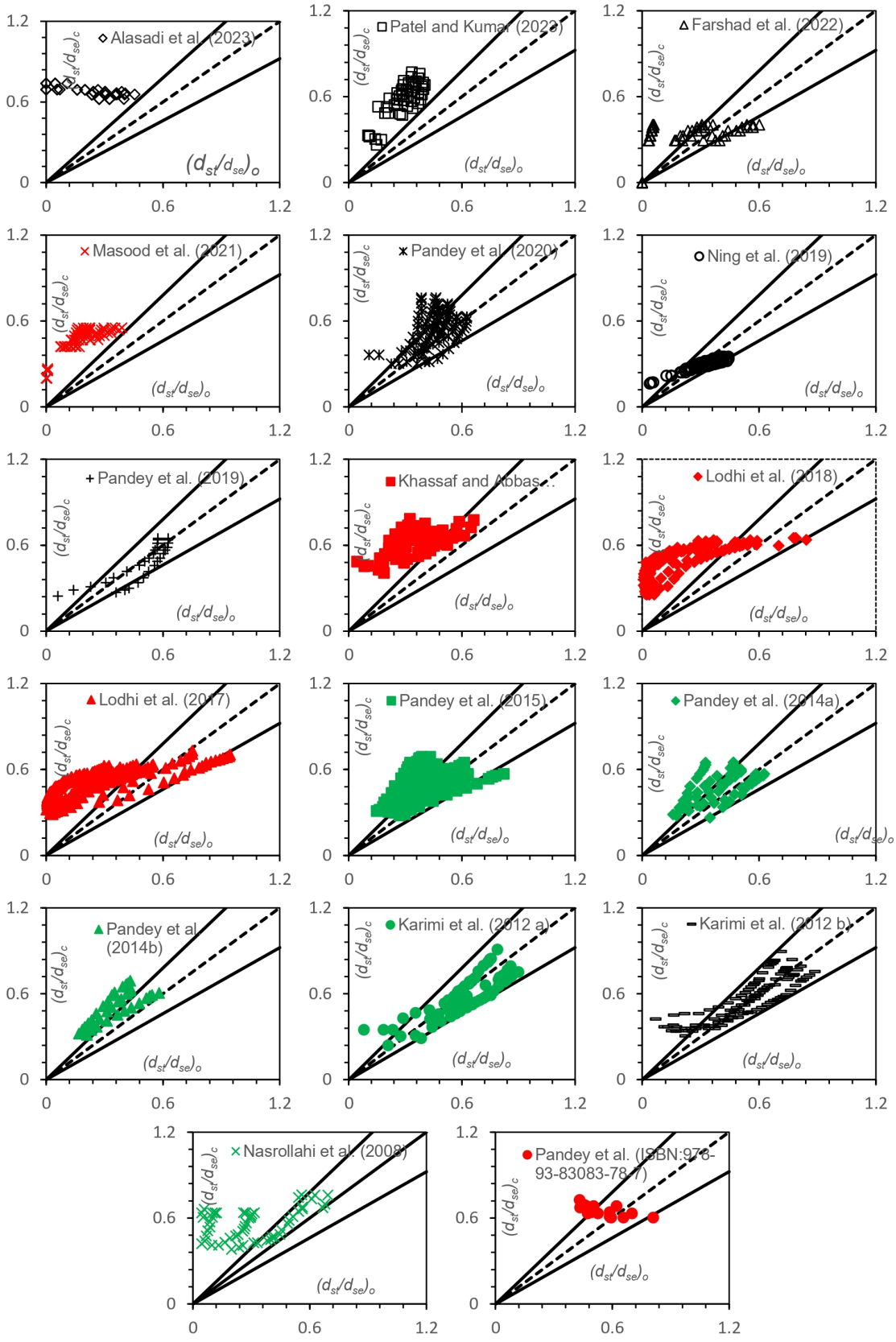

Fig. 8.4. Comparison of all literature data against the empirical formula of Nasrollahi et al. (2008).

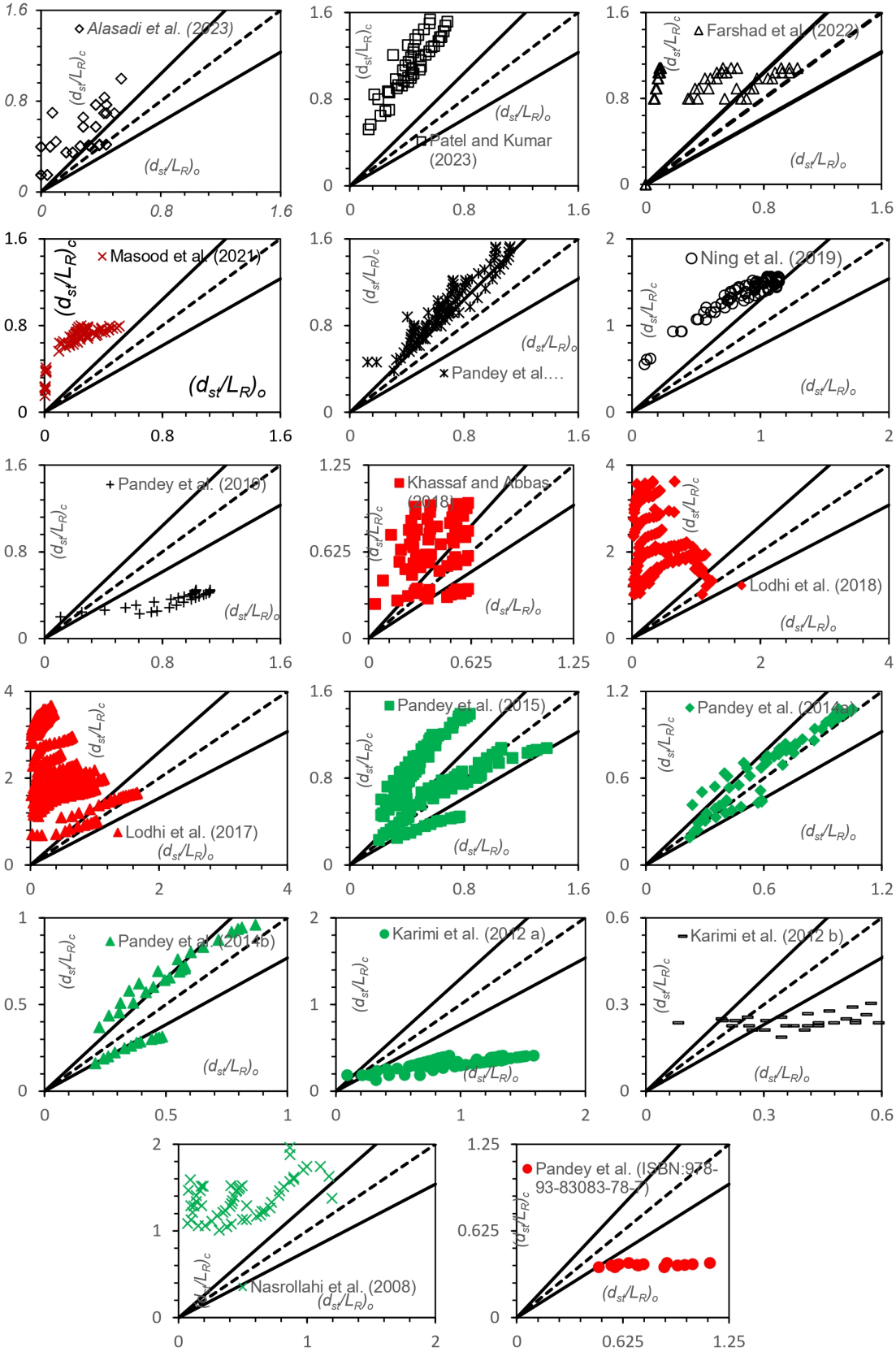

Fig. 8.5. Comparison of all literature data against the empirical formula of Kothyari et al. (2007).

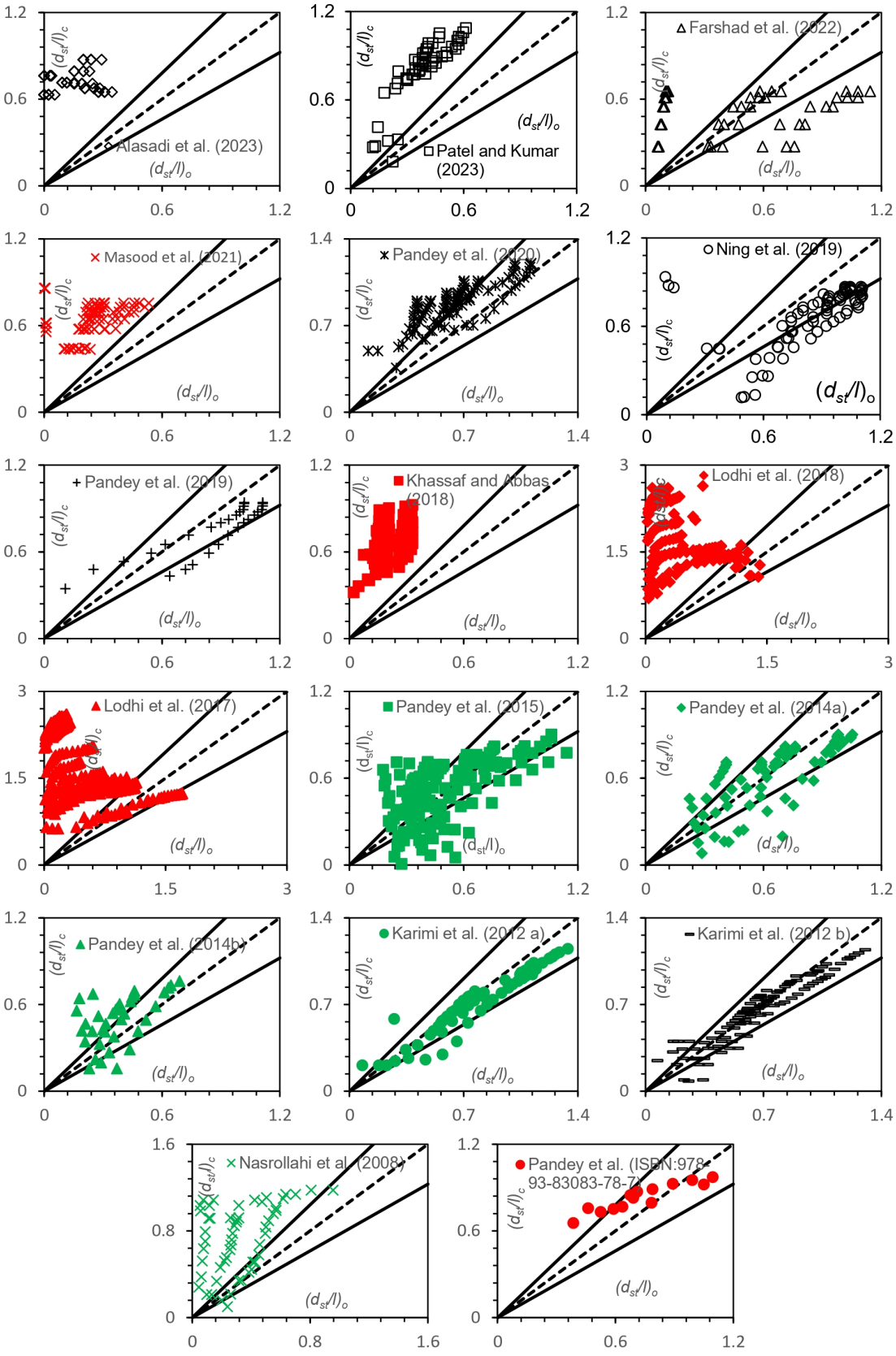

Fig. 8.6. Comparison of all literature data against the empirical formula of Yanmaz and Kose (2007).

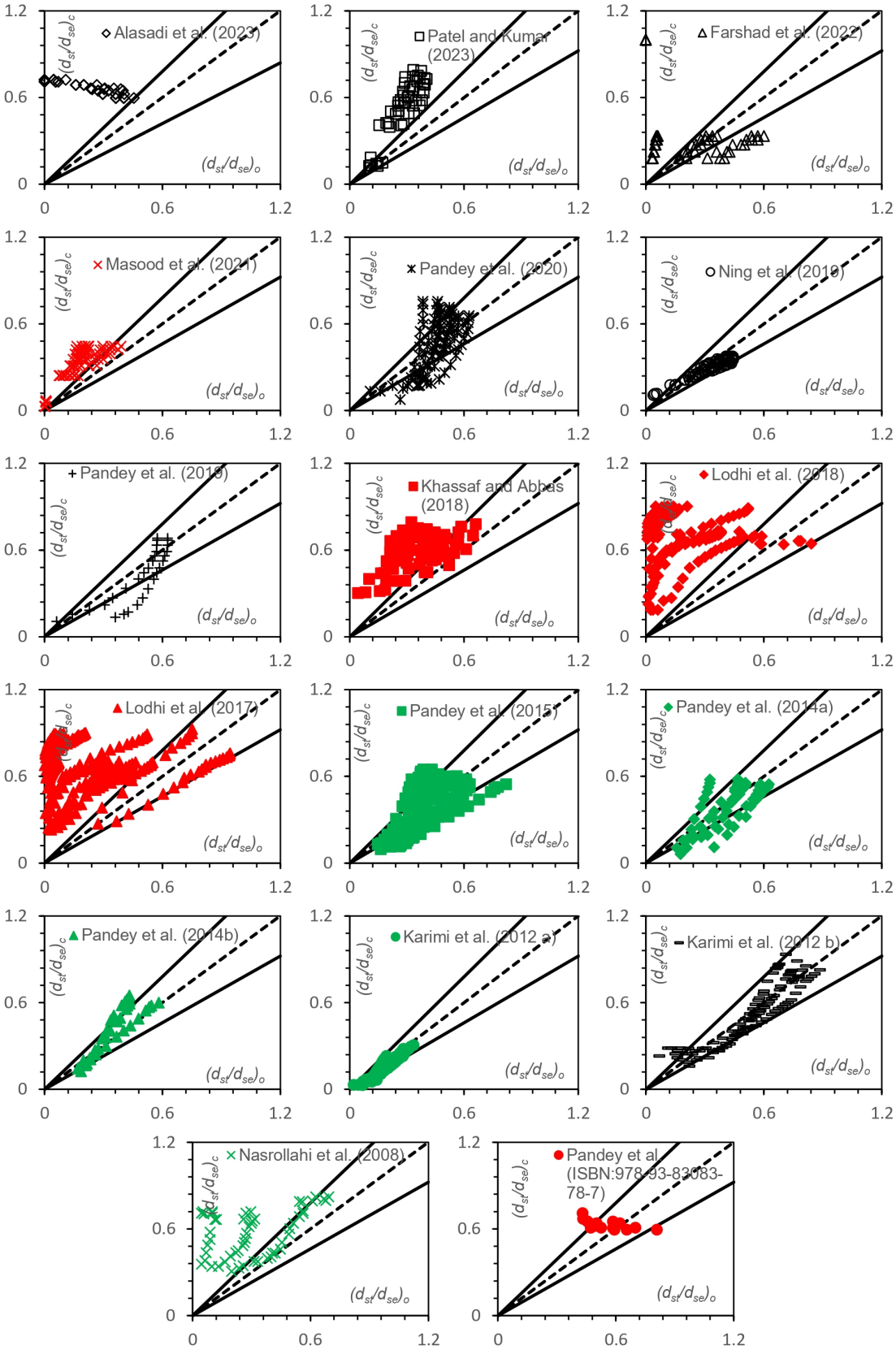

Fig. 8.7. Comparison of all literature data against the empirical formula of Coleman et al. (2003).

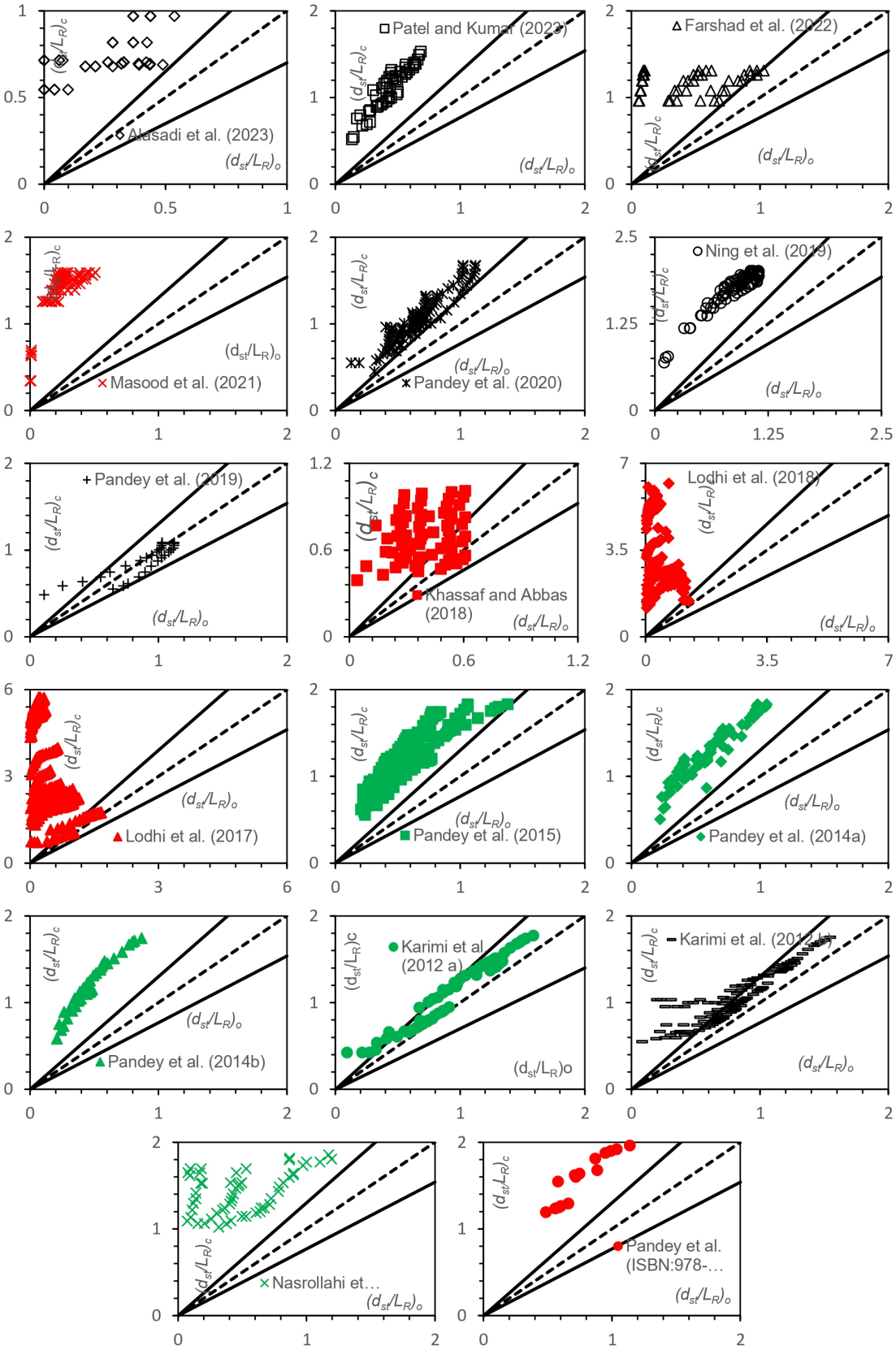

Fig. 8.8. Comparison of all literature data against the empirical formula of Oliveto and Hager (2002).

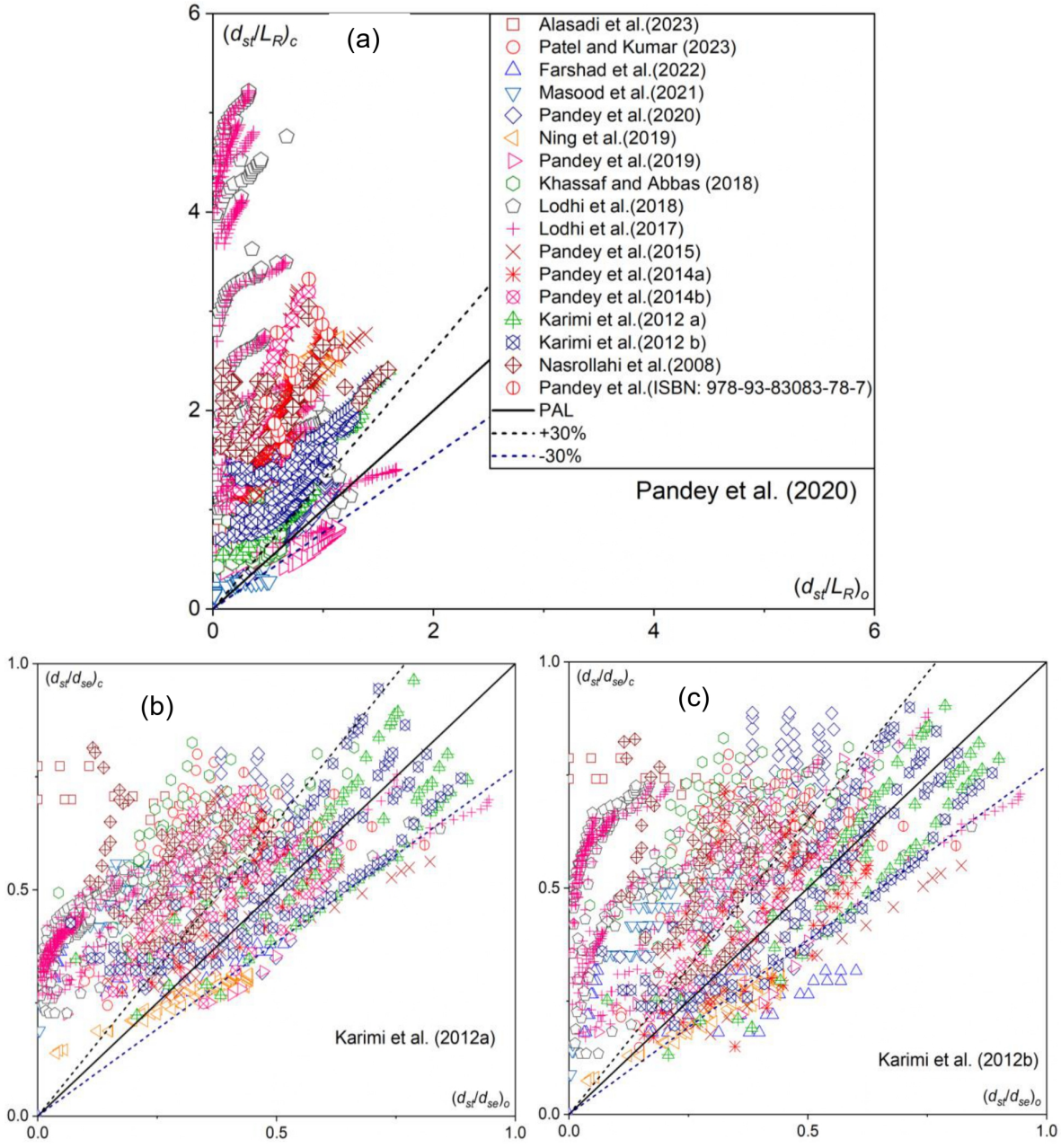
(a)
$(d_{st}/L_R)_c$
$(d_{st}/L_R)_o$
Alasadi et al.(2023)
Patel and Kumar (2023)
Farshad et al.(2022)
Masood et al.(2021)
Pandey et al.(2020)
Ning et al.(2019)
Pandey et al.(2019)
Khassaf and Abbas (2018)
Lodhi et al.(2018)
Lodhi et al.(2017)
Pandey et al.(2015)
Pandey et al.(2014a)
Pandey et al.(2014b)
Karimi et al.(2012 a)
Karimi et al.(2012 b)
Nasrollahi et al.(2008)
Pandey et al.(ISBN: 978-93-83083-78-7)
PAL
+30%
-30%
Pandey et al. (2020)
(b)
$(d_{st}/d_{se})_c$
$(d_{st}/d_{se})_o$
Karimi et al. (2012a)
(c)
$(d_{st}/d_{se})_c$
$(d_{st}/d_{se})_o$
Karimi et al. (2012b)

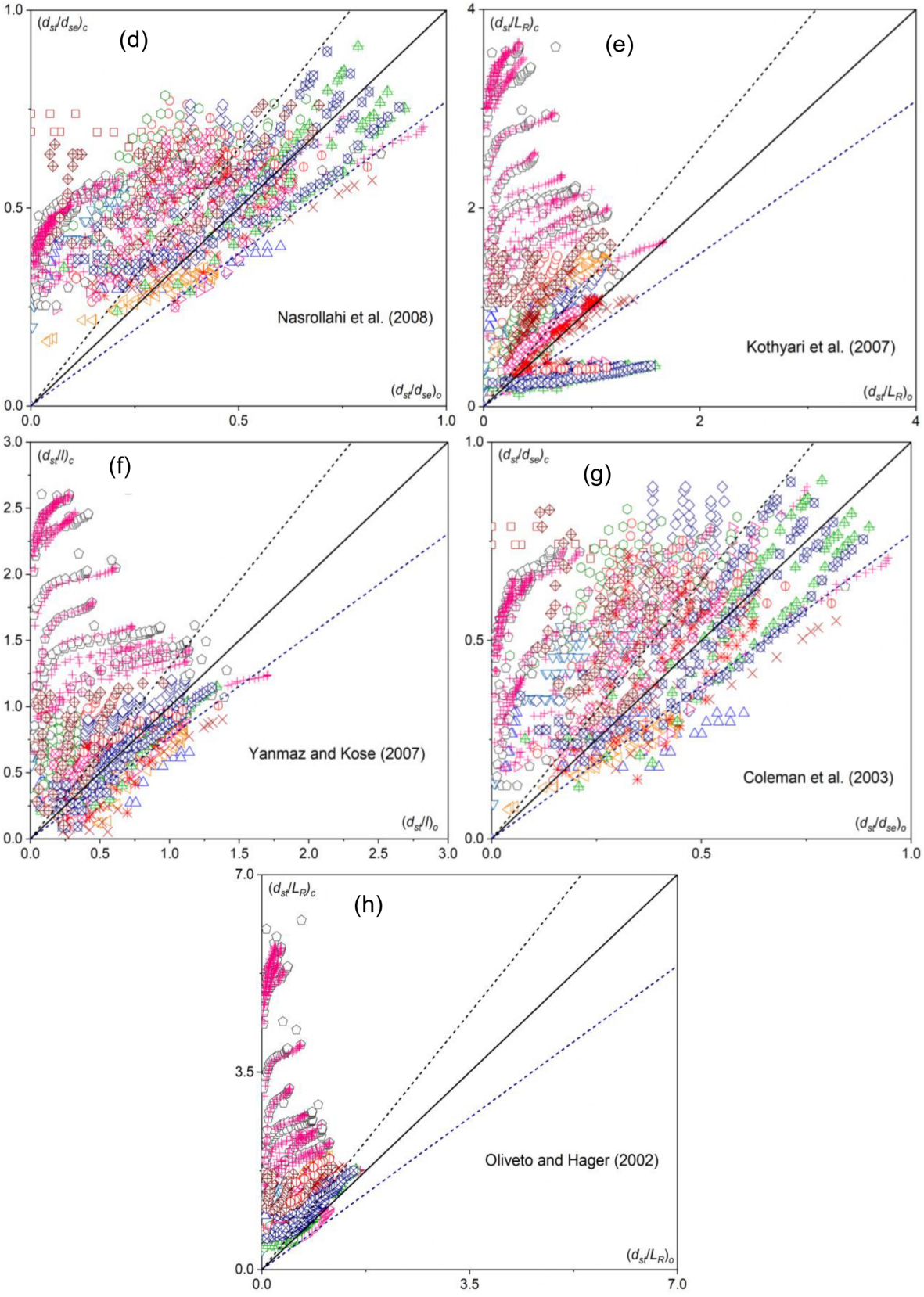

Fig. 8.9. Comparison of all literature data against the empirical formulas.

8.2 Findings and Interpretations

The findings reveal a novel temporal scour depth formula developed for spur dikes, followed by rigorous validation against existing empirical formulas. Statistical analysis assigns weightage to indicators (R^2, RMSE, NSE and MBE), illuminating the influence of each formula, including the newly developed one. Ultimately, a comprehensive ranking elucidates the superior performance of the most promising formulas over the past two decades in predicting scour depths around spur dikes. The details regarding the findings and interpretations are presented below.

8.2.1 New Formula Developed for Temporal Scour

Utilizing 932 data points out of 1670 data points, predictions are made regarding the time variation of scour depth under clear water scour conditions ($V/V_c \leq 1$). These findings serve as the basis for discussing how flow and spur dike design parameters influence the temporal evolution of spur dike scour depth. The study concludes by introducing a new predictive model for spur dike scour depth, which outperforms previous literature equations. Graphs are utilized to depict the trend lines and the significant correlations of these parameters with $(d_{st}/L_R)_o$.

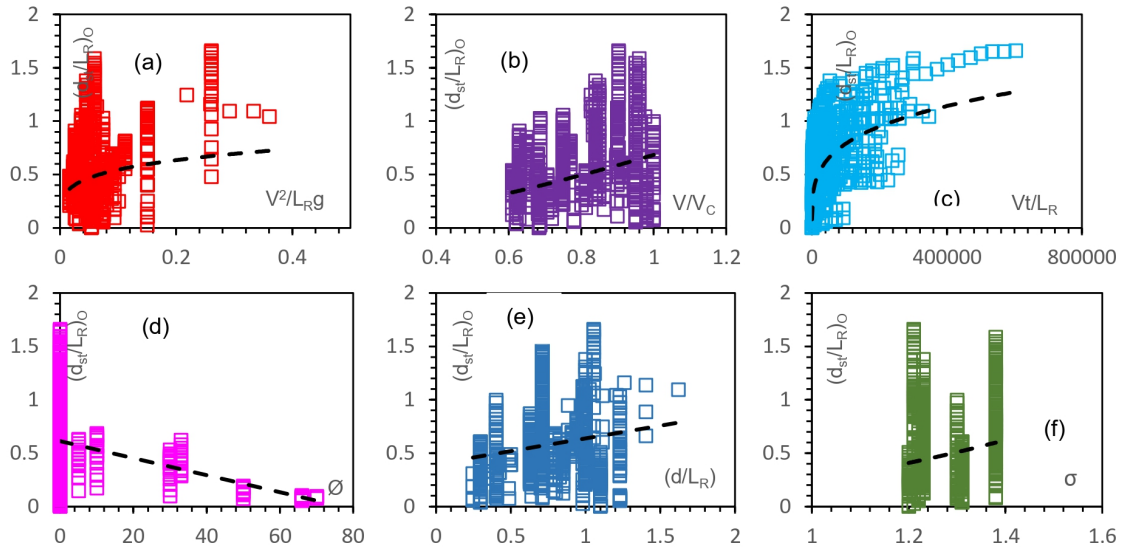

Fig. 8.10. Non-dimensional parameter graphs for 932 data points against $(d_{st}/L_R)_o$.

Here, in this study, a total of eight previously proposed formulas (Table 4.1) along with our newly proposed formula (Eq. 8.1), to compute d_{st}, have been considered in terms of their performance with 16 previous literature data. All data are taken with respect to the CWS condition.

$$\frac{d_{st}}{L_R} = (a_1) f_1\left[\left(\frac{V^2}{L_R g}\right)^{b_1}\right] f_2\left[\left(\frac{V}{V_C}\right)^{c_1}\right] f_3\left[\left(\frac{Vt}{L_R}\right)^{e_1}\right] f_4\left[(1-0.01\Phi)^{g_1}\right] f_5\left[\left(\frac{d}{L_R}\right)^{h_1}\right] f_6\left[(\sigma)^{i_1}\right] \quad (8.1)$$

The CWS prediction formulas are presented in the following form of the product of the individual parameter function. The scour function a_1 is estimated as 0.075 for the current study. The separate effects of the Re and Fr are eliminated after applying the dimensionality reduction

technique on the basis of the subset regression of the intra-parameter. The parameter functions are represented by Eqs. 8.2–8.7.

$$f_1\left[\left(\frac{V^2}{L_R g}\right)^{b_1}\right]=\left(\frac{V^2}{L_R g}\right)^{-0.144} \tag{8.2}$$

$$f_2\left[\left(\frac{V}{V_C}\right)^{c_1}\right]=\left(\frac{V}{V_C}\right)^{1.930} \tag{8.3}$$

$$f_3\left[\left(\frac{Vt}{L_R}\right)^{e_1}\right]=\left(\frac{Vt}{L_R}\right)^{0.188} \tag{8.4}$$

$$f_4\left[\left(1-0.01\Phi\right)^{g_1}\right]=\left(1-0.01\Phi\right)^{2.197} \tag{8.5}$$

$$f_5\left[\left(\frac{d}{L_R}\right)^{h_1}\right]=\left(\frac{d}{L_R}\right)^{0.659} \tag{8.6}$$

$$f_6\left[\left(\sigma\right)^{i_1}\right]=\left(\sigma\right)^{2.036} \tag{8.7}$$

All the parameter functions considered in Eq. (8.1), are shown in Figs. 8.10 (a-f).

The parameter function of V^2/L_Rg has taken power relationship (Fig. 8.10 a). The V^2/L_Rg graph illustrates the impact on the maximum dimensionless temporal scour depth (dst/L_R) variation, indicating a clear increase in the d_{st}/L_R ratio with rising V^2/L_Rg. The V^2/L_Rg predominantly relies on approach velocity and particle size.

The dimensionless scour depth increases with respect to the increase of the flow intensity (V/V_c) [Fig. 8.10(b)]. The parameter function of (V/V_c) follows the power law.

The parameter function of dimensionless time (Vt/L_R) has followed the power trend ([Fig. 8.10 (c)]. The Vt/L_R demonstrates a clear increase in temporal scour depth variation with higher values of Vt/L_R.

Porosity (Φ) has a notable influence on temporal scour depth variation, with changes in porosity [Fig. 8.10(d)], affecting sediment transport dynamics and consequently modifying scour depth over time. it is demonstrated that the trend line exhibits of linear relationship.

Figure 8.10e depicts the impact of the ratio of approach flow depth to the reference length of the spur dike on the dimensionless temporal scour depth variation. This ratio, known as flow shallowness (Lanca et al., 2013), affects scour depth, with temporal scour depth increasing as flow shallowness rises, particularly noticeable for smaller spur dike reference lengths. The trend of the parameter function of the d/L_R plot is followed as a linear relationship.

The parameter function σ (Fig. 8.10f) is represented by the power relationship trend, exerts a notable influence on temporal scour depth variation, reflecting the variability in sediment particle sizes. Higher standard deviations indicate a wider range of particle sizes, potentially leading to increased scour depth fluctuations over time.

8.2.2 Comparison of New and Literature Formulas Using Statistical Measures

A total of 932 test data were gathered from various literature sources for local bed scour ($V/V_c \leq 1$). From this pool, 728 data points (80% of the total) were randomly selected for constructing a regression model, which employed both Gauss-Newton and Levenberg-Marquardt methods. The remaining 204 data points (20%) were reserved for validating the regression model and comparing it with other empirical equations found in the literatures.

The temporal variation of scour depth (d_{st}) over time can be expressed as a function of several parameters including ρ, υ, g, d, V, D_{50}, ρ_s, V_c, l, H, h, Θ, φ, Re, F_d, σ, W, and t. To simplify the analysis, dimensional analysis was conducted resulting in non-dimensional parameters such as $L_R V/\upsilon$, $V^2/L_R g$, d/L_R, D_{50}/L_R, ρ_s/ρ, V/V_c, H/L_R, h/L_R, Θ, φ, W/L_R, σ, and Vt/L_R.

Moreover, 13 dimensional reduction methods were explored, among which the Subset regression method was deemed optimal. Non-dimensional parameters including $V^2/L_R g$, d/L_R, D_{50}/L_R, V/V_c, H/L_R, h/L_R, φ, σ, and Vt/L_R were identified for developing the regression model. Various nonlinear regression models were then formulated, leading to the final equation (Eq. 8.8) for estimating time-dependent scour depth.

$$\frac{d_{st}}{L_R} = (0.075)\left(\frac{V^2}{L_R g}\right)^{-0.144}\left(\frac{V}{V_C}\right)^{1.930}\left(\frac{Vt}{L_R}\right)^{0.188}(1-0.01\Phi)^{2.197}\left(\frac{d}{L_R}\right)^{0.659}(\sigma)^{2.036} \tag{8.8}$$

Table 8.1. Comparison between training and testing data.

COMPARE	R^2	RMSE	NSE	MBE	Pin (10%)	Pin (20%)	Pin (30%)
Training	0.84	0.13	0.96	0.003	36.26	62.91	77.06
Validation	0.83	0.13	0.96	-0.020	36.26	67.65	77.94

Figures 8.11, 8.12 and 8.13 show good agreement between the measured and developed regression model in training and validation. The coefficient of determination for the training and validation of the model are R^2=0.84 and R^2=0.83 respectively (Table 8.1). This figure indicates that almost 100% of the validation data are confined to ±10%,20% and 30% limits. Therefore, Eq. (8.8) is a practical and simple equation which can be used with high accuracy.

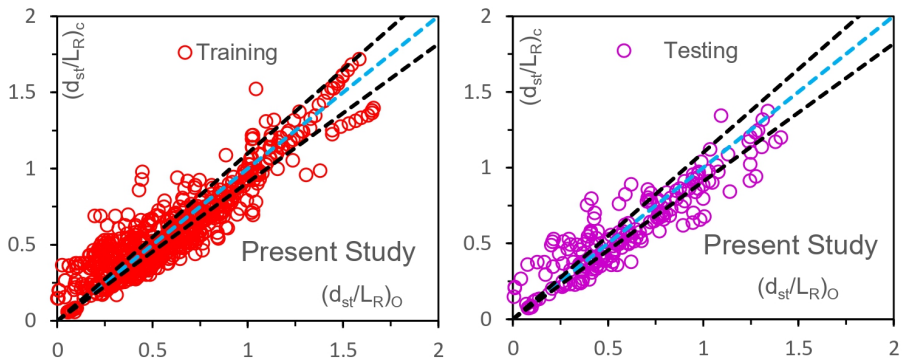

Fig. 8.11. Comparison between training and testing data for (±10% perfect agreement line, PAL).

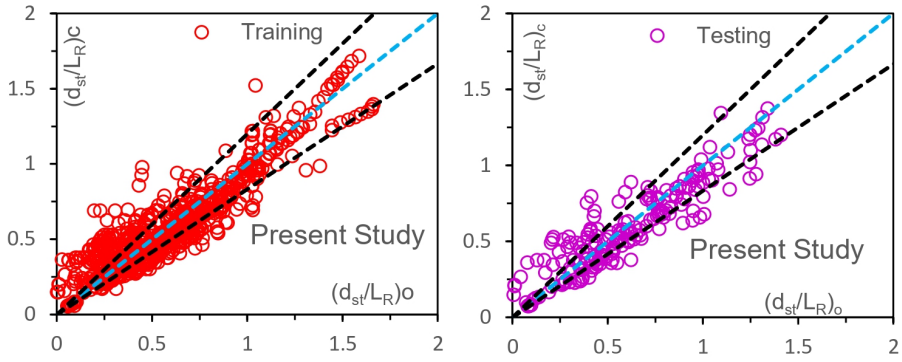

Fig. 8.12. Comparision between training and testing data for (± 20% PAL).

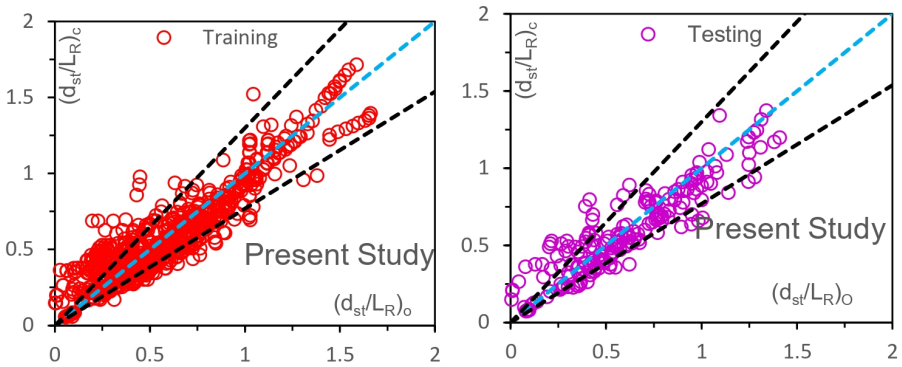

Fig. 8.13. Comparision between training and testing data for (± 30% PAL).

Based on Figures 8.11, 8.12, and 8.13, there is a noticeable inconsistency between the observed and calculated data, particularly at both low and high values of d_{st}/L_R. This discrepancy becomes apparent due to the exclusion of these parameters from the regression model (Eq. 8.8), leading to the observed mismatch between the observed and calculated data.

The accuracies of eight such formulas and the present study are checked graphically along with consideration of various statistical parameters. The formulas are checked not only with the direct statistical measures but with the weighting criteria of all the statistical measures assigned to them with the different weighting criteria mentioned in the discussion. Figs. (8.14, 8.16 and 8.18) show the ±10%, ±20%, and ±30% deviation from the line of the perfect fit between the observed and predicted normalized d_{st}.

In Figures 8.14, 8.16 and 8.18, the X axis represents the dimensionless observed scour depth $(d_{st}/L_R)_o$ and the Y axis represents the dimensionless computed scour depth $(d_{st}/L_R)_c$. The d_{st} data were taken either from the graphs in the same literature or directly from research groups who used other researchers' d_{st} data. As the data were extracted from the given figures from their respective literatures it may differ little from the original d_{st} data. It may slightly differ in original the time step also.

The non-linear regression models which are developed in this study and empirical equations were compared using validation data. First, the regression model (932 data) in the present study was compared with other empirical equations. The results are shown in Table 8.2. According to Table 8.2, the Nasrollahi et al. (2008) equation provides a better coefficient of determination

(R^2=0.57) than other literature equations. Similarly, the Coleman et al. (2003) equation provides better root mean square error (RMSE=0.30), better Nash-Sutcliffe efficiency (NSE=0.30), and better mean bias error (MBE=0.170) than other literature equations. According to Table 8.2, at 10% and 20% perfect agreement lines, the Yanmaz and Kose (2007) equation provides a better percentage in (P_{in} = 20.92, 38.95) respectively than other literature equations. Similarly, the Coleman et al. (2003) equation provides a better % in for a 30% perfect agreement line (P_{in} = 49.68) than other literature equations. The regression equation developed in this study, improved the results (R^2=0.84, RMSE=0.13, NSE=0.86, MBE=0.003, P_{in} (10%)=37.45, P_{in} (20%)=64.27, P_{in} 30% =78.43). The comparison of literature equations and Eq. (8.4) is shown in Figs. 8.14, 8.16 and 8.18. Scattering of the calculated time variation of scour depth data (Figs. 8.14, 8.16 and 8.18) indicates that the models that were developed may not provide suitable results for spur dikes. Equation (8.4) has a better agreement with observed data than other empirical equations.

Figures 8.15, 8.17, and 8.19 depict the numerical formulas for scour depth estimation derived from nine literature formulas plotted against computed versus measured normalized scour depth. In Figure 8.15, the Present study satisfies a maximum of 37.45% of d_{st} data, whereas Pandey et al. (2020) satisfy a minimum of 2.68% for a 10% error band, encompassing all literature formulas. Similarly, in Figure 8.17, the Present study satisfies a maximum of 64.27% of d_{st} data, with a minimum of 5.90% of d_{st} data being satisfied by Pandey et al. (2020) for a 20% error band, considering all literature formulas. Additionally, in Figure 8.19, the Present study satisfies a maximum of 78.43% of d_{st} data, while Pandey et al. (2020) satisfy a minimum of 13.52% for a 30% error band, encompassing all literature formulas. In Figures 8.15, 8.17, and 8.19, it is evident that the equation proposed in the Present study exhibits superior agreement with observed data compared to other empirical equations, while Pandey et al. (2020) demonstrate the poorest agreement with observed data among the empirical equations.

Table 8.2. Comparison between various models to predict time variation of scour depth.

Prediction Model	R^2	RMSE	NSE	MBE	P_{in} (10%)	P_{in} (20%)	P_{in} (30%)
Present Study	0.84	0.13	0.86	0.003	37.45	64.27	78.43
Yanmaz and kose (2007)	0.08	0.45	-0.54	0.200	20.92	38.95	46.89
Coleman et al. (2003)	0.51	0.30	0.30	0.170	20.06	36.70	49.68
Karami et al.(2012b)	0.49	0.31	0.26	0.190	20.82	34.44	45.06
Nasrollahi et al. (2008)	0.57	0.32	0.21	0.230	16.74	33.15	41.20
Karami et al.(2012a)	0.54	0.32	0.19	0.230	17.81	32.83	41.52
Oliveto and Hager (2002)	0.22	0.61	-1.89	0.490	12.45	24.25	29.18
Kothyari et al. (2007)	0.31	0.42	-0.33	0.220	10.62	22.10	34.87
Pandey et al. (2020)	0.06	1.08	-7.98	0.830	2.68	5.90	13.52

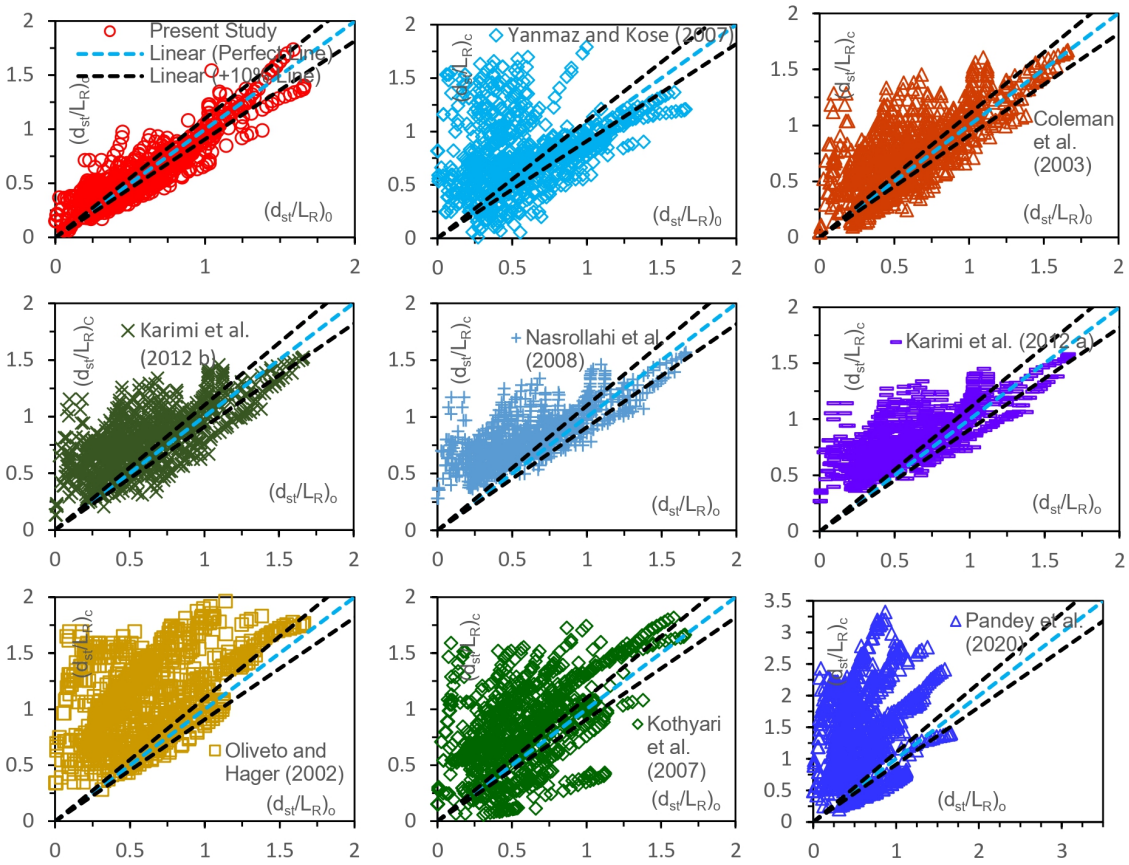

Fig. 8.14. Comparision of empirical equations for time variation of scour prediction (± 10% PAL).

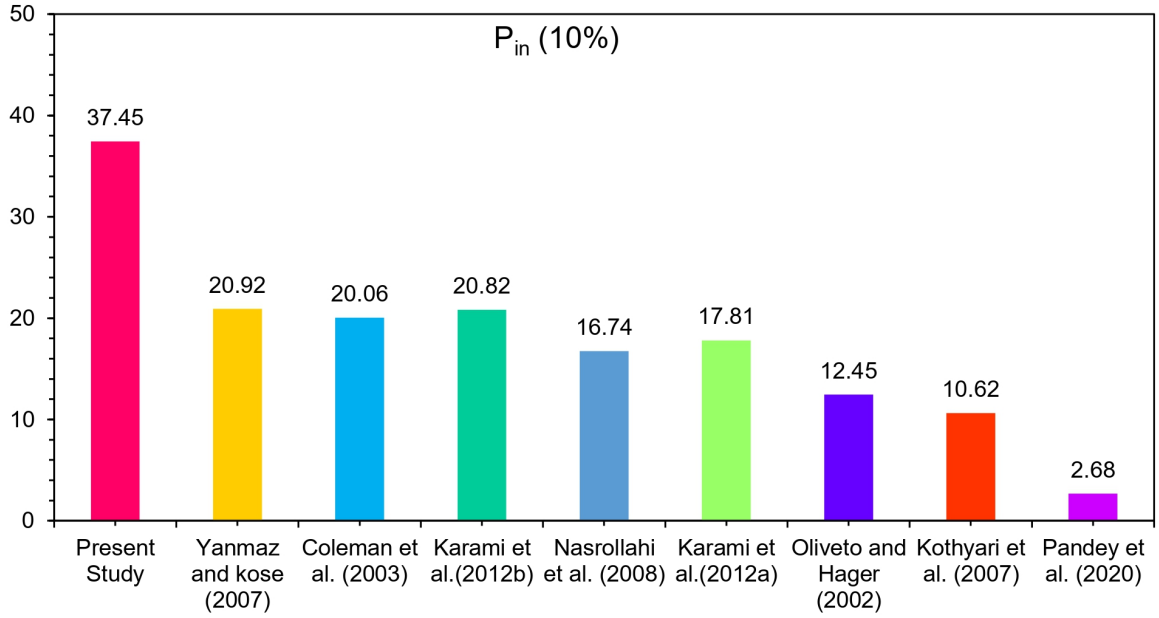

Fig. 8.15. Percentages in [p(in), 10%] considering all literature formulas.

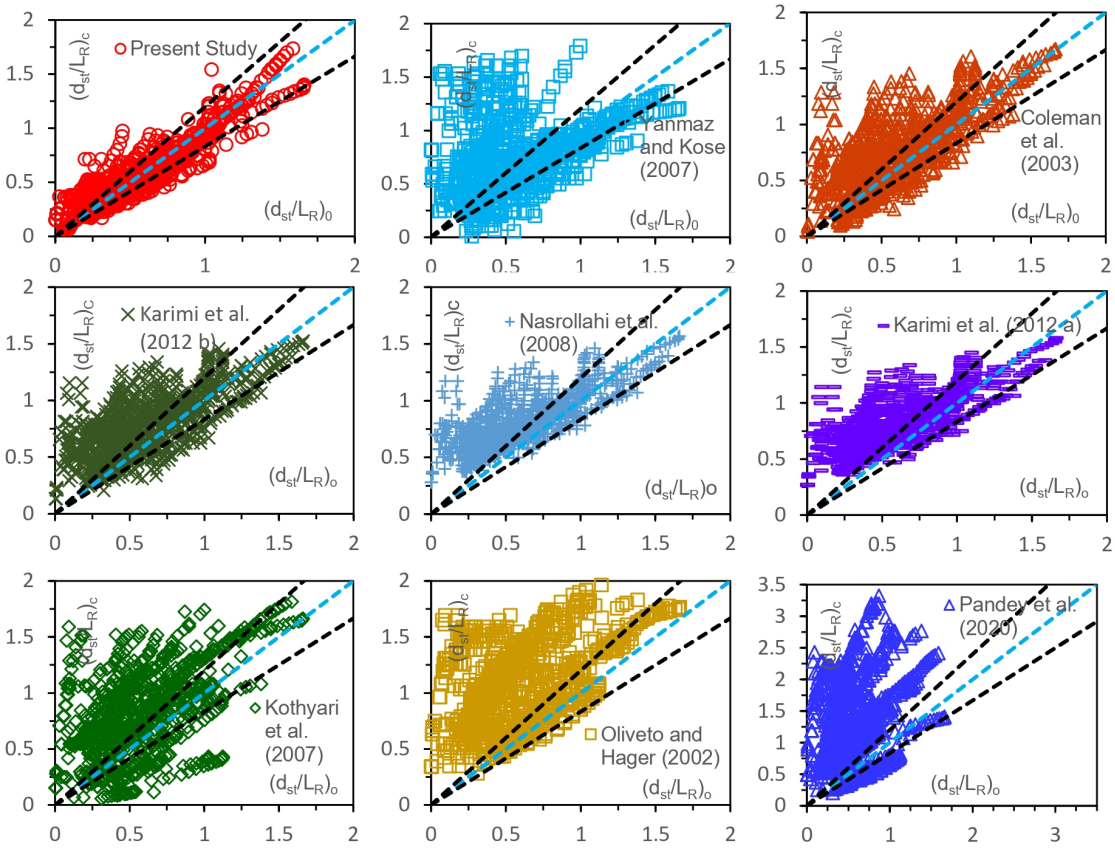

Fig. 8.16. Comparison of empirical equations for time variation of scour prediction (± 20% PAL).

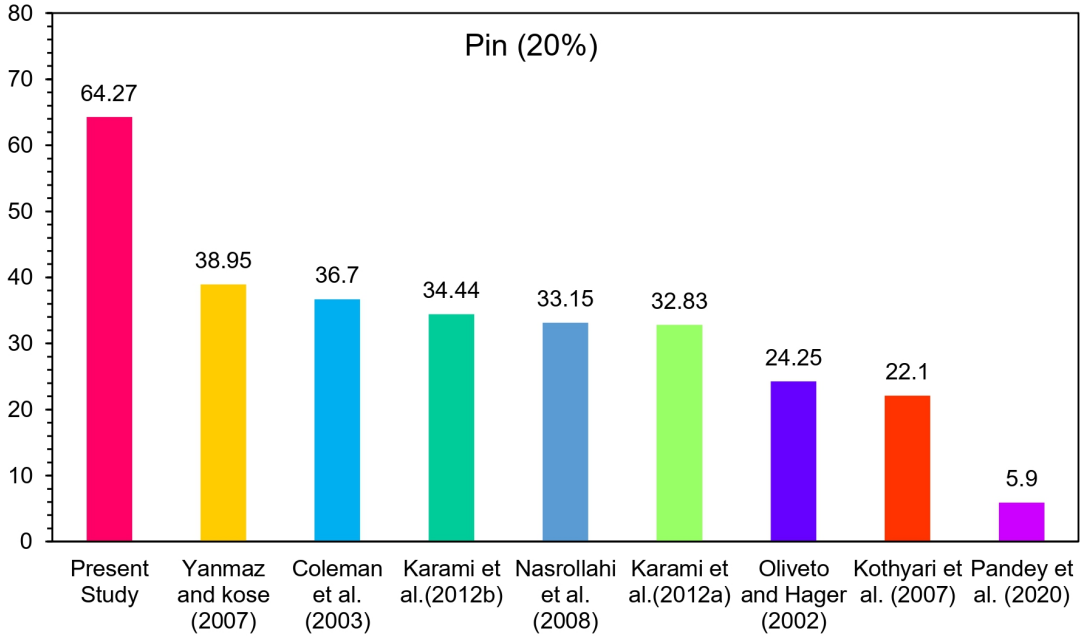

Fig. 8.17. Percentages in [p(in), 20%] considering all literature formulas.

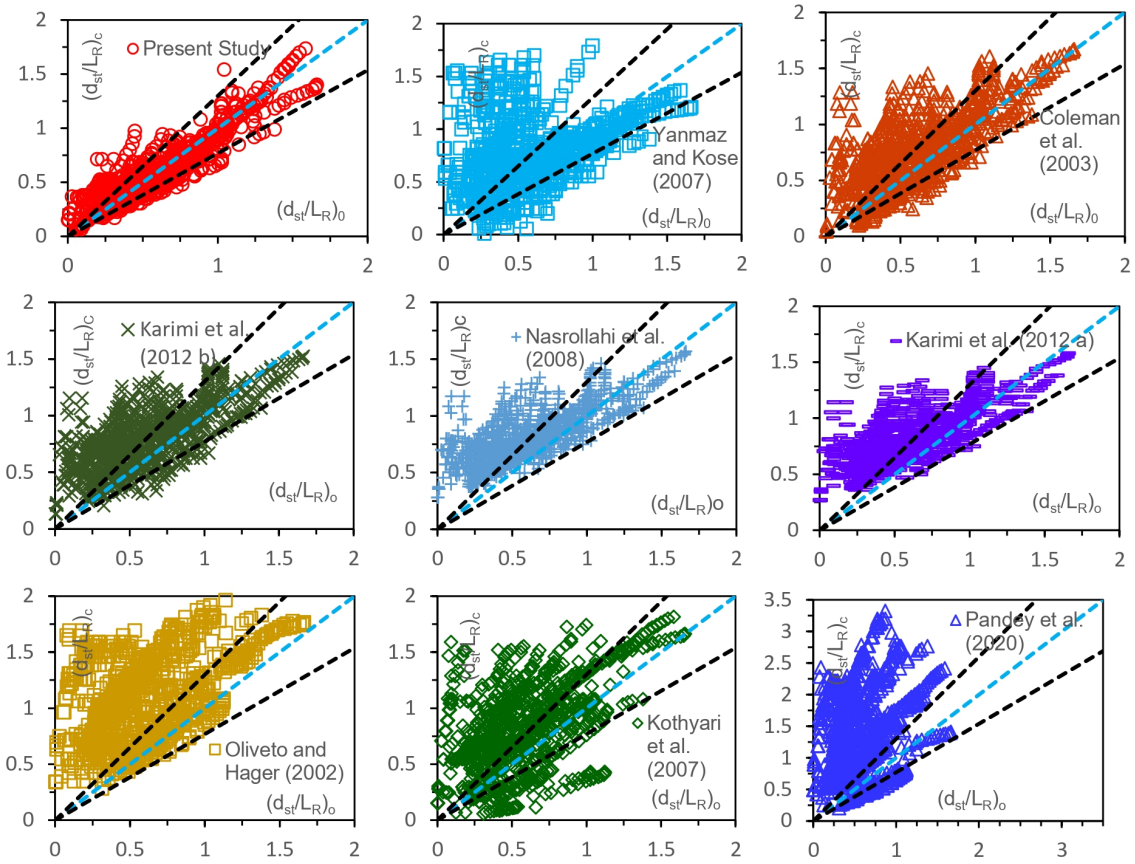

Fig. 8.18. Comparision of empirical equations for time variation of scour prediction (± 30% PAL).

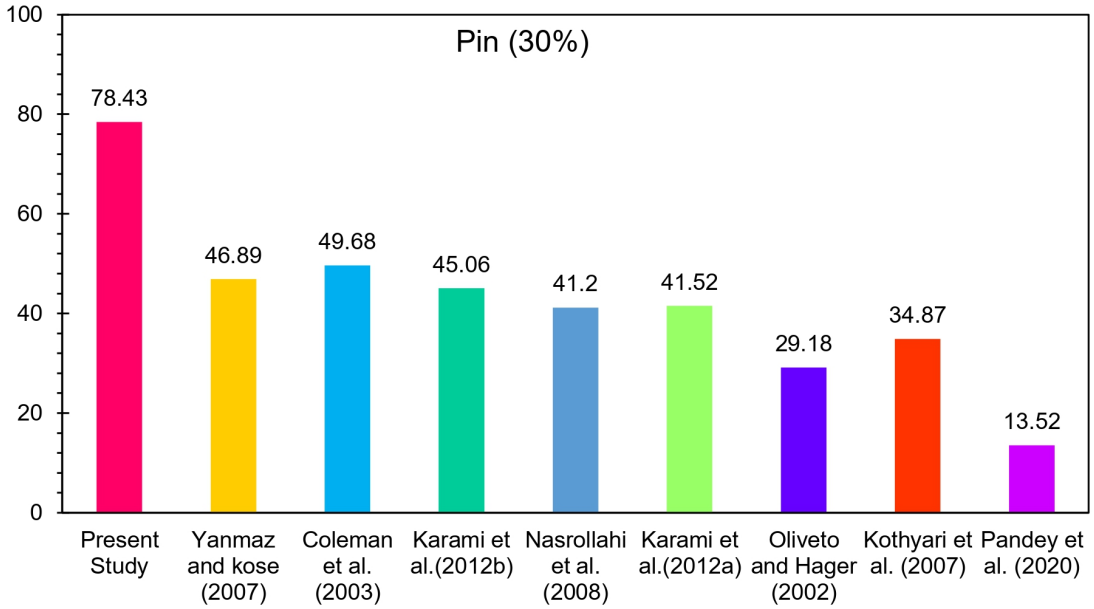

Fig. 8.19. Percentages in [p(in), 30%] considering all literature formulas.

8.2.3 Weightage and Ranking of Formulas

The assessment and prioritization of literature formulas and newly derived formula for predicting temporal scour depth employ various decision-making techniques like CRITIC, Entropy, and AHP. CRITIC (Criteria Importance Through Intercriteria Correlation) evaluates criteria consistency and significance, while Entropy quantifies decision-making uncertainty. AHP (Analytic Hierarchy Process) facilitates the prioritization of criteria through pairwise comparisons. Subsequently, PROMETHEE (Preference Ranking Organization Method for Enrichment Evaluations) and TOPSIS (Technique for Order of Preference by Similarity to Ideal Solution) methods are employed for ranking to determine the most effective formula for temporal scour depth prediction at spur dike.

8.2.3.1 Weight Criteria Technique

In multi-objective optimization (MOO) problems, importance weights are assigned, usually indistinguishable. However, in recent years, experts and researchers studying MOO issues have given much thought to weighting strategies. To assign relevance weights to responses in MOO, (Kumar et al. (2021) proposed different strategies. The performance of a formula cannot be controlled by any single benefit or cost criterion, evaluating all weighting criteria procedures at once is key to determining the significance of the various weighting criteria. Consequently, the weighting criteria for each indicator in the current study are determined using three different methods: (i) CRITIC, (ii) Entropy and (iii) AHP.

CRITIC Method

This method is based on how strongly the decision matrix's columns are correlated Diakoulaki et al. (1995). Following are the steps to calculate the indicators' weights.

Step I. The decision matrix and normalized matrix are calculated using Eqs. (8.9) and (8.10), respectively.

$$\left[Z_{ij}\right]_{kx1} = \begin{bmatrix} Z_{11} & Z_{12} & .. & Z_{1l} \\ Z_{21} & . & . & Z_{2l} \\ . & . & . & . \\ Z_{k1} & Z_{k2} & . & Z_{kl} \end{bmatrix} \ (i=1,2,....,k \text{ and } j=1,2,...,l) \tag{8.9}$$

$$M_{ij} = \frac{Z_{ij} - Z_{ij}^{\max}}{Z_{ij}^{\max} - Z_{ij}^{\min}} \tag{8.10}$$

where Z_{ij} presents the performance value of ith alternative on the j^{th} criterion.

Step II. The weight criteria are calculated using Eqs. (8.11) and (8.12),

$$Q_j = SD_j \sum_{k=1}^{1}\left(1 - R_{jk}\right) \tag{8.11}$$

$$W_j = \frac{C_j}{\sum_{j=1}^{1} C_j} \tag{8.12}$$

where R_{jk} is the CC between two criteria, and Q_j is the quantity of information contained in j^{th} criteria.

Entropy Weight Method (EWM)

The informational entropy concept and its theory have been applied before in statistical mechanics, information theory, hydrology, and water resources (e.g., Jaynes, 1957; Chiu,1987; Fiorentino et al., 1993; Singh, 2010, 2014; Moramarco et al., 2013), providing good results and an easy way to introduce probabilities into hydraulics. Informational entropy, Shannon entropy or simple entropy is defined in terms of probability. Taking into account the continuous random variable X, entropy is defined as (Eq. 8.13).

$$\Phi(X) = -\int_{-\infty}^{\infty} f(X)\ln f(X)dX = E\left[-\ln f(X)\right] \tag{8.13}$$

in which $\Phi(X)$ is the entropy, $f(X)$ is the probability density function of X, and E [ ] denotes expectation.

In this method, m indicators and n samples are set in the evaluation, and the measured value of the ith indicator in the j^{th} sample is recorded as xij.

The first step is the standardization of measured values (Li et al., 2012; Gorgij et al., 2017). The standardized value of the ith index in the jth sample is denoted as P_{ij}, and its calculation method is as follows (Eq. 8.14):

$$P_{ij} = \frac{X_{ij}}{\sum_{j=1}^{n} X_{ij}} \tag{8.14}$$

In the EWM, the entropy value E_i (Eq. 8.15) of the ith index is defined as (Dong et al., 2018)

$$E_i = \frac{\sum_{j=1}^{n} P_{ij}.\ln P_{ij}}{\ln n} \tag{8.15}$$

In the actual evaluation using the EWM, $P_{ij} \cdot \ln P_{ij} = 0$ is generally set when $P_{ij} = 0$ for the convenience of calculation. The range of entropy value E_i is [0, 1]. The larger the E_i is, the greater the differentiation degree of index i is, and more information can be derived. Hence, higher weight should be given to the index. therefore, in the EWM, the calculation method of weight w_i is (Liu et al., 2010; Amiri et al., 2014) (Eq. 8.16)

$$w_i = \frac{1 - E_i}{\sum_{i=1}^{m}\left(1 - E_i\right)} \tag{8.16}$$

Analytic Hierarchy Process (AHP)

Research written by Ling Yu says that the use of the Analytical Hierarchy Process (AHP) can provide optimal value, calculation formula and statistical data of each index, and even in the processing of qualitative index, also provide quantitative transformation method, sequentially to realize index evaluation of scientific, fairness and maneuver (Yu, 2016). The AHP is a decision support model developed by Thomas L. Saaty of the University of Pittsburg (Yu et al., 2017). AHP is the method for making the best decision when the decision maker has many criteria ([Ran, 2011). Stages in the AHP are as follows (Xu et al., 2017):

Step 1. Determine the problem then set the solution and compile the hierarchy of problems encountered;

Step 2. Define the criteria weight by comparing in pairs each criterion. This comparing process uses the priority scheme described in Table 8.3 (Morgan, 2017).

Table 8.3. Table of priority scheme.

Intensity of Interest	Information	Description
1	Both elements are just as important	Two elements have the same effect on a goal
3	One element is slightly more important than the other	Experience and judgment support a little more than other elements
5	One element is more important than the other	Experience and judgment are very strong in favor of one element over the other
7	One element is clearly more important than any other element	One of the strongest elements is preserved and dominant in practice
9	One of the most important elements of the other elements	Evidence favors a task in relation to another with the highest degree of reliability
2,4,6,8	Values between two adjacent consideration values	This value is given when there are two compromises between two options
Inverse	If activity "*i*" gets one number over activity "*j*", then "*j*" has its opposite value than "*i*"	

Step 3. Perform normalization on a pairwise comparison matrix by summing the value of each matched pair matrix column and then dividing each value from the column with the sum of the corresponding columns to obtain the normalization of the matrix (Eq. 8.17).

$$a_{jk} = \frac{X_{jk}}{\sum_{l=1}^{m} X_{lk}} \tag{8.17}$$

Step 4. Calculate the weight of synthesis by summing each column in the same row from the comparison normalization result of the matrix (Eq. 8.18).

$$\sum column = (k_1 + k_2 + k_3 + ... + k_n) \tag{8.18}$$

Step 5. Calculate the eigenvalues by multiplying each of the matched matrix columns in the same row, then being lifted by an existing criterion number (Eq. 8.19).

$$\lambda = (k_1 x k_2 x k_3 x ... x k_n)^{\frac{1}{n}} \tag{8.19}$$

Step 6. Calculate the priority weight of each criterion by means of the eigenvalues for each criterion divided by the total number of eigenvalues.

Step 7. Calculate the importance of each criterion by dividing the weight of synthesis by priority weight.

Step 8. Calculate the maximum eigen value (λmax) by dividing the total number of importance values by the number of criteria.

Step 9. Measure the consistency of use to ensure that judgment for decision making is of high consistency (Eq. 8.20).

$$CI = \frac{(\lambda_{max} - n)}{n} \tag{8.20}$$

where : *CI* = consistency Index λ_{max} = maximum eigenvalue, *n* = number of elements.

Step 10. Check consistency in the hierarchy provided that if the consistency ratio (*CI* / *IR*) is less than or equal to 0.1 then the result of the calculation (Eq. 8.21).is declared true (Aldrin et al., 2016). *IR* values can be seen in Table 8.4.

$$CR = \frac{CI}{IR} \tag{8.21}$$

where : *CR* = consistency ratio, *CI* = consistency index, and IR = index random consistency

Table 8.4. Index random consistency.

Matrix	1	2	3	4	5	6	7	8	9	10	11	12
IR	0	0	0.58	0.90	1.12	1.24	1.32	1.41	1.45	1.49	1.51	1.48

In this study, multi-attribute has been used for multi-attribute decision making. These weights of each attribute are found using (i) CRITIC, (ii) Entropy and (iii) AHP, shown in Figs. 8.19 (a), (b) and (c). respectively. The weights assigned to R^2, RMSE, NSE & MBE differ across methods, CRITIC method allocates 7%, 7%, 80% and 6% respectively, while the Entropy method assigns 8%, 5%, 76% and 5%, similarly, the AHP method distributes weights of 49%, 15%, 29% and 7% to the same criteria. So, the weight ranges of four statistical performance indicators R^2, RMSE, NSE and MBE using these four different weight criteria are 7–49%, 5–15%, 29–80%, and 6–11%, respectively. The highest weight is carried by NSE and the lowest weight by MBE.

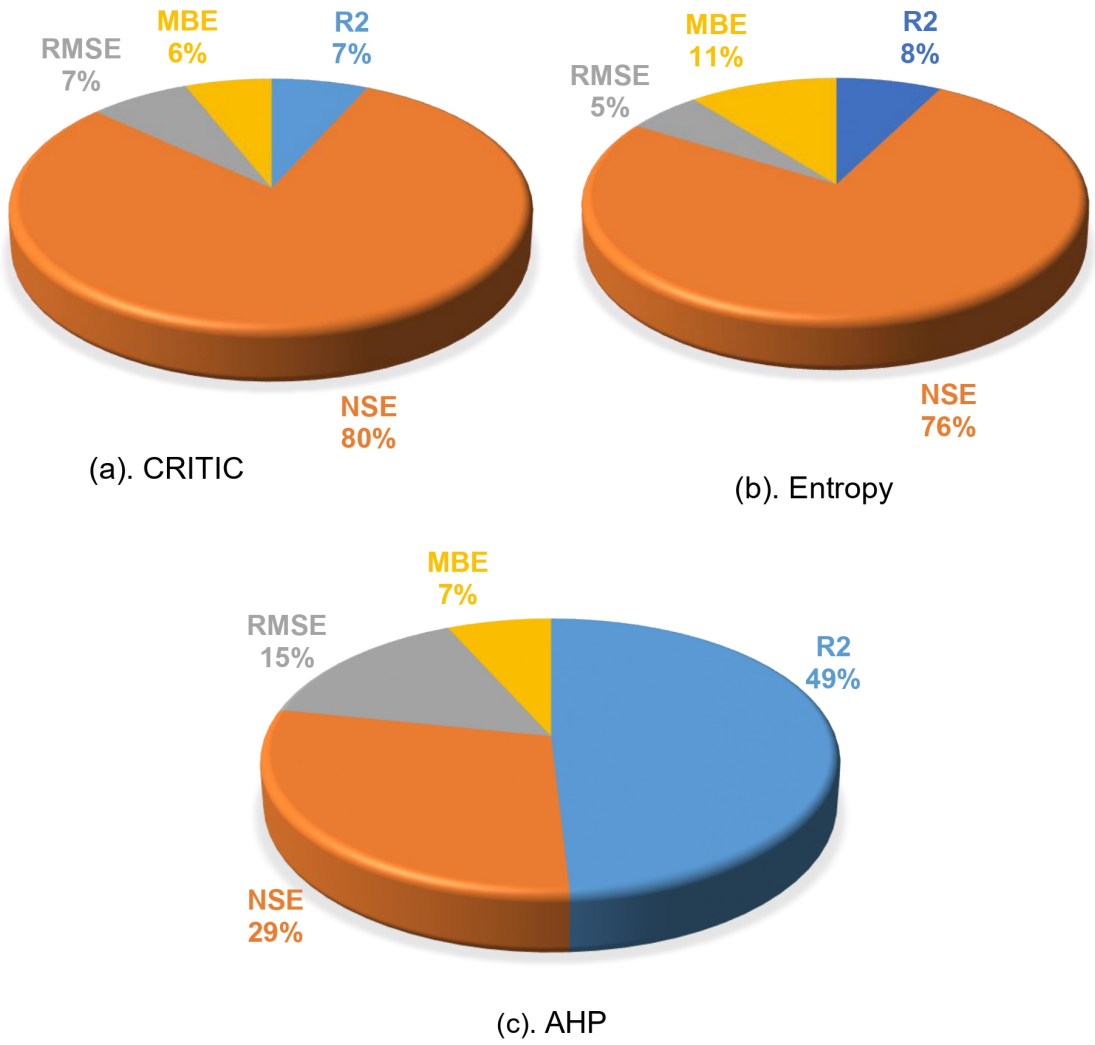

Fig. 8.19. Weight of beneficial and unfavorable criteria highlighted in pie-charts for (a) CRITIC, (b) Entropy and (c) AHP methods.

8.2.3.2 Ranking Criteria Technique

Ranking criteria techniques are systematic approaches employed in decision-making processes to assess and prioritize alternatives based on multiple criteria or attributes. These techniques are particularly useful when decision-makers need to evaluate options that involve trade-offs across various factors, such as cost, quality, time, and risk. By quantifying and structuring the decision-making process, ranking criteria techniques provide a methodical way to compare and select the most preferred alternatives. The Ranking criteria for each researcher in the current study are determined using two different methods: (i) PROMETHEE, and (ii) TOPSIS

PROMETHEE

PROMETHEE (Preference Ranking Organization Method for Enrichment Evaluations) and its variants, PROMETHEE I and PROMETHEE II, are multicriteria decision-making methods developed by Brans and Vincke in the early 1980s. While both PROMETHEE I and PROMETHEE II are based on the same fundamental principles, they differ in certain aspects of their implementation and the way they handle preference modeling and aggregation.
Following are the steps for PROMETHEE II (Complete ranking) (Brans and Vincke, 1985) to calculate the researchers' rankings.

Step 1. Normalize the Evaluation matrix (decision matrix)

The evaluation matrix (decision matrix) is normalized by dividing each element by the sum of its column to ensure all criteria are on the same scale for fair comparison.
For Beneficial criteria (Eq. 8.22).

$$R_{ij} = \frac{\left[X_{ij} - \min(X_{ij})\right]}{\left[\max(X_{ij}) - \min(X_{ij})\right]} (i = 1, 2..., m; j = 1, 2, ..., n) \tag{8.22}$$

For non-beneficial criteria (Eq. 8.23).

$$R_{ij} = \frac{\left[\max(X_{ij}) - X_{ij}\right]}{\left[\max(X_{ij}) - \min(X_{ij})\right]} (i = 1, 2..., m; j = 1, 2, ..., n) \tag{8.23}$$

Step 2. Calculate the evaluate differences of i^{th} alternative with respect to other alternatives

The differences in evaluation between the i^{th} alternative and other alternatives are computed by subtracting the normalized evaluation values of the alternatives from each other, considering each criterion separately.

Step 3. Calculate the preference function, P_j (a, b)

The preference function P_j (a, b) is computed for each pair of alternatives a and b based on their differences in evaluation values. This function typically takes into account parameters such as preference thresholds and shape functions to determine the degree of preference for one alternative over another for each criterion j.

$$\text{Condition: } D(Ma - Mb) \leq 0 \text{ , } P_j(a,b) = 0, \text{ if } R_{aj} \leq R_{bj}$$

$$\text{Condition: } D(Ma - Mb) > 0 \text{ , } P_j(a,b) = 0, \text{ if } R_{aj} > R_{bj}$$

Step 4. Calculate the aggregated preference, Π (a, b)

The aggregated preference Π (a, b) between alternatives a and $b$is calculated by aggregating the preference functions $P_j(a, b)$ over all criteria j. This aggregation can be performed using different methods such as the "outranking flow" approach, considering the net outranking flows between alternatives (Eq. 8.24).

$$\Pi(a,b) = \frac{\sum_{j=1}^{n} w_j P_j(a,b)}{\sum_{j=1}^{n} w_j} \tag{8.24}$$

Step 5. Determine the leaving and the entering outranking flows

The leaving outranking flow for each alternative is determined by summing the aggregated preferences over all alternatives that are outranked by it. The entering outranking flow is similarly determined by summing the aggregated preferences over all alternatives that outrank it.

Leaving (positive) flow for a^{th} alternative, ψ^{+} (Eq. 8.25).

$$\psi^{+} = \frac{1}{m-1} \sum_{b=1}^{m} \Pi(a,b), (a \neq b) \tag{8.25}$$

Entering (negative) flow for a^{th} alternative, ψ^{-} (Eq. 8.26).

$$\psi^{-} = \frac{1}{m-1} \sum_{b=1}^{m} \Pi(b,a), (a \neq b) \tag{8.26}$$

Step 6. Calculate the net outranking flow for each alternative

The net outranking flow for each alternative is computed by subtracting the leaving outranking flow from the entering outranking flow. This net outranking flow represents the overall preference of each alternative relative to others (Eq. 8.27).

$$\psi(a) = \psi^{+}(a) - \psi^{-}(a) \tag{8.27}$$

Step 7. Determine the ranking of all the considered alternatives depending on the value of φ

The ranking of alternatives is determined based on the values of the net outranking flow $\phi(a)$. Alternatives are ranked in descending order of their net outranking flow values, with higher values indicating higher preference.

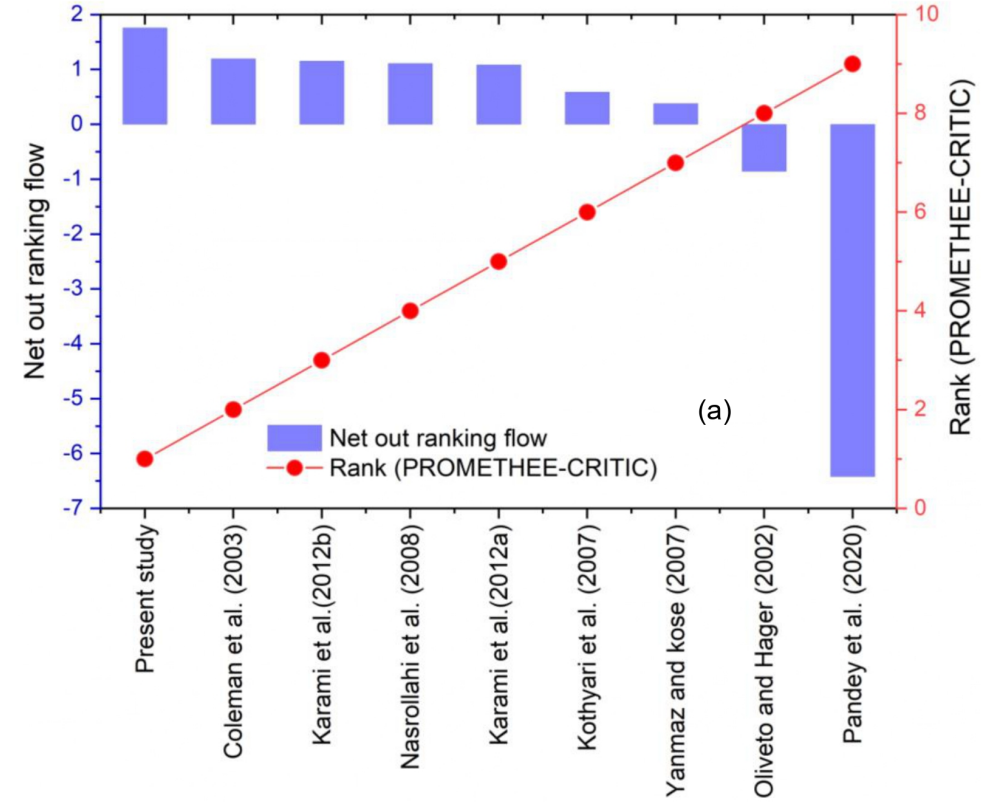
Net out ranking flow
Rank (PROMETHEE-CRITIC)
(a)
Net out ranking flow
Rank (PROMETHEE-CRITIC)
Present study
Coleman et al. (2003)
Karami et al.(2012b)
Nasrollahi et al. (2008)
Karami et al.(2012a)
Kothyari et al. (2007)
Yanmaz and kose (2007)
Oliveto and Hager (2002)
Pandey et al. (2020)

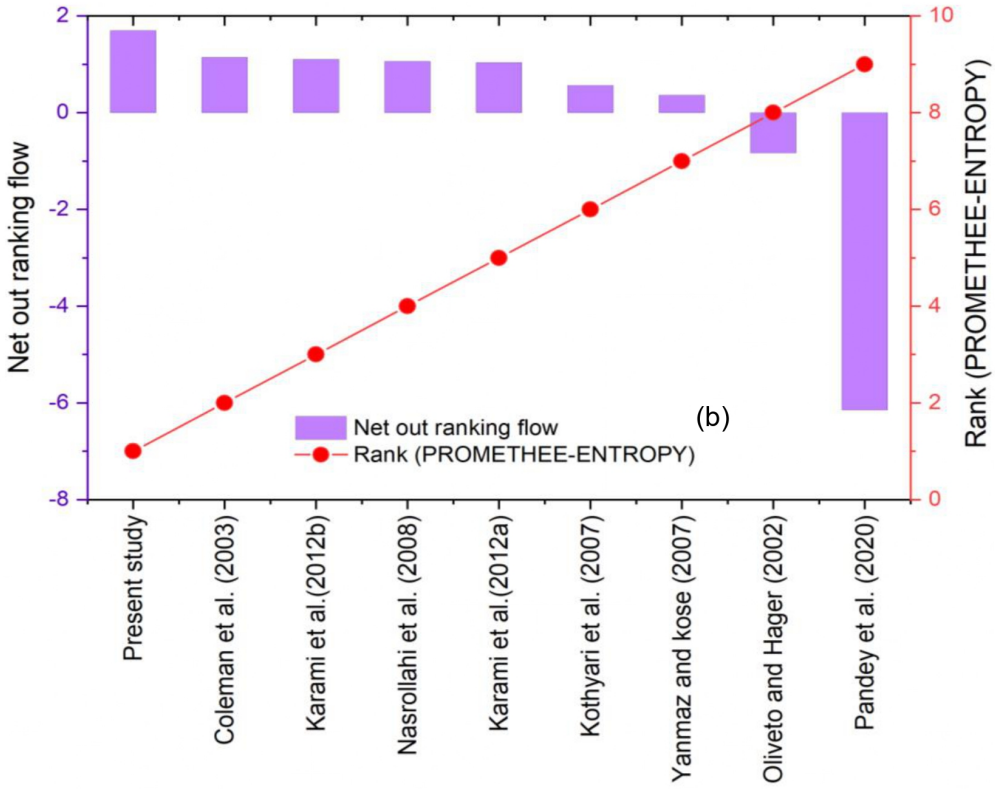
Net out ranking flow
Rank (PROMETHEE-ENTROPY)
(b)
Net out ranking flow
Rank (PROMETHEE-ENTROPY)
Present study
Coleman et al. (2003)
Karami et al.(2012b)
Nasrollahi et al. (2008)
Karami et al.(2012a)
Kothyari et al. (2007)
Yanmaz and kose (2007)
Oliveto and Hager (2002)
Pandey et al. (2020)

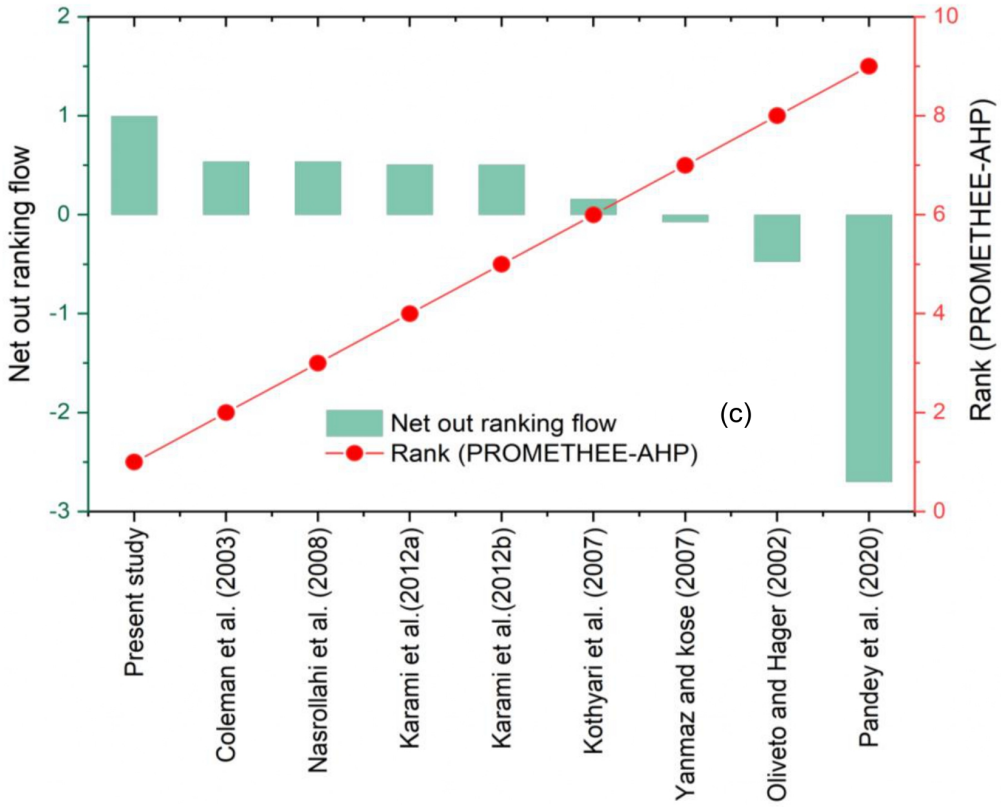

Fig. 8.20. Ranking of all formulas by PROMETHEE using three different weightage methods (a) CRITIC, (b) Entropy and (c) AHP.

TOPSIS

TOPSIS (Technique for Order Preference by Similarity to Ideal Solution) is a multi-criteria decision-making method that ranks alternatives by measuring their proximity to the ideal solution while simultaneously minimizing their distance from the negative ideal solution. It balances closeness to the ideal solution and remoteness from the negative ideal solution, providing a comprehensive ranking of alternatives. The method was introduced by Hwang and Yoon, 1981, and it has since been widely applied in various fields for decision-making under multiple criteria. Following are the steps for TOPSIS to calculate the researchers' rankings.

Step 1. Vector normalization for Normalized decision matrix

Normalize the decision matrix to bring all criteria to a common scale. This step ensures that the criteria are comparable and not biased by differences in measurement units (Eq. 8.28).

$$\overline{X_{ij}} = \frac{X_{ij}}{\sqrt{\sum_{j=1}^{n} X_{ij}^{\,2}}} \tag{8.28}$$

Step 2. Weighted Normalized decision matrix

Assign weights to each criterion based on their relative importance. These weights reflect the preferences or priorities of decision-makers and are typically determined through expert judgment or analytical methods.

Step 3. Ideal best and ideal worst for beneficial and non-beneficial criteria

Calculate the ideal solution and negative ideal solution for each criterion by identifying the maximum and minimum values, respectively, for each criterion across all alternatives.

V_j^+=indicates the ideal (best) value

V_j^-=indicates the ideal (worst) value

Step 4. Euclidean distance from Ideal Best and Ideal Worst

Calculate the Euclidean distance between each alternative and both the ideal and negative ideal solutions. This distance represents how far each alternative is from the ideal and negative ideal solutions for each criterion. (Eqs. 8.29 and 8.30).

$$\text{For Ideal Best, } S_i^+ = \left[\sum_{j=1}^{m}\left(V_v - V_j^+\right)\right]^{0.5} \tag{8.29}$$

$$\text{For Ideal Worst, } S_i^- = \left[\sum_{j=1}^{m}\left(V_v - V_j^-\right)\right]^{0.5} \tag{8.30}$$

Step 5. Relative Proximity

Determine the relative proximity of each alternative to the ideal and negative ideal solutions by calculating the similarity measures. Typically, the closeness coefficient (Closeness to the Ideal Solution) and the remoteness coefficient (Closeness to the Negative Ideal Solution) are computed.

Step 6. Performance score /TOPSIS Score

Calculate the TOPSIS score for each alternative by comparing its relative proximity to the ideal and negative ideal solutions. The TOPSIS score is often determined by subtracting the remoteness coefficient from the closeness coefficient (Eq. 8.31).

$$P_i = \frac{S_i^-}{S_i^+ + S_i^-} \tag{8.31}$$

Step 7. Ranking

Rank the alternatives based on their TOPSIS scores. Alternatives with higher TOPSIS scores are considered more favorable and are ranked higher.

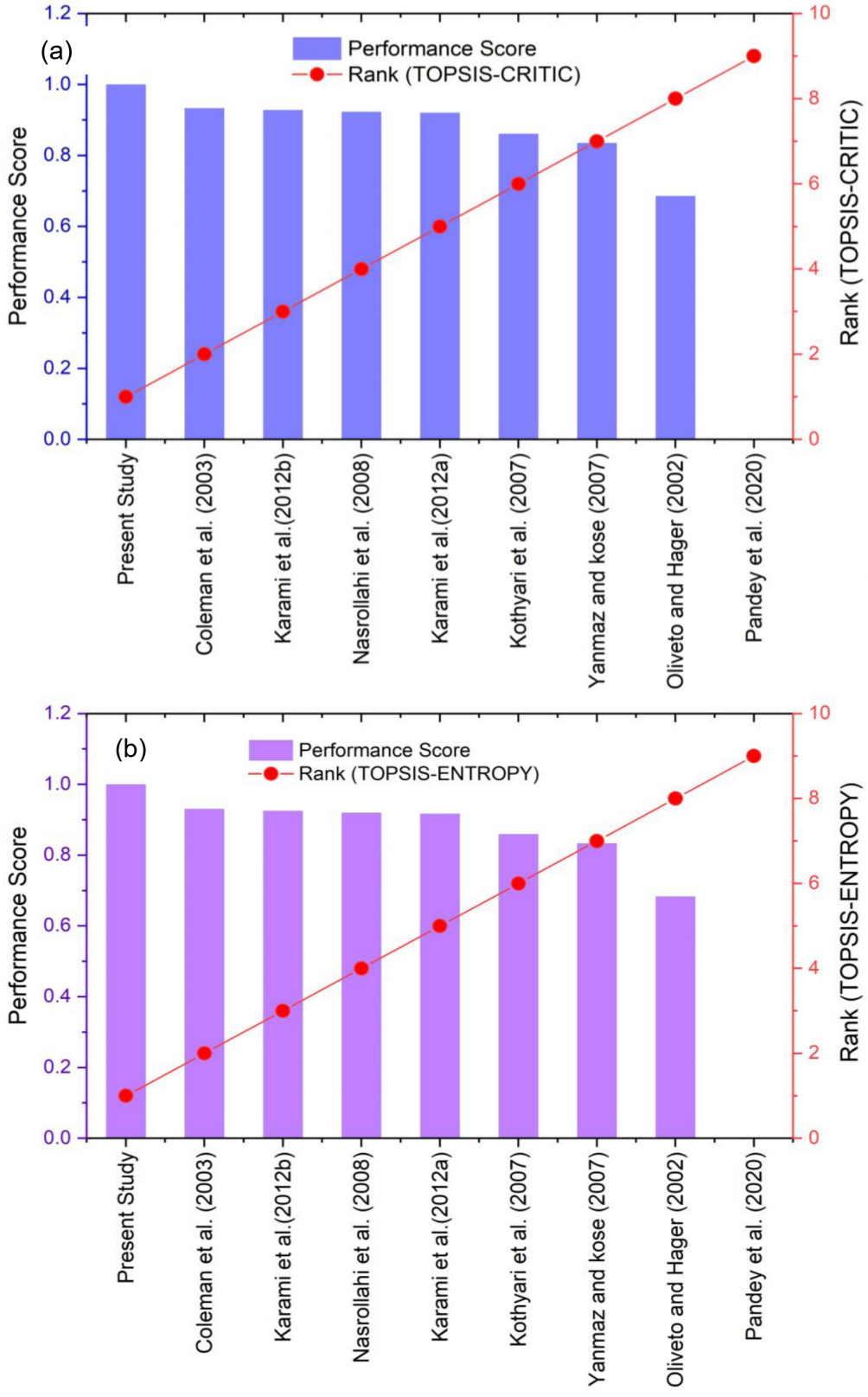
(a)
Performance Score
Rank (TOPSIS-CRITIC)
Performance Score
Rank (TOPSIS-CRITIC)
1.2
1.0
0.8
0.6
0.4
0.2
0.0
10
8
6
4
2
0
Present Study
Coleman et al. (2003)
Karami et al.(2012b)
Nasrollahi et al. (2008)
Karami et al.(2012a)
Kothyari et al. (2007)
Yanmaz and kose (2007)
Oliveto and Hager (2002)
Pandey et al. (2020)
(b)
Performance Score
Rank (TOPSIS-ENTROPY)
Performance Score
Rank (TOPSIS-ENTROPY)
1.2
1.0
0.8
0.6
0.4
0.2
0.0
10
8
6
4
2
0
Present Study
Coleman et al. (2003)
Karami et al.(2012b)
Nasrollahi et al. (2008)
Karami et al.(2012a)
Kothyari et al. (2007)
Yanmaz and kose (2007)
Oliveto and Hager (2002)
Pandey et al. (2020)

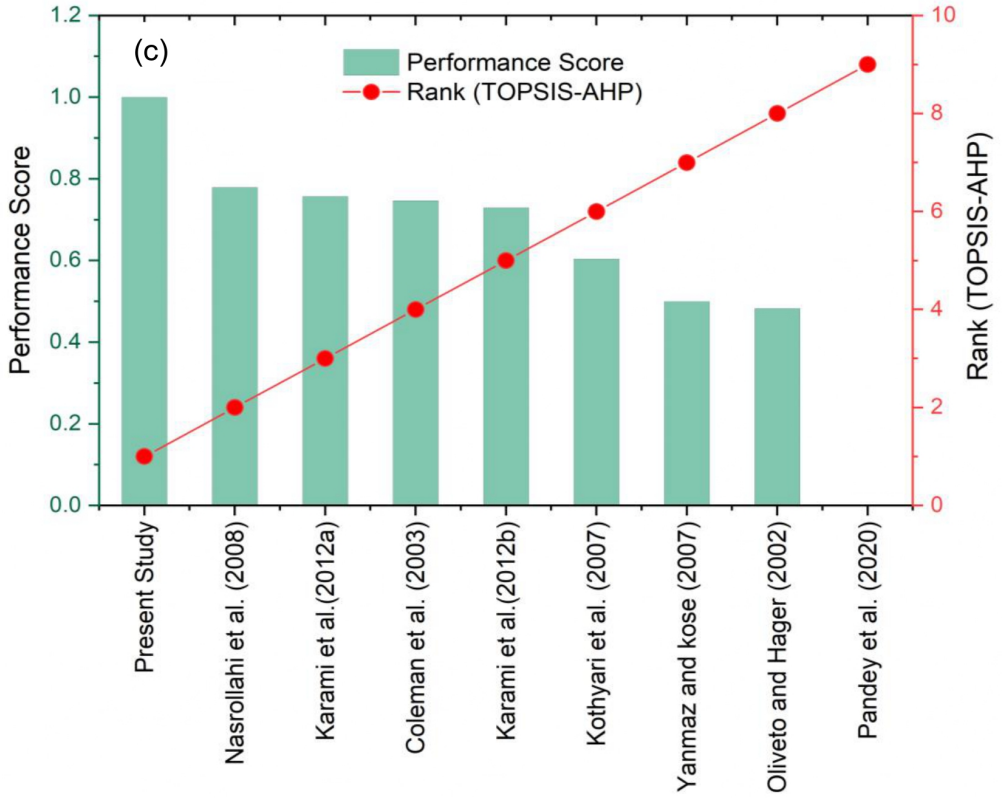

Fig. 8.21. Ranking of all formulas by TOPSIS using three different weightage methods (a) CRITIC, (b) Entropy and (c) AHP.

8.2.4 Overall Discussion

Literature data of d_{st} are analyzed to assess the accuracy of the computed d_{st} datasets by the aforementioned nine formulas in terms of four statistical performance indicators R^2, RMSE, NSE and MBE using PROMETHEE and TOPSIS (MADM technique in a deterministic scenario). Indicators' weights are calculated by (i) CRITIC, (ii) Entropy and (iii) AHP methods. Finally, a group decision approaching is used to aggregate the ranking for each d_{st} computation formula reported in the literatures. The results from the developed methodology are presented in the following sections.

The results of four performance indicators, two of which are beneficial criteria and the rest are unfavorable for the nine formulas for determining d_{st} are shown in Tables 8.5 and 8.6. The Net outranking flow (NORF) (Ψ) values are used by PROMETHEE and the Performance Score (PS) is used by TOPSIS to rank the d_{st} datasets for each formula, with a higher Ψ and PS value considered to indicate greater accuracy and vice versa. The NORF value is observed to vary between 1.76 (first rank) and -6.42 (last rank) for the CRITIC method, 1.70 (first rank) and -6.15 (last rank) for the Entropy method, and 0.9966 (first rank) and -2.6982 (last rank) for the AHP method throughout 9 formulas' ranks. Similarly, The PS value is observed to vary between 1.00 (first rank) and 0 (last rank) for the CRITIC, Entropy method, and the AHP method throughout 9 formulas' ranks. The weight distribution results of the three such methods are shown in Fig. 8.19.

Using the formula derived from the present study, it is found that within the 10% error band, 37.45% of data points lie which is the highest. The lowest data agreement has been found for Pandey et al. (2020) (Table 8.2) with 2.68% of data points lying within the 10% error band. Similarly, it is also found that within the 20% error band, 64.27 % of data points lie which is the highest. The lowest data agreement has been found for Pandey et al. (2020) (Table 8.2) with 5.90% of data points lying within the 20% error band. Again, it is found that within the 30% error band, 78.43% of data points lie which is the highest. The lowest data agreement has been found for Pandey et al. (2020) (Table 8.2) with 13.52% of data points lying within the 30% error band. Using PROMETHEE and TOPSIS, with the highest NORF and PS values, it has been also found that the newly developed formula performed best based on the CRITIC, Entropy method and as well as using the AHP method (Figs. 8.20 and 8.21), (Tables 8.5 and 8.6).

Among the 9 formulas accuracy of the Present Study formula is found highest by PROMETHEE and TOPSIS (Fig. 8.20 and 8.21) respectively. The accuracy of Coleman et al. (2003) formula is found close to the newly developed formula by PROMETHEE and TOPSIS, and Nasrollahi et al. (2008) also close to the newly developed formula by taking the weight of AHP using the TOPSIS method.

Among these nine d_{st}/L_R formulas, the formula derived in the present study gives the best accuracy as using the PROMETHEE and TOPSIS, all the beneficial and non-beneficial criteria are found better than the other eight formulas. In the case of Coleman et al. (2003) formula, the performance of the NORF value is found higher than the remaining seven formulas but the performances of the PS values for AHP weight using TOPSIS are not good. That is why Coleman et al. (2003) formula has been ranked just next after the present study formula on CRITIC, Entropy & AHP weightage methods. Pandey et al. (2020) formula has the last rank by both of the weight methods as well as the lowest agreement of data mainly due to negative NSE, very low R^2 and very high RMSE and MBE. There is a large degree of concordance between $(d_{st})_c$ and $(d_{st})_o$ in the formula derived in the current study. The main benefit of using the newly proposed formula is that it did not need any presumption or calculations of d_{se}, t_e to compute d_{st}.

Table 8.5. The ranking of the literature and the newly developed formula using PROMETHEE.

PROMETHEE	Weightage method					
	CRITIC		Entropy		AHP	
References	NORF	Ranking	NORF	Ranking	NORF	Ranking
Present study	1.76	1	1.70	1	1.00	1
Coleman et al. (2003)	1.20	2	1.15	2	0.54	2
Karami et al. (2012b)	1.16	3	1.11	3	0.54	5
Nasrollahi et al. (2008)	1.11	4	1.06	4	0.51	3
Karami et al.(2012a)	1.09	5	1.04	5	0.50	4
Kothyari et al. (2007)	0.59	6	0.56	6	0.16	6
Yanmaz and Kose (2007)	0.38	7	0.36	7	-0.07	7
Oliveto and Hager (2002)	-0.86	8	-0.83	8	-0.47	8
Pandey et al. (2020)	-6.42	9	-6.15	9	-2.70	9

Note: 'NORF'-Net out ranking flow

Table 8.6. The ranking of the literature and the newly developed formula using TOPSIS.

TOPSIS	Weightage method					
	CRITIC		Entropy		AHP	
References	PS	Ranking	PS	Ranking	PS	Ranking
Present Study	1.00	1	1.00	1	1.00	1
Coleman et al. (2003)	0.93	2	0.93	2	0.78	2
Karami et al. (2012b)	0.93	3	0.93	3	0.76	3
Nasrollahi et al. (2008)	0.92	4	0.92	4	0.75	4
Karami et al. (2012a)	0.92	5	0.92	5	0.73	5
Kothyari et al. (2007)	0.86	6	0.86	6	0.60	6
Yanmaz and Kose (2007)	0.84	7	0.83	7	0.50	7
Oliveto and Hager (2002)	0.69	8	0.68	8	0.48	8
Pandey et al. (2020)	0.00	9	0.00	9	0.00	9

Note: 'PS'-Performance Score

8.2.5 Limitations of The Present Study

The comprehensive approach to analyzing and selecting the most promising temporal scour depth formula for spur dikes in the study is acknowledged. Here are some potential limitations:

Data Quality and Availability: The accuracy and reliability of the results heavily rely on the quality and availability of the data collected from various graphs and literature sources. If the data is sparse, outdated, or inconsistent, it could introduce biases or errors in the analysis.

Assumptions and Simplifications: Dimensional analysis, subset regression, PCA, and other dimensionality reduction techniques often rely on simplifying assumptions. These assumptions may not always hold true in real-world scenarios, leading to potential inaccuracies in the results.

Generalizability: The findings of the study may be specific to the conditions, parameters, and datasets used in the analysis. Extrapolating these findings to different geographical locations, hydraulic conditions, or types of spur dikes may not be appropriate without further validation.

Weighting Methods: While weightage methods like CRITIC, ENTROPY, and AHP provide a systematic way to assign importance to different factors, the subjective interpretation of these weights could introduce bias into the analysis.

Ranking Methods: Techniques like TOPSIS and PROMETHEE are sensitive to the choice of parameters and normalization methods. Small changes in these parameters could lead to significantly different rankings, potentially affecting the selection of the most promising formula.

Model Validation: It's crucial to validate the selected formula against independent datasets or field measurements to assess its predictive accuracy and reliability. Failure to validate the chosen formula could lead to misleading conclusions.

Publication Bias: The study's reliance on existing literature may introduce publication bias, where only studies with positive or significant results are published, leading to an overestimation of the effectiveness of certain formulas.

Temporal Dynamics: Since the study focuses on temporal scour depth formulas, it's essential to consider the temporal variability of hydraulic conditions and scour processes. Failure to account for temporal dynamics could limit the applicability of the selected formula over different time scales.

Chapter 9
Conclusive Remarks

9.1 Conclusions

To determine the temporal scour depth around a Spur Dike, several researchers have conducted a series of studies in the vicinity of clear water scour and steady flow conditions. Several researchers have used various numerical, simulation models, and semi-empirical approaches based on sediment transport models to assess the depth of temporal scour (d_{st}) and proposed d_{st} prediction formulas.

Among them, the 8 most promising formulas derived over the last twenty years along with a newly derived formula have been considered in this study. The current study aims to identify the best predictor among them when it comes to determining d_{st} most accurately. Experimental data from 932 full temporal series provided by several research groups in the last 20 years are used to establish the accuracy of these formulas. A comparative study is performed by analyzing each formula with each set of experimental d_{st} data to verify the inter-correlation between observed and computed values of d_{st}.

The formulas are taken and checked performances for d_{st} prediction using four different statistical performance indicators such as R^2, RMSE, NSE and MBE. PROMETHEE and TOPSIS, multi attribute decision-making techniques are used to check the rank of each computational model to find the d_{st}.

The study remarks are given below

In general, the decisive dependent parameters are flow, bed sediment, Spur dike shape and time or more specifically Reynolds number, Froude number, flow shallowness, sediment coarseness, sediment uniformity coefficient and time. These are used in different combinations in the aforementioned formulas for developing the computational model for finding d_{st}.

It is observed that a minimum of 2.68% of d_{st} data are satisfied by Pandey et al. (2020)'s formula and a maximum of 37.45% of d_{st} data are satisfied by the newly developed formula for a 10% error band.

It is also observed that a minimum of 5.90% of d_{st} data are satisfied by Pandey et al. (2020)'s formula and a maximum of 64.27% of d_{st} data are satisfied by the newly developed formula for the 20% error band.

It is again also observed that a minimum of 13.52 % of d_{st} data are satisfied by the Pandey et al. (2020)'s formula and a maximum of 78.43% of d_{st} data are satisfied by the newly developed formula for the 30% error band.

The key ranking factor is 80% for NSE,7% for R^2, 7% for RMSE and 6% for MBE for the CRITIC method, and 76% for NSE,8% for R^2, 5% for RMSE and 11% for MBE for the Entropy method as well as 29% for NSE,49% for R^2, 15% for RMSE and 7% for MBE for the AHP method over 9 computational formulas. From this study, it is clear that the weight factors merely influence the ranking of the d_{st} prediction formulas.

The study addresses that several d_{st} prediction formulas were developed over time after 2002. After the newly proposed formula, Coleman et al. (2003) remain the 2nd ranking formula for calculating d_{st}. The accuracy of Nasrollahi et al. (2008), and Karimi et al. (2012a, b) formula are very close to it.

To make the d_{st} prediction formula, the present study proposes a new formula following Pandey et al. (2020) and others. Among all these formulas, the accuracy of the present formula is found highest.

9.2 Future Scopes

The future scopes of this study present several exciting opportunities for advancement in the field of predicting temporal scour depth for spur dikes

Data Exploration and Integration: Future research could focus on exploring and integrating data from diverse sources beyond Scopus, Google Scholar, and Google. This could include leveraging additional academic databases, field measurements, and experimental studies to enrich the dataset and enhance the robustness of the analysis.

Refinement of Analytical Techniques: Further refinement and optimization of analytical techniques such as dimensional analysis, subset regression, and PCA could improve the accuracy and efficiency of scour depth prediction models. Exploring novel approaches and algorithms tailored to the specific characteristics of scour processes could lead to more reliable predictions.

Validation and Comparison: Conducting rigorous validation and comparison studies to evaluate the performance of the proposed new formula against existing literature formulas is crucial. This involves assessing key metrics such as R^2 (coefficient of determination), RMSE (root mean square error), NSE (Nash-Sutcliffe efficiency), MBE (mean bias error), and percentage error to gauge the predictive accuracy and reliability of the formulas across different scenarios.

Integration of Weightage Methods: Integrating weightage methods such as CRITIC, Entropy, and AHP can provide a structured framework for assigning importance to various criteria and factors influencing scour depth prediction. Future research could explore the sensitivity of the results to different weighting schemes and criteria, ensuring transparency and consistency in the decision-making process.

Ranking Method Evaluation: Evaluating the effectiveness and robustness of ranking methods such as TOPSIS and PROMETHEE is essential. Future studies could investigate the sensitivity of rankings to variations in parameters and normalization techniques, as well as explore alternative ranking approaches to ensure comprehensive and reliable results.

Uncertainty Analysis: Conducting uncertainty analysis to quantify and characterize uncertainties associated with scour depth prediction models is critical. This involves assessing the sensitivity of model outputs to input parameters, identifying sources of uncertainty, and providing confidence intervals or probabilistic predictions to account for variability in predictions.

Practical Application and Implementation: Practical application and implementation of the developed models and methods in real-world engineering practice is essential. Collaborations with engineering firms, government agencies, and industry stakeholders can facilitate the deployment of these tools in hydraulic infrastructure design, maintenance, and management.

Continued Research Collaboration: Collaboration between researchers, practitioners, and stakeholders is key to advancing the field of scour depth prediction for spur dikes. Continued collaboration can foster knowledge exchange, data sharing, and interdisciplinary research efforts, ultimately driving innovation and improving the resilience of hydraulic infrastructure**.**

9.3 Notations

Notation used in this study-

B = Abutment width (m)
D = Sand diameter (m)
d = Depth of flow (m)
d_{se} = Equilibrium scour depth (m)
d_{sm} = Maximum scour depth (m)
d_{st} = Time dependent or instantaneous scour depth at time t (m)
D_{50} = Median grain size (m)
D_* = $D_{50}(\Delta g/\nu^2)^{1/3}$ Particle parameter
Fr = $V/(gy)^{0.5}$ Froude number of flow
F_d = $V/(\Delta g D_{50})^{0.5}$ Densimetric particle Froude number
$F_{d\beta}$ = Densimetric particle Froude number for the inception of sediment movement
F_{sm} = $(\sigma^{-1/3}. F_d)$ Densimetric Froude number for a sediment mixture
g = Acceleration due to gravity (m/sec^2)
H = Spur dike height (m)
h = Spur dike thickness (m)
L = Length of channel (m)
L_R = Reference length (m) = $(dl^2)^{1/3}$
l = Spur dike length (m)
N = Shape co-efficient for spur dike
n = Number of spur dike (number)
Q = Discharge of flow (m^3/sec)
Re = Reynolds number = VD_{50}/υ
R_h = $Wy/(W+2d)$ Hydraulic radius (m)
S_o = Bed slope
S_s = Spacing of spur dike (m)
T = Non dimensionless time function = $t\sigma^{1/3}/(\Delta g D_{50})^{0.5} L_R$
T_S = $(tD_{50}(\Delta g D_{50})^{0.5})/l^2$ Dimensionless time parameter
t = Time taken to reach temporal scour depth (sec)
t_b = Base time of hydrograph (sec)
t_e = Time taken to reach maximum or equilibrium scour depth (sec)
t_m = Time taken to reach maximum scour depth (sec)
V = Depth-averaged flow velocity (m/sec)
V_c = Critical flow velocity (m/sec)
V_* = Shear velocity in (m/sec)
V_{*c} = Critical shear velocity (m/sec)

W = Width of channel (m)
y = Depth of channel (m)
ρ = Density of water (kg/m^3)
ρ_s = Sediment density (kg/m^3)
Δ = (ρ_s/ρ -1) Relative density (dimensionless)
σ = $(D_{84}/D_{16})^{0.5}$ Sediment Gradation/Geometric Standard Deviation (dimensionless)
Θ = Spur dike orientation angle (degree)
φ = Spur dike degree of permeability (degree)
μ = Dynamic viscosity (kg/m-.sec)
ν = Kinematic viscosity (m^2/sec)
τ = Shear stress (N/m^2)
τ_c = Critical shear stress (N/m^2)
Θ_c = Shields formula
where $D_* > 150$; $\Theta_c = 0.055$
where $20 < D_* \leq 150$; $\Theta_c = 0.013\ D_*^{0.29}$
where $10 < D_* \leq 20$; $\Theta_c = 0.04\ D_*^{-0.61}$
where $4 < D_* \leq 10$; $\Theta_c = 0.14\ D_*^{-0.64}$
where $D_* \leq 4$; $\Theta_c = 0.24\ D_*^{-1}$
e = (l/W) element obstruction/constriction ratio

9.4 References

Akbar, Z., Pasha, G. A., Tanaka, N., Ghani, U., and Hamidifar, H. (2024). Reducing bed scour in meandering channel bends using spur dikes. *International Journal of Sediment Research*, Vol. 39, Issue 2, pp. 243-256. https://doi.org/10.1016/j.ijsrc.2024.01.001.

Alasadi, L. A. R., Khlif, T. H., and Hassan, F. A. (2023). Experimental investigation for the local scour around V-shaped spur-dikes. *Scientific Review Engineering and Environmental Sciences,* Vol. 32, Issue 1, pp. 69-86. https://doi.org/10.22630/ srees.4506.

Amiri, V., Rezaei, M., and Sohrabi, N. (2014). Groundwater quality assessment using entropy weighted water quality index (EWQI) in Lenjanat, Iran. *Environmental Earth Sciences*, Vol. 72, Issue 9, pp. 3479-3490. https://doi.org/10.1007/s12665-014-3255-0.

Azamathulla, H., Asce, M., Ghani, A.A., Zakaria, N.A., and Guven, A. (2010). Genetic Programming to Predict Bridge Pier Scour. *Journal of Hydraulic Engineering*, Vol. 136, Issue 3, pp. 165-169. https://doi.org/10.1061/(ASCE)HY.1943-7900.0000133.

Azamathulla, H.M., Deo, M.C., and Deolalikar, P.B. (2008). Alternative neural networks to estimate the scour below spillways. *Advances in Engineering Software*, Vol. 39, Issue 8, pp. 689-698. https://doi.org/10.1016/j.advengsoft.2007.07.004.

Ballio, F., and Orsi, E. (2001). Time Evolution of Scour around Bridge Abutments. *Water Engineering Research*, Vol. 2, Issue 4, pp. 243-259.

Barbhuiya, A. K., and Dey, S. (2004). Local scour at abutments: A review. *Sadhana-academy proceedings in engineering sciences, Eng. Sci*, Vol. 29, Issue 5, pp. 449-476. https://doi.org/10.1007/ BF02703255.

Barkdoll, B. D., Ettema, R. and Melville, B. W. (2007). Countermeasures to Protect Bridge Abutments from Scour. Report No.NCHRP-587, Transportation Research Board, Washington D.C, USA.

Brans, J. P., and Vincke, P. (1985). Note—A preference ranking organisation method: (the PROMETHEE method for multiple criteria decision-making). *Management Science*, Vol. 31, Issue 6, pp. 647-656. https://doi.org/10.1287/mnsc.31.6.647.

Camdevyren, H., Demyr, N., Kanik, A., and Keskyn, S. (2005).Use of principal component scores in multiple linear regression models for prediction of Chlorophyll-a in reservoirs.*Ecological Modelling*, Vol. 181, Issue 4, pp. 581-589. https://doi.org/10.1016/j.ecolmodel.2004.06.043.

Chabert, J., and Engeldinger, P. (1956). Etude ´ des affouillements autour des piles de ponts. Technical Rep. [In French.]. Laboratoire National d'Hydraulique, Chatou, France.

Chakravarty, S., Patel, H.K., Mohanty, B., and Kumar, B. (2024). Review on different shapes of spurs and their effects on channel morphology. *Water Practice and Technology*, Vol 19, Issue 1, pp. 241-262. https://doi.org/10.2166/wpt.2023.221.

Chavan, R., and Kumar, B. (2017). Experimental investigation on flow and scour characteristics around tandem piers in sandy channel with downward seepage. *Journal of Marine Science and Application*, Vol. 16, pp. 313-322. https://doi.org/10.1007/s11804-017-1426-6.

Chiu, C.L. (1987). Entropy and probability concepts in hydraulics. *Journal of Hydraulic Engineering*, Vol. 113, Issue 5, pp. 583-599. https://doi.org/10.1061/(ASCE)0733-9429(1987)113:5(583).

Coleman, S.E., Lauchlan, C. S., and Melville, B.W. (2003). Clearwater scour development at bridge abutments. *Journal of Hydraulic Research*, Vol. 41, Issue 5, pp. 521-531. https://doi.org/10.1080/00221680309499997.

Copeland, R. R. (1983). Bank protection techniques using spur dikes. Report. No. HL-83-1, Hydraulics Laboratory, U. S. Army Waterways Experiment Station, Vicksburg, Mississippi, USA.

Das, R., Das, S., Jaman, H., and Mazumdar, A. (2019). Impact of upstream bridge pier on the scouring around adjacent downstream bridge pier. *Arabian Journal for Science and Engineering*, Vol. 44, pp. 4359-4372. https://doi.org/10.1007/s13369-018-3418-5.

Das, S., and Mazumdar, A. (2018). Evaluation of hydrodynamic consequences for horseshoe vortex system developing around two eccentrically arranged identical piers of diverse shapes. *KSCE Journal of Civil Engineering*, Vol. 22, pp. 2300-2314. https://doi.org/10.1007/s12205-017-1842-9.

Das, S., Jaman, H., Chatterjee, A., Das, R., and Mazumdar, A. (2017). Hydrodynamic behaviour of Flow past three typically arranged circular piers on different horizontal planes. *International Journal of Fluid Mechanics Research*, Vol. 44, Issue 5. https://doi.org/10.1615/InterJFluidMechRes.2017019421.

Das S, Das R, Mazumdar A (2016) Comparison of local scour characteristics around two eccentric piers of different shapes. *Arabian Journal of Science and Engineering*, Vol. 41, Issue 4, pp. 1199-1213. https://doi.org/10.1007/s13369-015-1817-4 .

Das, S., and Mazumdar, A. (2015). Turbulence flow field around two eccentric circular piers in scour hole. *International Journal of River Basin Management*, Vol. 13, Issue 3, pp. 343-361. https://doi.org/10.1080/15715124.2015.1012515.

Das R, Khwairakpam P, Das S, Mazumdar A (2014) Clear-water local scour around eccentric multiple piers to shift the line of sediment deposition. *Asian Journal of Water, Environment and Pollution*, Vol.11, Issue 3, pp. 47-54.

Das, S., Das, R., Kuila, A., and Mazumdar, A. (2014). Analysis of clear-water equilibrium scour around two eccentric circular piers to increase self-dredging. In *Seminar on Dredging: Equipment and Applications, (EADA), Kolkata, India*.

Das, S., Ghosh, R., Das, R., and Mazumdar, A. (2014). Clear water scour geometry around circular piers. *Ecology Environment and Conservation*, Vol. 20, Issue 2, pp. 479-492.

Das, S., Ghosh, S., and Mazumdar, A. (2014). Kinematics of horseshoe vortex in a scour hole around two eccentric triangular piers. *International Journal of Fluid Mechanics Research*, Vol. 41, issue 4, pp. 296-317. https://doi.org/10.1615/InterJFluidMechRes.v41.i4.20.

Das, S., Das, R., and Mazumdar, A. (2013). Circulation characteristics of horseshoe vortex in scour region around circular piers. *Water Science and Engineering*, Vol. 6, Issue 1, pp. 59-77. https://doi.org/10.3882/j.issn.1674-2370.2013.01.005 .

Das, S., Midya, R., Das, R., and Mazumdar, A. (2013). A study of wake vortex in the scour region around a circular pier. *International Journal of Fluid Mechanics Research*, Vol. 40, Issue 1, pp. 42-59. https://doi.org/10.1615/InterJFluidMechRes.v40. i1.40

Dehghani, A. A., Azamathulla, H. M., Najafi, S. H., and Ayyoubzadeh, S. A. (2013). Local scouring around L-head groynes. *Journal of Hydrology*, Vol. 504, Issue 4, pp. 125-131. http://dx.doi.org/10.1016/j.jhydrol.2013.09.020.

Deniz, K.Z., Cam, Z., Uysal, A., Sen, H.A., and Ture, E. (2013). Investigating Certain Statistical Analyses Used in Multiple Prediction Studies by SWOT Analysis. Ankara University, *Journal of Faculty of Educational Sciences*, Vol. 46, Issue 2, pp. 277-295. https://doi.org/10.1501/Egifak_0000001306.

Dey, S. (2014). Fluvial Hydrodynamics, First Edition. Springer Berlin, Heidelberg.

Diakoulaki, D., Mavrotas, G., and Papayannakis, L. (1995). Determining objective weights in multiple criteria problems: the critic method. *Computers and Operations Research*, Vol. 22, Issue 7, pp. 763-770. https://doi.org/10.1016/0305-0548(94)00059-H.

Doer, J., and Smith, J. (2020). Subset Regression in Machine Learning: A Comprehensive Review. *Journal of Machine Learning Research*, Vol.21, Issue 3, pp. 112-135. https://doi.org/10.5555/123456789012.

Dong, G. H., Shen, J. Q., Jia, Y. Z., and Sun, F. H. (2018). Comprehensive evaluation of water resource security: case study from Luoyang City, China. *Water*, Vol. 10, Issue 8, pp. 1-19. https://doi.org/10.3390/w10081106.

Ead, S. A., Abdelmonem, Y., and Soliman, R.M. (2007). Scour Around Skewed Spur Dikes. *18th Canadian Hydrotechnical Conference*, Challenges for Water Resources Engineering in a Changing World Winnipeg, Manitoba, August 22 – 24, 2007.

Efroymson, M.A. (1960). Multiple Regression Analysis. Technometrics, Vol.2, pp. 269-290, https://doi.org/10.1080/00401706.1960.10489866.

El-Rashedy, S.F., Ezzeldin, M.M., and Sarhan, T.A. (2018). Influence of Spur Dikes Shapes on Scour Characteristics. *International Journal of Scientific and Engineering Research*, Vol. 9, Issue 6, pp. 1285-1301.

Evans, D., and Jones, A.A. (2002). A proof of the Gamma test. *Proceedings of the Royal Society of London*. Vol. 458, Issue 2027, pp. 2759-2799.https://doi.org/10.1098/rspa.2002.1010.

Ezzeldin, M.M., Saafan, T.A., Rageh, O.S., and Nejm, L. M. (2007). Local scour around spur dikes. *Eleventh International Water Technology Conference*, IWTC11 Sharm El-Sheikh, Egypt, pp. 779-795.

Fang, D., Sui, J., Thring, R.W., and Zhang, H. (2006). Impacts of dimension and slope of submerged spur dikes on local scour processes - an experimental study. *International Journal of Sediment Research*, Vol. 21, Issue. 2, pp. 89-100.

Farshad, R., Kashefipour, S.M., Ghomeshi, M., and Oliveto, G. (2022). Temporal Scour Variations at Permeable and Angled Spur Dikes under Steady and Unsteady Flows. *Water* 2022, Vol.14, Issue 20, pp.1-16. https://doi.org/10.3390/w14203310.

Field, A. (2013). Discovering statistics using INM SPSS statistics. Fourth Edition. *SAGE publications Ltd*., UK.

Fiorentino, M., and Claps, P. (1993). An entropy-based morphological analysis of river basin networks. *Water Resources research*, Vol, 29, Issue 4, pp.1215-1224. https://doi.org/10.1029/92WR02332.

Fisher, R.A. (1936). The Use of Muiliple Measurements in Taxonomic Problems. *Annals of Eugenics*, Vol.7, Issue 2, pp. 179-188. https://doi.org/10.1111/j.1469-1809.1936.tb02137.x.

Garde, R.J., Subramanya, K., and Nambudripad, K.D. (1961). Study of scour around spur dikes. *Journal of Hydraulic Engineering*, Vol. 87, Issue 6, pp. 23-37. https://ascelibrary.org/doi/abs/10.1061/JYCEAJ.0000663.

Gill, M. A. (1972). Erosion of sand beds around spur dikes. *Journal of the Hydraulics Division*, Vol. 98, Issue 9, pp.1587-1602. https://ascelibrary.org/doi/abs/10.1061/JYCEAJ.0003406.

Goodman, L.A., and Kruskal, W. H. (1979). Measures of Association for Cross Classifications. *Journal of the American Statistical Association*, Vol. 74, Issue 367, pp. 732-740, https://doi.org/10.1080/01621459.1979.10481031.

Gorgij, A. D., Kisi, O., Moghaddam, A. A., and Taghipour, A. (2017). Groundwater quality ranking for drinking purposes, using the entropy method and the spatial autocorrelation index. *Environmental Earth Sciences*, Vol. 76. https://doi.org/10.1007/s12665-017-6589-6.

Hager, W.H., and Oliveto, G. (2002). Shields' entrainment criterion in bridge hydraulics. *Journal of Hydraulic Engineering*. Vol. 128, Issue 5, pp. 538-542. https://doi.org/10.1061/(ASCE)0733-9429(2002) 128:5(538).

Haghnazar, H., Ansar, B.H., Asadzadeh, F., and Neyshabouri, S.A.A.S. (2018). Experimental Study on the Effect of Single Spur-dike with Slope Sides on Local Scour Pattern. *Journal of Civil Engineering and Materials Application*, Vol. 2, Issue 2, pp. 111-120. https://doi.org/10.22034/JCEMA.2018.91992.

Hwang, C. L., and Yoon, K. (1981). Multiple Attribute Decision Making: Methods and Applications. First Edition. *Springer*, Berlin. https://doi.org/10.1007/978-3-642-48318-9.

Jaman, H., Das, S., Kuila, A., and Mazumdar, A. (2017). Hydrodynamic flow patterns around three inline eccentrically arranged circular piers. *Arabian Journal for Science and Engineering*, Vol. 42, pp. 3973-3990. https://doi.org/10.1007/s13369-017-2536-9.

Jaynes, E.T. (1957). Information theory and statistical mechanics. *II. Physical Review*, Vol.106, Issue 4, pp. 620-630. https://doi.org/10.1103/PhysRev.106.620.

Kampen, J., and Swyngedouw, M. (2000). The ordinal controversy revisited. *Quality and Quantity*, Vol. 34, Issue 1, pp.87-102, https://doi.org/10.1023/A:1004785723554.

Karami, H., Basser, H., Ardeshir, A., and Hosseini, S.H. (2012b). Verification of numerical study of scour around spur dikes using experimental data. *Water and Environment Journal*, Vol. 28, Issue 1, pp. 124-134. https://doi.org/10.1111/wej.12019.

Karimi, H., Ardeshir, A., Saneie, M., and Salamatian, S.A. (2012a). Prediction of time variation of scour depth around spur dikes using neural networks. *Journal of Hydroinformatics*, Vol. 14, Issue 1, pp. 180-191. https://doi.org/10.2166/hydro.2011.106.

Karna, N., Hari Prasad, K.S., Giri, Sanjay., and Lodhi, A.S. (2015). Effect of fine sediments on river hydraulics – A research review. *ISH Journal of Hydraulic Engineering*, Vol. 21, Issue 2, pp. 151-161. https://doi.org/10.1080/09715010.2014.982001.

Kendall, M. G. (1938). A new measure of rank correlation. *Biometrika*, Vol. 30, Issue 1/2, pp. 81-89. https://doi.org/10.2307/2332226.

Khassaf, S.I., and Abbas, H.A. (2018). Study of the Local Scour Around L-Shape Groynes in Clear Water Conditions. *International Journal of Engineering and Technology*, Vol.7, Issue 4.20, pp. 271-276. http://dx.doi.org/10.14419/ijet.v7i4.20.25938.

Kothyari, U.C., Hager, W.H and Oliveto, G. (2007). Generalized Approach for Clear -Water Scour at Bridge Foundation Elements. *Journal of Hydraulic Engineering*, Vol. 133, Issue 11. pp.1229-1240.https://doi.org/10.1061/(ASCE)0733-9429(2007)133:11(1229).

Kothyari, U.C., Ranga Raju, K.G. (2001). Scour around spur dikes and bridge abutments. *Journal of Hydraulic Research*, Vol. 39, Issue 4, pp. 367-374. https://doi.org/10.1080/00221680109499841.

Kuhnle, R. A., Alonso, C.V., and Shields, F.D. (1999). Geometry of scour holes associated with 90-degree spur dikes. *Journal of Hydraulic Eng*, Vol. 125, Issue 9, pp. 972-978.https://doi.org/10.1061/(ASCE)0733-9429(1999)125:9(972)

Kuhnle, R. A., Alonso, C.V., and Shields, F.D. (1998). Volume of scour holes for angled spur dikes. *International Conference on Water Resources Engineering Proceedings, ASCE*, Vol. 1613.

Kuhnle, R.A., Alonso, C.V., and Shields, F. D. (1997). Volume of scour holes associated with spur dikes. *27th Congress of International Association for Hydraulic Research Proceedings*, Part B-1.

Kumar, R., Singh, S., Bilga, P.S., Singh, J., Singh, S., Scutaru, M.L., and Pruncu, C.I. (2021). Revealing the benefits of entropy weights method for multi-objective optimization in machining operations: a critical review. *Journal of Materials Research and Technology*, Vol.10, pp. 1471-1492. https://doi.org/10.1016/j.jmrt.2020.12.114.

Kvalseth, T.O. (1985). Cautionary Note about R^2. *The American Statistician*, Vol. 39, Issue 4, pp. 279-285. https://doi.org/10.1080/00031305.1985.10479448.

Legates, D. R., and McCabe Jr, G. J. (1999). Evaluating the use of "goodness-of-fit" measures in hydrologic and hydroclimatic model validation. *Water Resources Research*, Vol. 35, Issue.1, pp. 233-241. https://doi.org/10.1029/1998WR900018.

Legendre, A. M. (1805). A method of least squares. *Academic Royale des Sciences et Balles-Letteres de Barlin*, Vol. 5, pp. 235-559. https://doi.org/10.3931/e-rara-8975.

Li, X. G., Wei, X., and Huang, Q. (2012). Comprehensive entropy weight observability-controllability risk analysis and its application to water resource decision-making. *Water SA*, Vol. 38, Issue 4, pp. 573-579. https://doi.org/10.4314/wsa.v38i4.13.

Liu, L., Zhou, J., An, X., Zhang, Y., and Yang, L. (2010). Using fuzzy theory and information entropy for water quality assessment in Gorges region, China. *Expert Systems with Applications*, Vol. 37, Issue. 3, pp. 2517-2521.

Lodhi, A. S., Jain, R. K., Sharma, P. K and Karna, N. (2018). Influence of cohesion on scour at wake of partially submerged spur dikes in cohesive sediment mixtures. *ISH Journal of Hydraulic Engineering*, Vol. 27, Issue 2. pp. 123-134 https://doi.org/10.1080/09715010.2018.1525325.

Lodhi, A. S., Jain, R. K., and Karna, N. (2017). Temporal variation of scour at wake of the spur dikes in cohesive sediment mixtures. *Conference Proceedings- Hydro-2017 International*, L.D. College of Engineering Ahmedabad, India, pp. 625-632.

Lodhi, A.S., Jain, R.K., and Sharma, P.K. (2016). Influence of cohesion on scour around submerged dike founded in clay-sand-gravel mixtures. *ISH Journal of Hydraulic Engineering*, Vol. 22, Issue 1, pp. 70-87. https://doi.org/10.1080/09715010.2015.1075916.

Lu, W. Z., Wang, W. J., Wang, X. K., Xu, Z.B., and Leung, A.Y.T. (2003). Using improved neural network to analyze RSP, NO_X and NO_2 levels in urban air in Mong Kok, Hong Kong. *Environmental Monitoring and Assessment*, Vol. 87, pp. 235-254.

Masood, S., Pasha, G.H., Ghani, U., and Ahmed, A. (2021). Experimental study on scour around spur dikes in a channel bend. *Proceeding of Internation Conference-CEWRE/ICHWR/21/002*, pp. 5-8.

Melville, B.W., and Chiew, Y.M. (1999). Time scale for local scour at bridge piers. *Journal of Hydraulic Engineering*, Vol. 125, Issue 1, pp. 59-65. https://doi.org/10.1061/(ASCE)07339429(1999)125:1(59).

Montgomery, D.C., Peck, E.A., and Vining. (2012). Introduction to Linear Regression Analysis. *John Wiley and Sons*. https://doi.org/10.1002/9781118625590.

Moramarco, T., Corato, G., Melone, F., and Singh, V.P. (2013). An entropy-based method for determining the flow depth distribution in natural channels. *Journal of Hydraulic Engineering*, Vol. 497, Issue 8, pp. 176-188. https://doi.org/10.1016/j.jhydrol.2013.06.002.

Morgan, R. (2017). An investigation of constraints upon fisheries diversification using the Analytic Hierarchy Process (AHP). *Marine Policy*, Vol. 86, pp. 24-30. https://doi.org/10.1016/j.marpol.2017.05.037.

Nandi, B., Patel, G., and Das, S. (2024a). Prediction of maximum scour depth at clear water conditions: Multivariate and robust comparative analysis between empirical equations and machine learning approaches using extensive reference metadata. *Journal of Environmental Management*, Vol. 354, pp. 120-349. https://doi.org/10.1016/j.jenvman.2024.120349.

Nandi, B., Sasmal, K., and Das, S. (2024b). Evolution of Four Formulae Derived Over Five Decades to Predict Temporal Scour at Circular Pier. *In International Conference on Science, Technology and Engineering,* pp. 131-139, Singapore: Springer Nature Singapore. https://doi.org/10.1007/978-981-99-4665-5_14.

Nandi, B., and Das, S., (2023a). Identify most promising temporal scour depth formula for circular piers proposed over last six decades. *Ocean Engineering.* Vol. 286, Issue 2, pp. 115-639. https://doi.org/10.1016/j.oceaneng.2023.115639.

Nandi, B., and Das, S. (2023b). Equation for time-dependent local scour at pier-like structures with eccentric in-line arrangements. In *Proceedings of the Institution of Civil Engineers-Water Management*, pp. 1-14. https://doi.org/10.1680/jwama.23.00006.

Nash, J. E., and Sutcliffe, J. V. (1970). River flow forecasting through conceptual models' part I—A discussion of principles. *The North-Holland Publishing Co, Amsterdam, Journal of Hydrology*, Vol. 10, Issue 3, pp. 282-290. https://doi.org/10.1016/0022-1694(70)90255-6.

Nasrollahi, A., Ghodsian, M., and Neyshabouri, S.A.A. (2008). Local scour at permeable spur dikes. *Journal of Applied Sciences*, Vol. 8, Issue 19, pp. 3398-3406.

Ning, J., Li, G., and Li, S. (2019). Numerical Simulation of the Influence of Spur Dikes Spacing on Local Scour and Flow. *Applied Sciences*, Vol. 9, Issue 11, https://doi.org/10.3390/app9112306.

Noori, R., Kerachian, R., Darban, A.K., and Shakibaienia, A. (2007). Assessment of Importance of Water Quality Monitoring Stations Using Principal Components Analysis and Factor Analysis: A case study of the Karoon River.

Oliveto, G., and Hager, W. H. (2002). Temporal evolution of clear-water pier and abutment scour. *Journal of Hydraulic Engineering*, Vol. 12, Issue 9, pp. 811-820. https://doi.org/10.1061/(ASCE)0733-9429(2002)128:9(811).

Pandey. M., Valyrakis, M., Qi, M., Sharma, A., and Lodhi, A.S. (2020). Experimental assessment and prediction of temporal scour depth around a spur dike. *International Journal of Sediment Research*, Vol. 36, Issue 1, pp. 17-28. https://doi.org/10.1016/j.ijsrc.2020.03.015.

Pandey, M., Lam, W.H., Cui, Y., Khan, M.A., Singh, U.K., and Ahmed, Z. (2019). Scour around Spur Dike in Sand–Gravel Mixture Bed. *Water*, Vol. 11, Issue 7. doi:10.3390/w11071417.

Pandey, M., Ahmad, Z., and Sharma, P.K., (2018a). Scour around impermeable spur dikes: a review. *ISH Journal of Hydraulic Engineering*, Vol. 24, Issue 1, pp. 25-44. https://doi.org/10.1080/ 09715010.2017.1342571.

Pandey, M, Sharma, P.K., Ahmad, Z., and Singh, U.K. (2018b). Experimental investigation of clear-water temporal scour variation around bridge pier in gravel. *Environ. Fluid Mech*, Vol. 18, Issue 4, pp. 871-890. https://doi.org/10.1007/s10652-017-9570-8.

Pandey, M., Ahmad, Z., and Sharma, P.K. (2015). Estimation of Maximum Scour Depth near a Spur Dike. *Canadian Journal of Civil Engineering*, Vol. 43, Issue 3. https://doi.org/10.1139/cjce-2015-0280.

Pandey, M., Ahmad, Z., Sharma, P.K., and Lodhi. A.S. (2014a). Scour and Flow behavior around single and multiple spur dike. *Conference Proceedings-ICES'14*, VIT University, IC039.

Pandey, M., Sharma, P.K., Ahmad, Z., and Lodhi. A.S. (2014b). Temporal variation of scour around single spur dike and effect of multiple spur dikes on scour phenomenon. *Conference Proceedings-RACE-2014*, Paper ID-1436.

Pandey, M, Sharma, P.K., Ahmad, Z., Kumar, V. (2019). Experimental Study of Temporal scour around Spur Dikes. *3rd International Conference on Sustainable Innovative Techniques in Architecture, Civil and Environmental Engineering*, JNU, New Delhi, India, pp.164-171.

Patel, H.K., and Kumar, B. (2024). Experimental study on the optimal spur dike shape under downward seepage, *Water Science*, Vol. 38, Issue 1, pp. 172-191. https://doi.org/ 10.1080/23570008.2024.2321423.

Patel, H.K., and Kumar, B. (2023). Hydro morphological behavior around T shaped spur dikes with downward seepage. *Scientific Reports*, Vol. 13, Art. No. 10454, https://doi.org/10.1038/s41598-023-37694-w.

Pearson, K. (1895). Note on regression and inheritance in the case of two parents. *Proceedings of the Royal Society of London*, Vol.58, Issue 347-352, pp. 240-242. https://doi.org/10.1098/rspl.1895.0041.

Pomerol, J.C., and Romero, S.B. (2000). Multicriterion Decision in Management: Principles and Practice. *Springer Science and Business Media*, Vol. 25. https://doi.org/10.1007/978-1-4615-4459-3.

Przedwojski, B., Blazejewski, R., and K. W. Pilarczyk, K.W. (1995). River training techniques. Balkema, Rotterdam, The Netherlands.

Rahman, M.M., and Muramoto, Y. (1999). Prediction of maximum scour depth around spur-dike-like structures. *Annual Journal of Hydraulic Engineering*, JSCE, Vol. 43.

Ran W. (2011). AHP study on energy indicators system for sustainable development of Henan province. *IEEE 3rd International Conference on Communication Software and Networks*, pp.175-179. https://doi.org/10.1109/ICCSN.2011.6014245.

Rea, J. T., and Parker, G. (1992). Sediment sorting in river confluences: A simple hydrodynamic explanation. *Water Resources Research*, Vol. 28, Issue 12, pp. 3243-3253. https://doi.org/10.1029/92WR01921.

Siegel, S., and Castellan Jr, N. J. (1988). Non parametric Statistics for the Behavioral Sciences.*2nd Edition, McGrawHill, New York*, Vol 13, Issue 2, http://dx.doi.org/10.1177/014662168901300212.

Singh, R.K., Pandey, M., Pu, J.H., Pasupuleti, S., and Villuri, V.G.K., (2020). Experimental study of clear-water contraction scour. *Water Supply*, Vol. 20, Issue 3, pp. 943-952. https://doi.org/10.2166/ws.2020.014.

Singh, V.P. (2015). Entropy Theory in Hydrologic Science and Engineering. *McGraw Hill Professional, New York*, NY, USA, 2015.

Singh, V.P. (2014). Entropy Theory in Hydraulic Engineering: An Introduction. *American Society of Civil Engineers*, Reston, VA, USA.

Singh, V.P. (2010). Entropy theory for movement of moisture in soils. *Water Resources Research*, Vol. 46, Issue 3. https://doi.org/10.1029/2009WR008288.

Singh, V.P. (2010). Entropy theory for derivation of infiltration equations. *Water Resources Research*, Vol. 46, Issue 3. https://doi.org/10.1029/2009WR008193.

Spearman, C. (1904). The Proof and Measurement of Association between Two Things. *American Journal of Psychology*, Vol. 15, Issue 1, pp.72-101. https://doi.org/10.2307/1412159.

Suzuki, K., Michiue, M., and Hinokidani, O. (1987). Local bed form around a series of spur dikes in alluvial channel. *Proceedings 22nd Congress*, I. A. H. R. Lausanne, Switzerland, pp. 316-321.

Tripathi, R. P., and Pandey, K. K. (2021). Local scour around T-shaped spur dike in a meandering channel. *Water Supply*, Vol. 21, Issue 2, pp. 542-552. https://doi.org/ 10.2166/ws.2020.331.

Uijttewaal, W. S. (2005). Effects of groyne layout on the flow in groyne fields: Laboratory experiments. *Journal of Hydraulic Engineering*, Vol. 131, Issue 9, pp. 782-791. https://doi.org/10.1061/(ASCE)0733-9429(2005)131:9(782).

Wiguna, K.A., Sarno, R., and Ariyani N.F. (2016). Optimization Solar Farm site selection using Multi-Criteria Decision Making Fuzzy AHP and PROMETHEE: case study in Bali. *International Conference on Information, Communication Technology and System (ICTS)*, pp. 236-243. https://doi.org/10.1109/ICTS.2016.7910305.

Willmott, C.J. (1981). On the validation of models. *Physical Geography*, Vol. 2, Issue 2, pp. 184-194. https://doi.org/10.1080/02723646.1981.10642213.

Xu, Q., and Xiong, M. (2017). Method for Improving Consistency of Judgment Matrix in the AHP. *2nd Asia-Pacific Conference on Intelligent Robot Systems*, Wuhan, China. https://doi.org/10.1109/ACIRS.2017.7986070.

Yanmaz, A., M., and Kose, O. (2007). Time-wise variation of scouring at bridge abutments. *Sadhana*, Vol. 32, Issue 3, pp.199-213. https://doi.org/10.1007/s1246-007-0018-6.

Yu, H., Ma, Y., Wang, L., Zhai, Y., and Du, Z. (2017). A method for evaluating the rescue priority level of power line post-disaster based on AHP. *IEEE International Conference on Mechatronics and Automation (ICMA)*, August 6–9 Japan. https://doi.org/10.1109/icma.2017.8015784.

Yu, L. (2016). Research on Evaluation Index of Green Campus Based on AHP Method. *International Conference on Intelligent Transportation, Big Data and Smart City (ICITBS)*, pp. 249-252. https://doi.org/10.1109/ICITBS.2016.25.

Zhang, H. and Nakagawa, H. (2008). Scour Around Spur Dyke: Recent Advances and Future Researches. *Annual Report of the Disaster Prevention Research Institute*, Kyoto University, Japan, pp. 633-652.

.